

Università degli Studi di Salerno



Department of Chemistry and Biology “Adolfo Zambelli”

PhD in Chemistry – XXXIII Course

Dottorati innovativi con caratterizzazione industriale PON “Ricerca e
Innovazione” 2014- 2020

PhD Thesis on

Synthesis of New Water Reducer Superplasticizers for Building Materials

Academic tutors:

Prof. Carmine Gaeta

Prof. Carmen Talotta

Industrial tutor:

Dr. Rocco Gliubizzi

Ph.D. coordinator:

Prof. Claudio Pellecchia

Ph.D. Student:

Clotilde Capacchione

Serial number:

8800100043

Academic year 2020/2021

Summary

Abstract.....	5
Chapter 1: Introduction.....	11
1.1 The world of concrete: overview of chemical and mineralogical nature of cement clinker phases.....	11
1.2 The hydration of Portland cement	16
1.3 Superplasticizers for building materials and their action mechanism	19
1.4 Abram's law for cement mortars.....	26
1.5 Industrial methods to investigate the admixtures effect on building materials	30
Chapter 2 - Research aims and thesis outline	35
Chapter 3 - Dispersing and Retarding Properties of Water-Soluble Tetrasulfonate Resorcin[4]arene and Pyrogallol[4]arene Macrocycles in Cement-based Mortar	40
3.1 General overview	40
3.2 Synthesis and characterization of resorcin[4]arene, pyrogallol[4]arene and methyl-resorcinarene tetrasulfonated macrocycles	46
3.2.1. Synthesis and characterization of the derivative 1	48
3.2.2 Synthesis and characterization of the derivatives 2,3.....	53
3.3 Products testing of dispersing and retarding properties of derivatives	53
3.4 Conclusions	66

3.5 Experimental section with details for the synthesis of derivatives 1, 2 and 3.	67
3.6 Applicative workability tests of derivative 1,2 and 3 on fresh mortar.....	70
Chapter 4: Poly(EthyleneGlycol)/β-Cyclodextrin Pseudorotaxanes as Sustainable Dispersing and Retarding Materials in Cement-Based Mortar	74
4.1 General overview	74
4.2 Synthesis and characterization of the polymeric axis mPEG-Phth 9 and mPEG-Mal 10	86
4.3 Formation and characterization of pseudorotaxanes mPEG-Phth@- β CD 12, mPEG-OH@- β CD 13 and mPEG-OH@- β CD 14.....	101
4.5 Conclusions	122
4.6 Experimental section with details for the synthesis of derivatives 9, 10, 11, 12, 13 and 14.....	123
4.7 Applicative workability tests of derivative 12, 13 and 14 on fresh mortar	129
Chapter 5: Modified carboxymethylcellulose-based scaffolds as new potential ecofriendly superplasticizers with a retardant effect for mortar: from the synthesis to the application.....	132
5.1 General overview	132
5.2 Synthesis of new water-soluble carboxymethylcellulose-based SPs	139
5.3 Products testing the dispersing and retarding properties of derivatives....	141
5.4 Conclusions	157

5.5 Experimental section for the synthesis of derivatives 15-21	158
5.6 Characterization and testing through applicative tests on mortar	159
6. Summary	164
6.1 Final conclusions.....	164

Abstract

This industrial PhD project is focused on the development of new additives called Superplasticizers (SPs) that are particularly interesting for the engineering of construction field. These attracting molecules are organic compounds that are employed for building materials to improve their fresh workability capability and their mechanical properties in the hardened state. Their ability to disperse cement grains is due to their structure: they contain negatively charged functional groups that can interact with the positive charges present on the surface of the cement granules, thus avoiding the collapse of the cement particles and consequently making it fluid. Even if they are added in low quantity, they decrease the amount of needed mixing water and control the setting time without losing fluidity of the pastes, which results in higher strength and better durability of final materials.

Dispersants have given an important and fundamental improvement in materials engineering during the last century, in the late twenties the first-generation additives were developed from by-products obtained from the paper firm. Due their important applications in engineering field, research has been focused on the development of new and more performing plasticizers such as naphthalene/melamine sulfonate derivatives and polycarboxylate esters/ethers, that represent the second and third generation of additives.

To supply to the growing demand of new and more performing admixtures, the scientists have been pushing forward with breakthroughs

in technology and knowledge. This PhD project fits into this contest and its aim is to provide innovative solutions for this framework.

At first, we propose a study^{1,2} to investigate the role of new unconventional plasticizers on concrete, respect to the polymeric counterpart that are currently commercially available. In particular the attention was turned on the synthesis of new macrocycles, based on resorcin[4]arene and pyrogallol[4]arene, functionalized with polar groups, such as sulfonate groups to increase their solubility in aqueous systems. The presence of negatively charged groups, linked to the pre-organized skeleton of the macrocycles, strongly influenced the cement conglomerate by modifying both the flowability of the cementitious paste and the setting time of the hardened product.

Even though the SP additives currently on the market show high performances, the challenge of our time is to study new types of innovative, eco-sustainable and highly performing super-plasticizers for future industrial applications. Prompted by these considerations, we designed mPEG@ β -cyclodextrin pseudorotaxanes³ obtained by inclusion

¹ Capacchione, C.; Talotta, C.; Neri, P.; Bruno, I.; Pauciulo, A.; Bartiromo, A.R.; Gliubizzi, R.; Gaeta, C. Synthesis of new Water Reducer Plasticizers for concrete, gypsum and clay. XXXIX National Conference of the Division of Organic Chemistry - SCI, CDCO, Turin (Italy), 8-11th September, 2019. Poster session.

² Capacchione, C.; Picariello, D.; Della Sala, P.; Talotta, C.; Neri, P.; Bruno, I.; Pauciulo, A.; Bartiromo, A. R.; Gliubizzi, R.; Gaeta, C. Dispersing and Retarding Properties of Water-Soluble Tetrasulfonate Resorcin[4]arene and Pyrogallol[4]arene Macrocycles in Cement-Based Mortar. *ACS Omega* **2020**, *5*, 18218–18225. [10.1021/acsomega.0c01837]

³ Capacchione, C.; Della Sala, P.; Bruno, I.; Pauciulo, A.; Bartiromo, A.R.; Iannece, P.; Neri, P.; Talotta, C.; Gliubizzi, R.; Gaeta, C. Poly(Ethylene Glycol)/ β -Cyclodextrin Pseudorotaxane Complexes as Sustainable Dispersing and Retarding Materials in a Cement-Based Mortar. *ACS Omega* **2021**, *6*, 12250–12260. [DOI: 10.1021/acsomega.1c01133].

inside the cavity of the β -CD of a polymeric chain of PEG functionalized with carboxylic group. In fact, it is well known that in the highly alkaline environment of cement, the carboxylate groups act as anchor on, while the poly(ethylene oxide) side chains included inside the β -CD protrude from the cement surface into the pore solution to produce steric hindrance. From the analysis of their effect on mortar, these SPs were considered as new second generation additives.³

Finally, last part of the PhD project was carried on during the research period at the *Chair of Construction Chemistry and Polymeric Materials ChemPoWer under the Prof. Andrea Osburg's supervision, Deputy Head of the F. A. Finger Institute for Building Materials Engineering at Bauhaus-Universität Weimar*. In detail, the aim of the abroad research period was to design, synthesize and evaluate the influence and the properties of new bio-based additives, starting from modified sugars like cellulose derivatives that were proposed in this thesis.⁴ It was studied their synthesis and their possible application as new candidates for SPs for cementitious systems. Through the reduction of the dimension of the cellulose backbone and the introduction of anionic functional groups on their structure, it was possible to observe their behaviour as superplasticizers: indeed, this kind of additives showed the capability to increase the flowability properties and the setting time of cement.

⁴ Capacchione, C.; Partschefeld, S.; Gliubizzi, R.; Gaeta, C.; Osburg A. Modified carboxymethylcellulose-based scaffolds as new potential ecofriendly superplasticizers with a retardant effect for mortar: from the synthesis to the application. *Manuscript accepted on the 23rd of June 2021*.

Glossary of terms

SPs – Superplasticizers

βCD – β cyclodextrin

PCE – Polycarboxylate ethers/esters

WR – Water Reducers

HRWR – High-Range Water Reducers

ASTM – American Society for Testing and Materials International

DIN – Deutsches Institut für Normung

BS – British Standards

SNF - Poly-β-naphthalene sulfonate

SMF - Poly-melamine sulfonate

CEM II 42.5R – Normalized cement

CEN NormenSand – Normalized sand

bwoc – by weight of cement

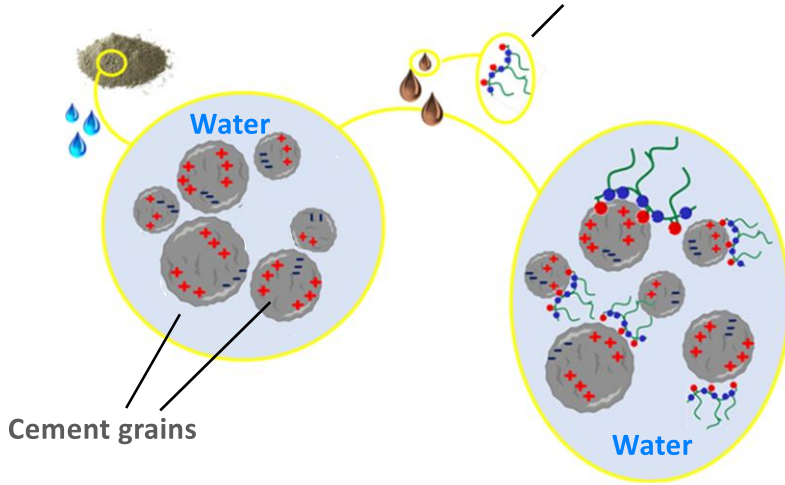
PCM-β-CD - poly-carboxymethyl-β-cyclodextrin

PEG - polyethylene glycol

mPEG - Poly(ethylene-glycol) methyl ether

Superplasticizers

Example of superplasticizer of III generation



Chapter 1: Introduction

1.1 The world of concrete: overview of chemical and mineralogical nature of cement clinker phases

The concrete is the most used product in houses and residences: it is a paste with binder capacity that it is composed of cement, a grey fine powder mixed with water, sand and stones. Many efforts have been concentrated on the investigations of the binder compounds nature and on the development of tailored compounds that through specific structural features are able to interact with chemicals beyond concrete. Starting from the evaluation of cement composition, it is possible to highlight the key parameters inside the cementitious paste that are reflected in the final properties of mortar, such as the mechanical strength. The chemical composition of cement is linked to the origin of the powder and its application in the urban constructions depends on the specific standards recognized by the Italian State and by the European Union.

Cement-producing countries are spread all over the world, indeed between the main global producers and consumers there are China, USA,

Australia, India, meanwhile between the EU countries such as Germany, France, Switzerland, and Italy are considered as the major producers.⁵

The choice of the proper cement type is a crucial aspect for the durability of cementitious materials, and it shall follow the appropriate standards valid in the area of application.

The UNI EN 197-1 states that there are 5 kinds of cement, 27 subtypes and 6 strength classes, all in compliance with the current legislation.

According to the current legislation, the normalized cement is termed CEM followed by the notation of the type. There are 5 main categories of cement as follows:

- The **Type I** is the most common cement, it is also called Ordinary Portland cement and it is mainly composed of 95-100% of only clinkers and of 5% of minor accessory minerals that are present in all the other categories in the same percentage;
- The **Type II** is a Portland-composite cement that contains clinkers and additional composites that are present in the 19 subtypes in different percentages (from the 6-20% until the 21-35%) such as limestone, blast furnace slag, silica fume, natural or natural calcined pozzolana, siliceous and calcareous volcanic ash;
- The **Type III** is also called blast furnace cement due to the percentage of blast furnace slag that could be in the range of 36-65%;

⁵ Josephin, A.; Dhanalakshmi, J.; Ambedkar, B. Experimental investigation on rice husk ash as cement replacement on concrete production. *Constr. Build. Mater.*, **2016**, *127*, 353–362.

- The **Type VI** is a Pozzolanic cement and the abundance of cinders from pozzolana and volcanic ash could be in the range of 11-35% or 36-55% by weight of cement;
- The **Type V** is another kind of composite cement, it is made of clinkers, blast furnace slag, natural or natural calcined pozzolana and siliceous ash in the percentage of 18-30% or 31-50%.

Cement is classified with another fundamental parameter, the strength class: it is defined by measuring the early strength of a cement at either 2 and 7 days and it shall be conforming to the requirements in EN 196-1.

Each type of the 6 strength standards includes two classes of early strength: one class shows an ordinary early strength, so it is defined with **N**, instead the other one that provides a high early strength, is indicated with **R**.

Finally, the compressive strength of concrete is also defined with **32.5**; **42.5** and **52.5 mPa** values that reflect the mechanical strength of the hardened final material.

Cement clinkers are obtained burning and crushing raw materials such as shells, rocks, limestones, clay at very high temperatures such as 1450 °C in rotary ovens called “kiln”, hence the reason why cement constituents are named clinkers.⁶ The production of cement is a process with high energy and environmental impact. Indeed, it is estimated that 1 ton of cement leads to produce the same amount of CO₂, contributing annually

⁶ Kurdowski, W. Cement and Concrete Chemistry; Springer: Dordrecht, 2014.

Table 1. Typical mineralogical composition of OPC clinker phases.

Clinkers minerals	%	Clinkers minerals	%
SiO₂	20	K₂O	1
Al₂O₃	6	Na₂O	1
Fe₂O₃	3	SO₃	2
CaO	63	Others	1
MgO	1.5	GV	2
TiO₂	0.19	TV	0.5
MnO	0.3		

In addition to these compounds, where SO₃ works as precursor of sulfates mix generated from the hydration reactions of cement, there are other compounds such as MgO, TiO₂, Mn₂O₃, K₂O, Na₂O and others called “alkali” which are present in discrete amounts and are therefore referred to as "minorities". However, this does not refer to their importance, in fact they are responsible for affecting the kinetic of cement hardening and the final mechanical strength of the product and for reacting with some aggregates affecting the structure of the hardened concrete causing it to flake.

The clinkers composition is defined with a specific notation: every kind of oxide that is present in different percentages is conventionally symbolized with a letter (for example CaO = **C**; SiO = **S**; Al₂O₃ = **A** and

Fe₂O₃ = F).⁸ The mineralogical composition of cement clinkers is attributed to 4 different classes of compounds also called “phases” that are showed in the **table 2**:

Table 2. Clinkers phases composition of typical Ordinary Portland Cement determined through the Bogue calculation.⁹

Chemical name	Chemical formula	Shorthand notation	% wt
<i>Tricalcium silicate</i>	3CaO·SiO ₂	C ₃ S	54.1
<i>Dicalcium silicate</i>	2CaO·SiO ₂	C ₂ S	16.6
<i>Tricalcium aluminate</i>	3CaO·Al ₂ O ₃	C ₃ A	10.8
<i>Tetracalcium aluminoferrite</i>	4CaO·Al ₂ O ₃ ·Fe ₂ O ₃	C ₄ AF	9.10
<i>Gypsum</i>	CaSO ₄ ·H ₂ O	CSH ₂	

1.2 The hydration of Portland cement

Adding water to the cement powder means to let the hydration reactions to start: aluminates quickly react with water, but they don't contribute too much to the development of mechanical properties of the hardened mortar. The rapid interaction of aluminates with water gives an immediate loss of plasticity (quick setting) resulting in hydrated alluminates

⁸ Midness,S.; Young, J.F.; Darwin, D.; *Concrete*; Prentice-Hall: Upper Saddle River NJ, 1981.

⁹ Taylor, H. F. W. Modification of the Bogue calculation. *Adv. Cem. Res.* **1989**, *2*, 73–77.

compounds with a sheet-like morphology. Calcium sulfate is added to the cement powder to regulate the hardening time; indeed, it retards the hydration of aluminates. In addition, the primary ettringite $3\text{CaO}\cdot\text{Al}_2\text{O}_3\cdot 3\text{CaSO}_4\cdot 32\text{H}_2\text{O}$ is formed by reaction between CaSO_4 and C_3A (tricalcium aluminate Table 2). The fibers of ettringite cover the surface of C_3A and C_4AF (tetracalcium aluminoferrite) sheets and hinder, for a short time, the contact between water and aluminates. The responsible of the hardening of concrete are the silicates: C_3S (tricalcium silicate, Alite) and C_2S (dicalcium silicate, Belite) are the main classes of silicates in concrete. They show a different hydration rate, indeed the C_3S have a faster hydration kinetic than C_2S . In the short period, higher is the amount of C_3S , and smallest is the mechanical strength development. The silicate hydrates, the C-S-H, have a fiber-like morphology and for this reason they are responsible of the development of the mechanical properties of the hardened materials.

The cement hydration process could be monitored by isothermal calorimetry. This method is very useful to explain the chemical processes behind concrete: the heat released from the exothermic hydration reactions and the rate of the hydration process.

It is possible to determine the rate of heat evolution during time of hydration of cement that takes 28 days. Immediately after the contact between cement grains and water, the first period is characterized by a very strong and fast exothermic reaction that it is followed by a temporary dormant or quiescent phase. At the end of this step, cementitious paste is starting to lose its plasticity and workability meanwhile the heat reaction accelerates until the achievement of the maximum of the curve described

in **Figure 2**, that consists in the end of the fluidification capability of the cementitious paste. The evolution of this period is called setting time and it is observed in the timescale of hours. The final step is the hardening process of the mortar or concrete that ends 28 days after the preparation of the paste.

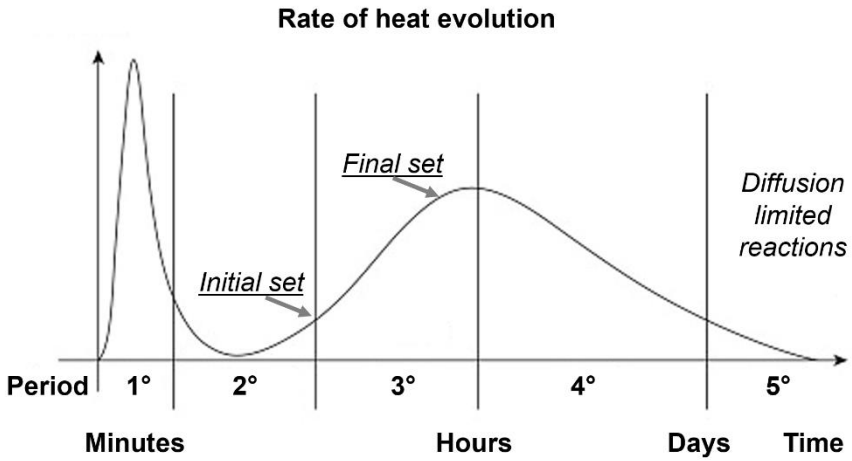


Figure 2. Example of the evolution of heat hydration cement reactions during time.¹⁰

¹⁰ Pacheco-Torgal, F.; Ivanov, V.; Karak, N.; Jonkers H.; Biopolymers and Biotech Admixtures for Eco-Efficient Construction Materials; 1st Ed.; Woodhead Publishing, 2016, 464.

1.3 Superplasticizers for building materials and their action mechanism

Superplasticizers are a family of fascinating chemical additives with important applications in engineering field, indeed the introduction of these synthetic dispersants represents one of the most important improvement of the concrete technology in the modern society.

The main function of SPs is to decrease the amount of needed mixing water and to control the setting time without affecting the fluidity of the pastes, which results in higher strength and better durability of final materials such concrete, gypsum and clay.

To be used, superplasticizers must meet quality standards both in terms of properties and methods for checking uniformity between batches. ASTM, DIN or BS are national specifications that define the requirements that additives must meet to be certified.

As function of the reduction capability of the additives, they can be also labelled as defined by ASTM C494 / C 494-M-1992 as Water Reducers (WR, type A) or High-Range Water Reducers (HRWR, type F) when they reduce the quantity of water until the 5% and 30%.

Water-reducing additives can be also classified into further classes according to the influence they can have on setting times: the admixtures of type D (WR) and type G (HRWR) show retarding properties, instead

the superplasticizers or type E (WR) are very well known for their accelerating properties.¹¹

In detail, **retardant additives** extend the setting time rate, retaining the initial workability of the cementitious pastes. They are widely used in many applications, such as for long-distance transport of concrete from the batching plant to the job site particularly in hot climates or for pumping of concrete mixes for oil wells where temperatures of over 90 °C are usually reached. This class of additives can be employed to recycle concrete residues into cement trucks returned from mixing sites for subsequent reuse to preserve the environmental health. Setting times and mechanical strength are parameters of concrete that are strongly influenced by temperature. For example, in hot climates, setting times are significantly reduced and this effect can affect the performance of concrete. In these adverse climatic conditions (e.g. 35 °C), it is very useful to use retardant admixtures which restore the setting points compared to concrete produced in less adverse climatic conditions (20 °C). Obviously, the retarder also manifests itself in cold climates (e.g. 5 °C) with a different ratio.

The properties of the cementitious material can be manipulated to the point of achieving a totally opposite effect at a very early stage: this is the case with **accelerating admixtures**, another class of admixtures able to speed up the early hydration steps.¹² Their application is particularly

¹¹ Spiratos, N.; Pagè, M.; Mailvaganam, N.P.; Malhotra, V.M.; Jolicoeur, C.; Superplasticizers for concrete: fundamentals, technology and Practice; Marquis, Quebec, Canada, 2006.

¹² Rosskopf, P.; Linton, F.; Pepler, R. Effect of Various Accelerating Chemical Admixtures on Setting and Strength Development of Concrete. *J. Test. Eval.*, **1975**, *4*, 322-330.

required in the winter season when, due to low temperatures, hydration of the cement slows down initially.¹³

According to the C 1017 / 1017M-98 standard¹⁴, fluidificants can be further classified into Type I and Type II SPs: Type I SPs are defined as plasticizers and are able to give fluidity to the mix to which they are added, while Type II SPs are also defined as plasticizers and retarders as they perform a dual effect as fluidizers and agents able to prolong the setting time of cementitious systems.

The pioneer additives in modern times were by-products of cellulose obtained from organic materials, primarily lignins, contained in the recovery of industrial waste of paper firms (**Figure 3**).

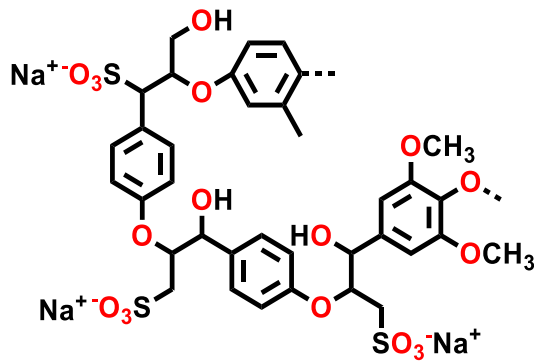


Figure 3. Lignin sulfonate SPs or LS.

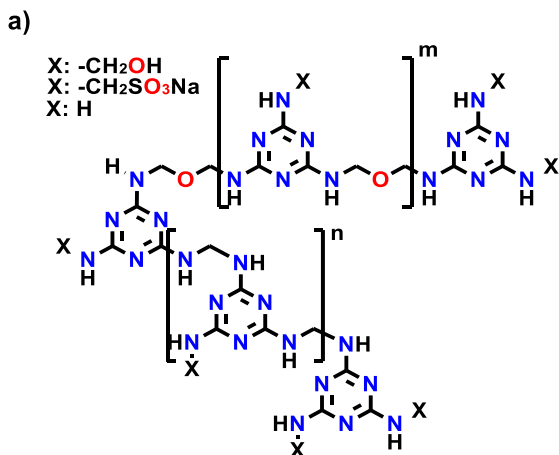
Instead, the first synthetic products were developed in Japan and in Germany ten years later, starting from raw materials obtained from

¹³ Lazzara, G. *Nanotechnologies and Nanomaterials for Diagnostic, Conservation and Restoration of Cultural Heritage*; 1st edition.; Elsevier: Cambridge, MA, 2018.

¹⁴ ASTM C1017 / C1017M-98, Standard Specification for Chemical Admixtures for Use in Producing Flowing Concrete, ASTM International, West Conshohocken, PA, 1998.

petroleum feedstocks. For almost fifty years, superplasticizers were mostly divided into two big sections of polymeric admixtures: the polyβ-naphthalene sulfonate and poly-melamine sulfonate derivatives group also labelled as SNF and SMF respectively (**Figure 4**).^{15,16}

SNF and SMF are water-soluble organic polymers bearing anionic SO_3^- groups.³ Sulfonated polymers are obtained by sulfonation of monomeric aromatic units and successive formaldehyde condensation, and following this approach, a variety of materials (other than SNF and SMF) were obtained such as sulfonated phenolic resins.



¹⁵ Mezhov, A.; Ulka, S.; Gendel, Y.; Diesendruck, C. E.; Kovler, K. The Working Mechanisms of Low Molecular Weight Polynaphthalene Sulfonate Superplasticizers. *Constr. Build. Mat.* **2020**, *240*, 117891.

¹⁶ Wang, H.; Yang, X.; Xiong, W.; Liu, X.; Zhang, Z. Synthesis and the Effects of New Melamine Superplasticizer on the Properties of Concrete. *ISRN Chemical Engineering* **2013**, *2013*, 1–6.

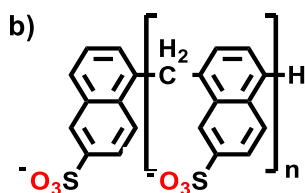


Figure 4. Chemical structure of dispersants of second generation: a) Sulfonated Naphthalene Formaldehyde condensates (SNF) and b) Sulfonated Melamine Formaldehyde condensates (SMF).

The last generation of additives is represented by the Polycarboxylate esters or PCEs¹⁷ (**Figure 5**) that attract a lot of attention because of their superior performance in cementitious systems. Indeed, if compared to SNF, they can fluidize mortars with a lower water/cement ratio and with their lower dosages and enhance the slump retention ability.^{18,19}

¹⁷ T. Hirata, Japanese Patent JP 84, 2022 (S59-018338), (1981).

¹⁸ Zhang, Y.; Kong, X. Correlations of the dispersing capability of NSF and PCE types of superplasticizer and their impacts on cement hydration with the adsorption in fresh cement pastes. *Cem. Concr. Res.* **2015**, *69*, 1–9.

¹⁹ Uchikawa, H.; Hanehara, S.; Sawaki, D. The role of steric repulsive force in the dispersion of cement particles in fresh paste prepared with organic admixture. *Cem. Concr. Res.* **1997**, *27*, 37–50.

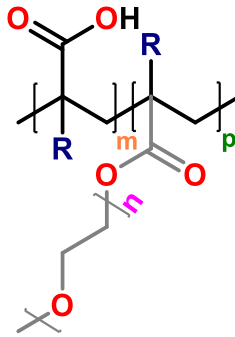


Figure 5. The chemical structure of Polycarboxylate ether/ester superplasticizers (PCE).

The action mechanism of superplasticizers is linked to their chemical nature: the anionic charged groups of SNF and SMF cause the adsorption of superplasticizer molecules on the hydrating surface of the grains (**Figure 6**).

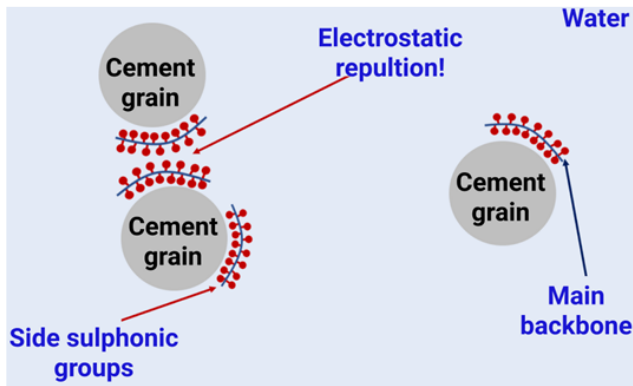


Figure 6. Schematic illustration of the mechanism of action of SPs: a) electrostatic effect of charged polymers such as the SNF/SMF superplasticizers.

This effect leads to the formation of a double ionic layer of positively and negatively charged ions that conveys to the grains surface a final negative potential; that causes the break-up of the cementitious agglomerates thus liberating the trapped water among the neighbouring particles to induce the cement flocculation phenomenon, as described by the Ottewill–Walker equation.^{20,21}

The mode of action of PCEs is slightly different in comparison with the one observed with the second-generation additives. This aspect is due to the peculiar brush structure of PCEs: indeed, they are composed by a main backbone bearing anionic groups that is fundamental to neutralize the surface charges on the cement particles and by collateral side chains that induce short-range repulsive forces between cement grains (**Figure 7**).^{22,23,24,25}

²⁰ Hirata, T.; Ye, J.; Branicio, P.; Zheng, J.; Lange, A.; Plank, J.; Sullivan, M. Adsorbed Conformations of PCE Superplasticizers in Cement Pore Solution Unraveled by Molecular Dynamics Simulations. *Sci. Rep.* **2017**, *7*, No. 16599.

²¹ Ottewill, R. H.; Walker, T. S. The influence of non-ionic surface-active agents on the stability of polystyrene latex dispersions. *Kolloid-Z.u.Z.Polymer* **1968**, *227*, 108–116.

²² Yoshioka, K.; Sakai, E.; Daimon, M.; Kitahara, A. a, A. Role of steric hindrance in the performance of superplasticizers for concrete. *J. Am. Ceram. Soc.* **2005**, *80*, 2667–2671.

²³ Nkinamubanzi, P.-C.; Mantellato, S.; Flatt, R. J. Superplasticizers in Practice. In *Science and Technology of Concrete Admixtures*; Elsevier; 2016, 353–377.

²⁴ Spiratos, N.; Page, M.; Mailvaganam, N. P.; Malhotra, V. M.; Jolicoeur, C. *Superplasticizers for Concrete: Fundamentals, Technology, and Practice*; Supplementary Cementing Materials for Sustainable Development: Ottawa, 2003.

²⁵ Plank, J.; Sakai, E.; Miao, C. W.; Yu, C.; Hong, J. X. Chemical admixtures - Chemistry, applications and their impact on concrete microstructure and durability. *Cem. Concr. Res.* **2015**, *78*, 81–99.

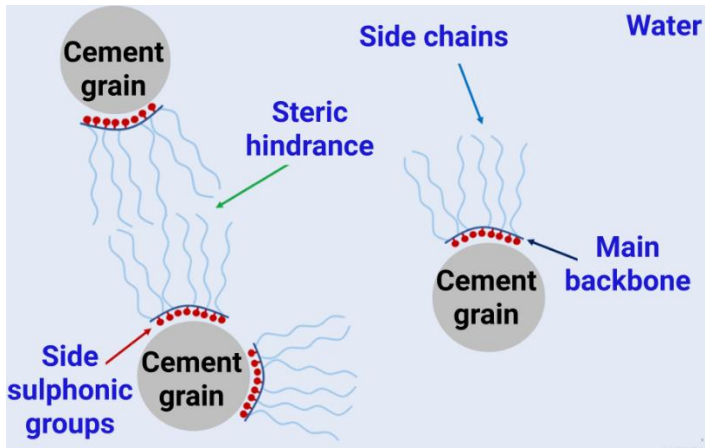


Figure 7. Cartoon of the mechanism of action of third generation SPs where it is observed the combination of charging repulsion effect with the steric hindrance of the PCEs.

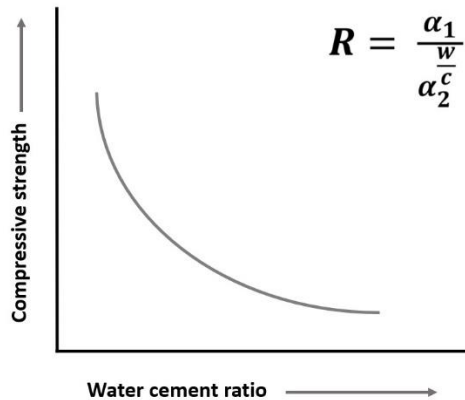
The type and the molecular weight of the additives can differently affect the performance of the SPs: the repulsion effect of the side chains of the acrylate-type polymers such as the PCEs, is very dominant in comparison with the electrostatic phenomenon, that plays a key role for the sulfonated products (SNF/SMF); in addition to this, the performance can be strongly influenced by the Mw.

1.4 Abram's law for cement mortars

The quality of the cement matrix that surrounds the skeleton components of concrete (such as sand, gravel or crushed stones) strongly influences the final properties of the hardened products such as mechanical strength, durability, permeability.

A dense and compact cement paste is able to ensure a high-quality conglomerate only if the starting aggregates are compact, thick and mechanically resistant and if the capillary porosity is very reduced.

The key parameters to reduce the capillary porosity and consequently to increase the mechanical resistance to compression are the degree of hydration of the cement and the water/cement ratio. The theory which allows to correlate the mechanical strength properties of concrete, assumed as a measure of concrete quality, and the quantity of water inside the cementitious mix was proposed in 1918, with the studies of the American researcher Duff Abrams²⁶ proposed in **Figure 8**:



²⁶ Rao, G.A. Generalization of Abrams' law for cement mortars. *Cem. Concr. Res.* **2001**, *31*, 495-502.

R = Average compressive strength (MPa);

α_1 ; α_2 = constants related to the type of employed cement powder and to the experimental conditions;

w/c = water quantity / binder quantity;

Figure 8. Abram's law.

According to this theory, in line with the increase of the compressive strength, as the w/c ratio decreases, there are improvements in other mechanical properties (e.g. flexural and tensile strength, elastic modulus), enhancements in durability and reductions in water permeability.

There is a reason why the reduction of the water content of the mix and therefore of the w/c ratio with the same cement dosage turns into a beneficial effect on the cement matrix and consequently on the properties of the whole mix. In the **Figure 9** it is represented the schematic situation of two adjacent cement granules under two different conditions for the w/c ratio (a and b). The greater amount of water results in a greater distance between the cement granules and therefore, at the same degree of hydration for example at the mixing time and in the middle of the hydration process, the fibrous crystals of hydrated cement appear less intertwined.

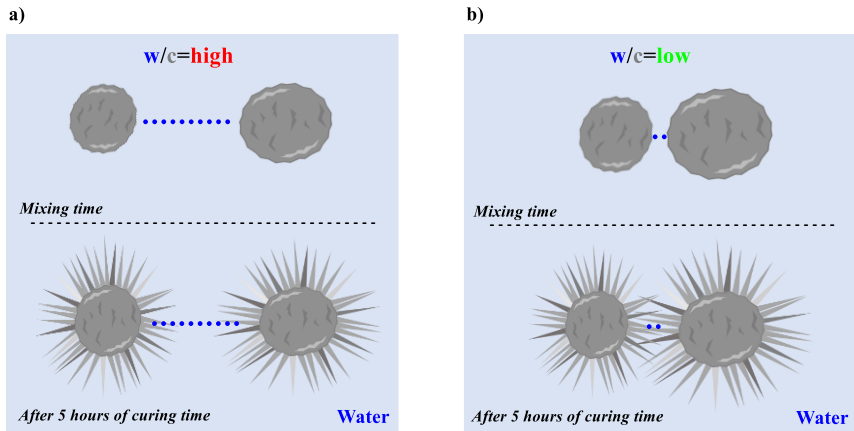


Figure 9. Schematic example of the influence of w/c ratio effect on the morphology of a cement paste with the same curing time.

The influence of w/c ratio on the morphology of a cement paste with the same curing time (5 h) can be investigated and in the literature, it is widely known that the microstructure of pastes with the lowest w/c ratio appear much less porous, more densified, thus less permeable, and more mechanically resistant due to the lower volume content of capillary pores. As a result of the reduction of the w/c ratio within a certain range (e.g. 0.80-0.30) and the microstructural modification of the cement matrix, the quality of the concrete with the same degree of hydration improves (i.e. cement type, curing time and temperature).²⁷

²⁷ Collepari, M. *Gli additivi per calcestruzzo: come funzionano e come si impiegano*; Tintoretto: Villorba (TV), 2012.

1.5 Industrial methods to investigate the admixtures effect on building materials

Slump and setting tests are normalized simple and quick industrial methods used for the investigation of the effect of SPs on matrices of different nature. Indeed, in order to implement newly synthesised chemicals on the market, they must be tested according to specific high-quality standards. Specifications and instructions of the use of these tests are covered with UNI EN 12350-2, respectively in the paragraph 4.3.3 and 4.4.2.

1.5.1 Slump test. In particular, the **Slump/flow table test** has been one of the most widely used methods for determining the consistency and workability of cementitious paste, since 1922 because of the numerous benefits associated with its use. Due to its simplicity and practicality, this investigation gives information that is very important for analysing the effect of SPs in real time on mortars and concrete. It involves the use of a specific normalized equipment and specific experimental conditions.

The slump test determines the workability of freshly made cementitious systems before their setting. The test is carried out mixing cement powder, water, sand and additive into a mortar mixer (**Figure 10 1a**) and filling the metallic mould, the Abram's cone with the obtained paste (**Figure 10 1b**). The cone is vertically raised, the binder is assessed with 15 shots (**Figure 10 1c**) and then the diameter values in millimetres

(called “*spread*”) of the pastes are measured three times after 4, 30, 60, 90 and 120 minutes (**Figure 10**) and an average value is registered.

The slump value is a parameter used to indicate the workability of the cement mix that it is influenced by several factors:

- Chemical properties of the materials (particle size distribution, moisture content, temperature of the cementitious materials etc.);
- Dosage and nature of additives;
- Air content of the cement;
- Water content of the cement paste;
- Time elapsed from mixing the cement to the time of the test;
- Cement sampling and equipment used for mixing and transport.

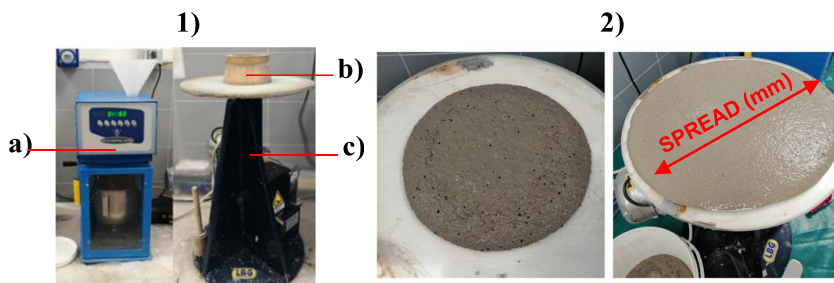


Figure 10. 1) Workability tests apparatus: a) mortar mixer, b) Abram's cone (UNI EN 12350-2) and c) automatic lifter; 2) Spread diameter

measurements of experimental samples with different fluidificat behaviour.

According to the UNI EN 206-2006 and UNI 11104:2004 standards, 5 consistency classes are identified on the basis of the slump test, as shown in **Table 3**.

Table 3. Consistency classes of cement

Class	Slump [mm]
S1 Dry (Kerb backing, dry fill and sloping slabs etc.)	10 – 40
S2 Standard (Foundations, Slabs and other general structures)	50 – 90
S3 Wet (Foundations, slabs, Pumping concrete)	100 – 150
S4 Very Wet (Foundations, slabs, Pumping and Piling concretes)	160-210
S5 Self Levelling (Foundations, slabs, Pumping and Piling concretes)	≥220

1.5.2 Vicat test. The Vicat test defines the time (in minutes) when the cement paste loses its fluidity and turns into a rigid matrix: this is the so-called “setting time”. The setting time apparatus is reported in **Figure 11** and it is composed by a ruler (**Figure 11 a**), a needle (**Figure 11 b**) and a

mould (**Figure 11 c**). The Vicat Needle Test^{28,29} is one of the most employed methods to investigate the changing into the properties of cement matrixes at an early stage in civil engineering. The Vicat needle apparatus consists of a moveable rod with a needle at one end. The rod slides through a frame, where an indicator on the rod moves over a scale mounted to the frame. A specimen of fresh cementitious paste is placed in a conical ring below the frame. The needle is placed on the cement paste specimen and allowed to settle under its own weight. The depth of penetration is recorded from the scale. Each subsequent reading is taken at a different location on the paste specimen. The test is completed when the distance between the needle and the base-plate is 6 ± 3 mm.

²⁸ Trtnik, G.; Turk, G.; Kavčič, F.; Bosiljkov, V. B. Possibilities of using the ultrasonic wave transmission method to estimate initial setting time of cement paste. *Cem. Concr. Res.* **2008**, *38*, 1336–1342.

²⁹ Zhang, M. H.; Sisomphon, K.; Ng, T. S.; Sun, D. J. Effect of superplasticizers on workability retention and initial setting time of cement pastes. *Constr. Build. Mater.* **2010**, *24*, 1700–1707.

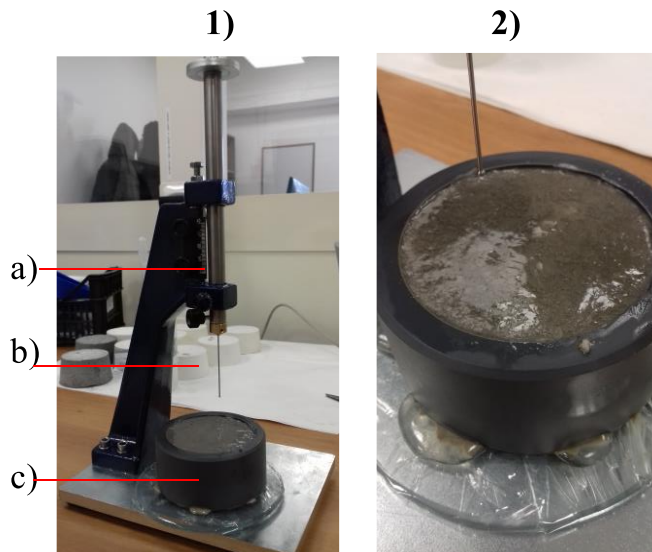


Figure 11. Setting time system: a) rule, b) needle and c) mould.

The setting time coincides with the hydration of C_3S and C_3A , which react with water with different kinetics. Literature studies have shown that C_3S controls the setting time of the cement paste and reacts quickly. The factors influencing the setting time are the temperature of the site, the water/cement ratio and the presence of accelerating additives. In particular, high temperatures, high content of water inside the cementitious pastes and retardant admixtures delay the workability retention.

Chapter 2 - Research aims and thesis outline

Due to the continuous demand for new additives in the field of materials engineering, many efforts have been focused on the design of new high-performance admixtures for concrete applications. In this PhD thesis project, we propose to carry out the synthesis and the development of new additives, with high industrial performance.

In the **chapter 3** we will describe the synthesis of water-soluble macrocyclic derivatives named resorcin[4]arenes and pyrogallol[4]arenes,^{1,2} in order to design new unconventional plasticizers with tailored properties to fit the needed features of SPs. In particular, we will report the synthesis of water soluble resorcin[4]arene derivatives bearing sulfonate groups and the analysis of their dispersing properties in cement based mortars. The design strategy of water-soluble resorcin[4]arene as SPs is based on the idea to exploit both, the presence of negatively charged groups (sulfonate), and the steric hindrance caused by the macrocycle. We envisioned that the anionic chains could anchor to the cement particles by electrostatic interactions, while the steric effects of the macrocycle backbone could increase the fluidity of the final concrete as shown in **Figure 12**.

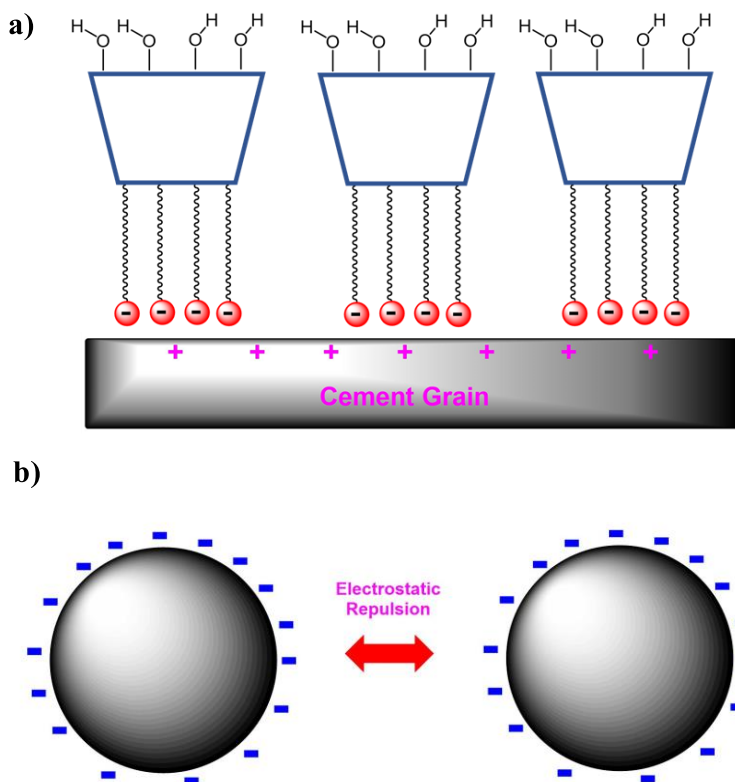


Figure 12. Sketch of the fluidizing mechanism envisioned for the sulfonate-macrocycles.^{1,2}

However, the construction materials engineering has evolved significantly over the last few years, especially for the concerns of the ecological aspects related to the use of SPs nowadays available on the market. Therefore, the need of eco-friendly and high-performing additives has increasingly emerged in the field of construction materials and for this reason, in the **chapter 4** we will report the design of green

admixtures based on eco-sustainable cyclodextrin-based pseudorotaxanes obtained by host-guest interaction.³

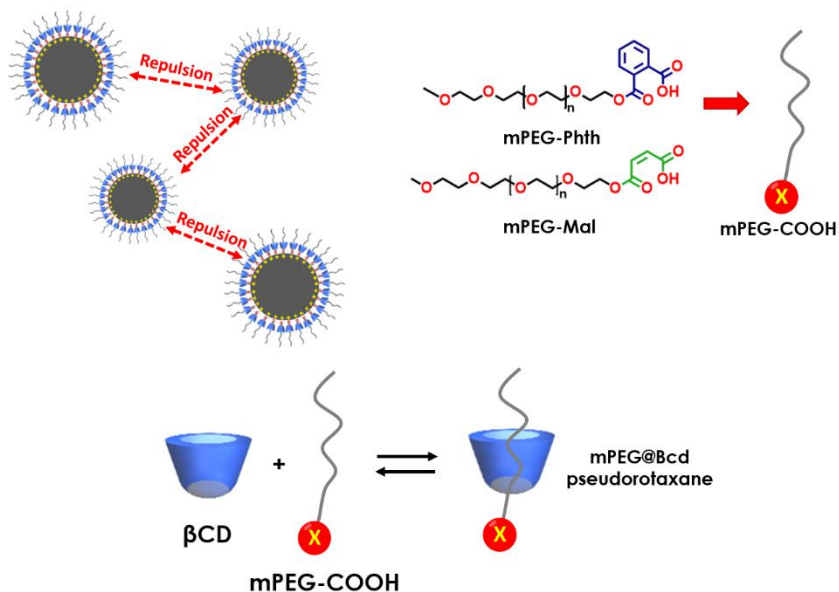


Figure 13. The dispersing mechanism between cement particles envisioned after absorption of mPEG-COOH@ β -CD pseudorotaxanes on the cement particles.

As shown in the **Figure 13**, these pseudorotaxanes will be produced by complexation of β -cyclodextrin with PEG-based polymeric chains bearing carboxylic functions. Their formation occurs by a simple self-assembly equilibrium in which the linear PEG derivative (axle in **Figure 13 b**) is threaded through the cyclodextrin (wheel) upon simple mixing in

aqueous solvent at room temperature and usually the process does not involve any work-up procedure. Thus, an interpenetrated architecture (pseudorotaxane in **Figure 13 c**) is formed in which the liner molecule (axle) is threaded through the macrocycle derivative (wheel) driven by intermolecular secondary interactions between them. Clearly, these are ideal experimental conditions for practical and industrial applications. In detail, we envisioned that the carboxylic functions of the axle could act as anchors to adsorb on the cement surface (**Figure 13 a**) through coordination with metal centers, while the pseudorotaxane architecture constituted by β -CD wheel threaded along the PEG axle would protrude from the cement surface to generate steric hindrance. The scope is to investigate how the presence of this polymeric species within the cyclodextrin could influence the properties of the cement paste and thus leading to the design of eco-sustainable, high-performance superplasticisers.³

Lastly, the enquiries will be focused on the research and development of new carboxymethylcellulose-based SPs as innovative superplasticizers for mortar systems (**Chapter 5**).⁴ These studies were carried on during the research period at the *Chair of Construction Chemistry and Polymeric Materials ChemPoWer under the supervision of the Prof. Andrea Osburg, Deputy Head of the F. A. Finger Institute for Building Materials Engineering at Bauhaus-Universität Weimar*. In detail, the abroad research period was mainly concentrated on the investigation about carboxymethylcellulose. This complex biopolymer is widely known as a thickening agent, so its modification was very challenging. To achieve the desired goal, we checked different hydrolysis times and temperatures

of the reactions to explore different experimental conditions. The hydrolyzed carboxymethylcellulose-based material will be functionalized with sulfoethyl groups that will act as anchoring functions to improve the interaction with the cementitious grains (**Figure 14**).

Finally, in order to have a holistic view on their effect on mortars, a complete investigation of final settled specimens properties will be reported into the **Chapter 5**.

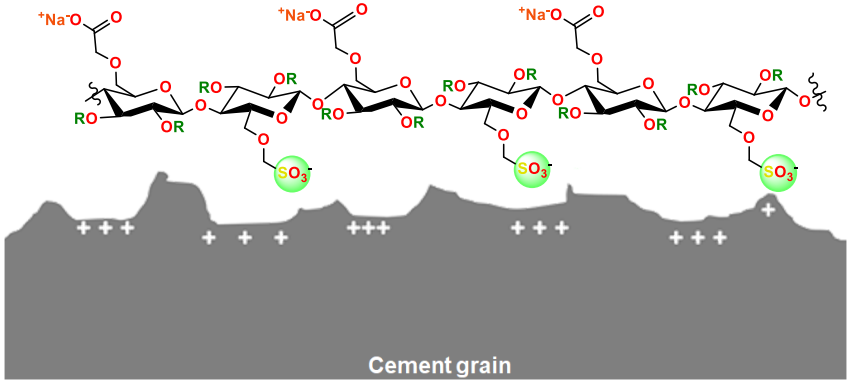


Figure 14. Mode of action envisioned for the adsorption of sulfoethyl-carboxymethylcellulose on the cement grain.⁴

Chapter 3 - Dispersing and Retarding Properties of Water-Soluble Tetrasulfonate Resorcin[4]arene and Pyrogallol[4]arene Macrocycles in Cement-based Mortar

3.1 General overview

Pyrogallol[4]arene and resorcin[4]arene are macrocycles (**Figure 15**),^{30, 31, 32, 33} constituted by 1,2,3-trihydroxybenzene and 1,3-dihydroxybenzene aromatic units, respectively, that are bridged at meta positions by –CHR– groups.^{34,35,36,37}

³⁰ Cram, D. J.; Cram, J. M. Container Molecules and Their Guests, Monographs in Supramolecular Chemistry; Stoddart, J. F., Ed.; Royal Society of Chemistry: Cambridge, 1994.

³¹ Della Sala, P.; Gaeta, C.; Navarra, W.; Talotta, C.; De Rosa, M.; Brancatelli, G.; Geremia, S.; Capitelli, F.; Neri, P. Improved Synthesis of Larger Resorcinarenes. *J. Org. Chem.* **2016**, *81*, 5726–5731.

³² Gaeta, C.; Della Sala, P.; Talotta, C.; De Rosa, M.; Soriente, A.; Brancatelli, G.; Geremia, S.; Neri, P. A Tetrasulfate-Resorcin[6]Arene Cavitand as the Host for Organic Ammonium Guests. *Org. Chem. Front.* **2016**, *3*, 1276–1280.

³³ Brancatelli, G.; Geremia, S.; Gaeta, C.; Della Sala, P.; Talotta, C.; De Rosa, M.; Neri, P. Solid-State Assembly of a Resorcin[6]Arene in Twin Molecular Capsules. *Cryst. Eng. Comm.* **2016**, *18*, 5045–5049.

³⁴ Timmerman, P.; Verboom, W.; Reinhoudt, D. N. Resorcinarenes. *Tetrahedron* **1996**, *52*, 2663–2704.

³⁵ Aoyama, Y.; Tanaka, Y.; Sugahara, S. Molecular Recognition. 5. Molecular Recognition of Sugars via Hydrogen-Bonding Interaction with a Synthetic Polyhydroxy Macrocyclic. *J. Am. Chem. Soc.* **1989**, *111*, 5397–5404.

³⁶ Avram, L.; Cohen, Y. Self-Recognition, Structure, Stability, and Guest Affinity of Pyrogallol[4]Arene and Resorcin[4]Arene Capsules in Solution. *J. Am. Chem. Soc.* **2004**, *126*, 11556–11563.

³⁷ Beyeh, N. K.; Kogej, M.; Åhman, A.; Rissanen, K.; Schalley, C. A. Flying Capsules: Mass Spectrometric Detection of Pyrogallarene and Resorcinarene Hexamers. *Angew. Chem. Int. Ed.* **2006**, *45*, 5214–5218.

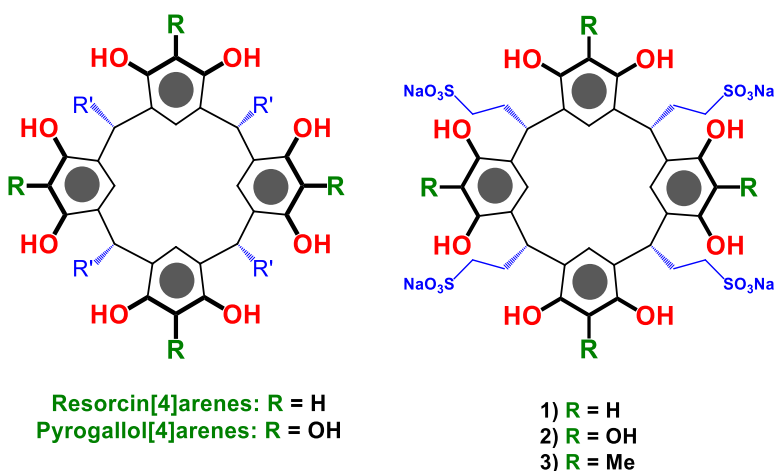


Figure 15. Chemical drawing of native resorcin[4]arenes, pyrogallol[4]arenes and their sulfonate derivatives **1–3** synthesized in this work.^{1,2}

In the resorcinarene and pyrogallolarene nomenclature we distinguish the upper rim (or exo rim) bearing OH functions from the lower rim (or endo rim) (**Figure 15**). The structure of these compounds was studied for the first time in 1940 by Niederl³⁸ and Vogel. They analysed the molecular weight of the species produced by the condensation reaction between different aldehydes and resorcinol with a ratio of 1:1, and proposed the

³⁸ Niederl, J. B.; Vogel, H. J.; Aldehyde—Resorcinol Condensations. *J. Am. Chem. Soc.* **1940**, *62*, 2512-2514.

tetrameric cyclic structure of the resorcin[4]arene. Their results were later confirmed by X-ray crystal structure analysis.³⁹

Resorcin[n]arenes and pyrogallol[n]arene macrocycles have gained a pivotal role in several fields of supramolecular chemistry such as molecular recognition,⁴⁰ molecular switches,⁴¹ porous materials,⁴² supramolecular catalysis,⁴⁴ and nanoscale architectures.^{46,47} One key feature of these macrocycles is their synthetic and conformational versatility, indeed it is possible to change the nature of the monomeric unit, and of the aldehyde that, in turn, determines the nature of the substituents on the methine bridges.

³⁹ Erdtman, H.; Högberg, S.; Abrahamsson, S.; Nilsson, B.; Cyclooligomeric phenol-aldehyde condensation products I. *Tetrahedron Lett.* **1968**, *9*, 1679-1682.

⁴⁰ He, Q.; Vargas-Zuniga, G. I.; Kim, S. H.; Kim, S. K.; Sessler, J. L. Macrocycles as Ion Pair Receptors. *Chem. Rev.* **2019**, *119*, 9753-9835.

⁴¹ Sansone, F.; Baldini, L.; Casnati, A.; Ungaro, R. Calixarenes: from biomimetic receptors to multivalent ligands for biomolecular recognition. *New J. Chem.* **2010**, *34*, 2715-2728.

⁴² Shetty, D.; Skorjanc, T.; Raya, J.; Sharma, S. K.; Jahovic, I.; Polychronopoulou, K.; Asfari, Z.; Han, D. S.; Dewage, S.; Olsen, J. C.; Jagannathan, R.; Kirmizialtin, S.; Trabolsi, A. Calix[4]arene-Based Porous Organic Nanosheets. *ACS Appl. Mater. Interfaces* **2018**, *10*, 17359-17365.

⁴³ Bew, S. P.; Burrows, A. D.; Duren, T.; Mahon, M. F.; Moghadam, P. Z.; Sebestyen, V. M.; Thurston, S. Calix[4]arene-based metal-organic frameworks: towards hierarchically porous materials. *Chem. Commun.* **2012**, *48*, 4824-4826.

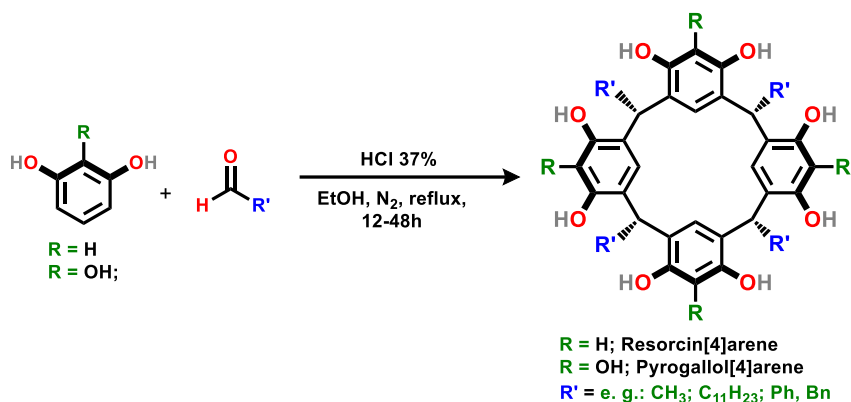
⁴⁴ Zhang, Q.; Catti, L.; Tiefenbacher, K. Catalysis inside the Hexameric Resorcinarene Capsule. *Acc. Chem. Res.* **2018**, *51*, 2107-2114.

⁴⁵ La Manna, P.; De Rosa, M.; Talotta, C.; Rescifina, A.; Floresta, G.; Soriente, A.; Gaeta, C.; Neri, P. Synergic Interplay Between Halogen Bonding and Hydrogen Bonding in the Activation of a Neutral Substrate in a Nanoconfined Space. *Angew. Chem., Int. Ed.* **2020**, *59*, 811-818.

⁴⁶ Shi, T.H.; Tong, S.; Wang, M.-X. Construction of Hydrocarbon Nanobelts. *Angew. Chem., Int. Ed.* **2020**, *59*, 7700-7705.

⁴⁷ Shi, T.H.; Guo, Q.H.; Tong, S.; Wang, M.X. Toward the Synthesis of a Highly Strained Hydrocarbon Belt. *J. Am. Chem. Soc.* **2020**, *142*, 4576-4580.

A review recently reported by Coleman and co-workers⁴⁸ highlighted some very interesting industrial applications of these macrocycles in the biopharmaceutical field, where they were used for their capability of interacting with biomolecules such as peptides, proteins, lipids.⁴⁸ The molecular recognition properties of these compounds were exploited for the synthesis of molecular traps, for the sensing of hazardous compounds and for sequestering environmental pollutants.^{49,50,51}



Scheme 1. Generical strategy for the synthesis of resorcinarenes/pyrogallarenes.^{52,53}

⁴⁸ Da Silva, E.; Lazar, A. N.; Coleman, A. W. Biopharmaceutical Applications of Calixarenes. *J Drug Deliv. Sci. Technol.* **2004**, *14*, 3–20.

⁴⁹ Kumar, S.; Chawla, S.; Zou, M. C. Calixarenes Based Materials for Gas Sensing Applications: A Review. *J Incl. Phenom. Macrocycl. Chem.* **2017**, *88*, 129–158.

⁵⁰ Shimojo, K.; Goto, M. Solvent Extraction and Stripping of Silver Ions in Room-Temperature Ionic Liquids Containing Calixarenes. *Anal. Chem.* **2004**, *76*, 5039–5044.

⁵¹ Mouradzadegun, A.; Elahi, S.; Abadast, F. Synthesis of a 3D-Network Polymer Supported Bronsted Acid Ionic Liquid Based on Calix[4]Resorcinarene via Two Post-Functionalization Steps: A Highly Efficient and Recyclable Acid Catalyst for the Preparation of Symmetrical Bisamides. *RSC Adv.* **2014**, *4*, 31239–31248.

The resorcin[4]arene and pyrogallol[4]arene macrocycles are synthesized through the acid-catalyzed condensation of resorcinol⁵² or pyrogallol⁵³, respectively, with aromatic or aliphatic aldehydes stirred under reflux in ethanol (**Scheme 1**).

A convenient synthesis of the resorcin[4]arene (**Scheme 1**) was proposed in literature by Donald J. Cram and co-workers, who described the new resorcinol-based macrocycles by a detailed solid-state study.⁵² Some years later, Mattay and co-workers⁵³ reported the synthesis of the pyrogallol[4]arene (**Scheme 1**), and showed that these macrocycles self-assembled into supramolecular systems as confirmed by ESI-MS spectra.⁵³

As previously reported by X-ray and NMR studies, resorcin[4]arene and pyrogallol[4]arene macrocycles adopt a three-dimensional structure that remind a calix (**Figure 16**) in which the OH groups at the upper rim form a belt of intramolecular H-bonds.

⁵² Tunstad, L. M.; Tucker, J. A.; Dalcanale, E.; Weiser, J.; Bryant, J. A.; Sherman, J. C.; Helgeson, R. C.; Knobler, C. B.; Cram, D. J. Host-guest complexation. 48. Octol building blocks for cavitands and carcerands. *J. Org. Chem.* **1989**, *54*, 1305–1312.

⁵³ Gerkenmeier, T.; Iwanek, W.; Agena, C.; Frohlich, R.; Kotila, S.; Näther, C.; Mattay, J. Self-Assembly of 2,8,14,20-Tetraisobutyl-5,11,17,23-tetrahydroxyresorc[4]arene. *Eur. J. Org. Chem.*, **1999**, 2257–2262.

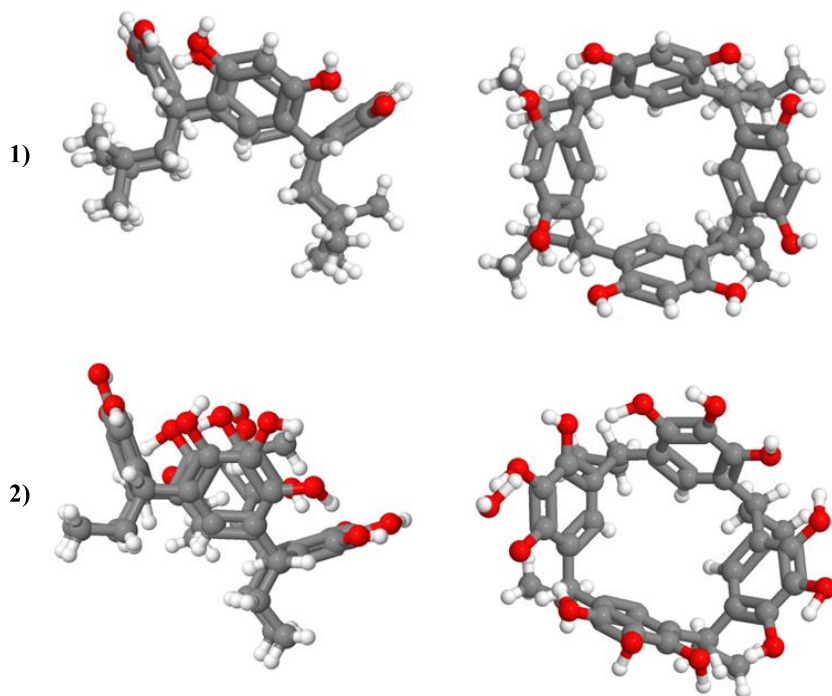


Figure 16. X-ray structures of resorcin[*n*]arene and pyrogallol[4]arene derivatives: 1) CSD Entry: QOHFEZ and 2) CSD Entry: ACAWUW.

The upper rim of the resorcin[4]arenes and pyrogallol[4]arenes (**Figure 15**) are adorned with 8 and 12 polar OH groups, respectively, while each methine bridge bears a substituent whose nature depends on the structure of the aldehyde used during the initial synthesis of the macrocycle (see **Scheme 1**). At this regards Kobayashi and co-workers⁵⁴ reported the

⁵⁴ Kobayashi, K.; Asakawa, Y.; Kato, Y.; Aoyama, Y. Complexation of Hydrophobic Sugars and Nucleosides in Water with Tetrasulfonate Derivatives of Resorcinol Cyclic

synthesis of water-soluble resorcin[4]arene, pyrogallolarene and methylresorcin[4]arene derivative **1**, **2** and **3** (**Scheme 2**) bearing -CH₂CH₂SO₃⁻ groups on the bridged moiety.

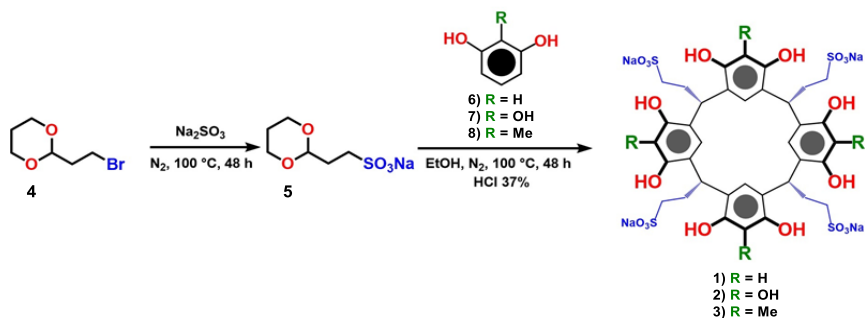
These macrocycles **1** and **2** can be considered as ideal candidates for applications as SPs because they show high solubility in water due to the presence of sulfonate groups.⁵⁴

In contrast to sulfonate aromatic polymers which are widely used as SPs, no data have been reported on the dispersing capacities of sulfonate - macrocyclic derivatives until now.

In addition, probably the presence of polar hydrophilic OH groups at the upper rim of **1**, **2** and **3** somehow affect their dispersing abilities. Prompted by these considerations we have synthesized macrocycles **1**, **2** and **3**² and studied their properties as SPs additive.

3.2 Synthesis and characterization of resorcin[4]arene, pyrogallol[4]arene and methyl-resorcinarene tetrasulfonated macrocycles

Tetramer Having a Polyhydroxy Aromatic Cavity: Importance of Guest-Host CH- π Interaction. *J. Am. Chem. Soc.* **1992**, *114*, 10307–10313.

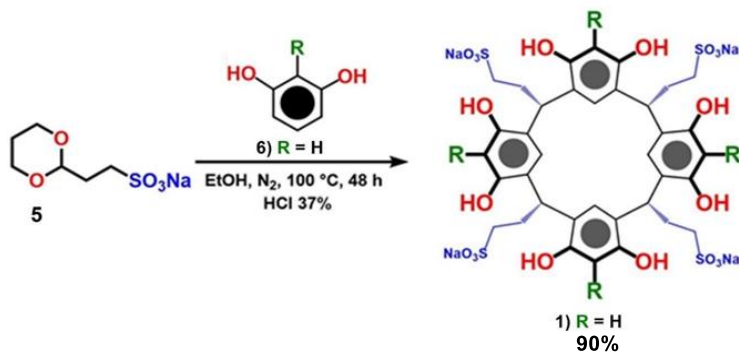


Scheme 2. Synthesis of derivatives **1**, **2** and **3**.⁵⁴

Resorcin[4]arene derivatives have a hydrophobic cavity that makes them poorly water soluble. In view of their chemical nature, a substituent bearing a sulfonate group was anchored on the methine bridges of all the three macrocycles **1**, **2** and **3** with the aim to increase their solubility in an aqueous environment.⁵⁴ With the aim to obtain the protected sulfonated aldehyde **5**, the derivative **4** was added to an aqueous solution of sodium sulphite and the two-phase system was refluxed under nitrogen atmosphere for 48 hours. The organic phase was separated, while the aqueous phase containing the key precursor **5** was collected and added to the ethanolic solution of the aromatic monomer **6**, **7** or **8** in the presence of HCl. The resulting mixture was stirred under reflux,^{1,2} following a modified procedure of the one reported by Kobayashi's group⁵⁴ (**Scheme 2**). The solution was refluxed for 48 h, and finally, the products **1**, **2** and **3** were collected by filtration, washed with methanol, and dried in vacuo in 90 %, 92 % and 80 % of yield, respectively.

The formation of the desired compounds was investigated through comparison of the ^1H NMR and ^{13}C NMR spectra with those reported in literature⁵⁴ and finally confirmed by mass spectra analysis. Moreover, DFT-optimized structures displayed that the macrocycles **1**, **2** and **3** were able to adopt a bowl-shaped 3D structure stabilized through H-bonding intramolecular interactions. FT-IR spectra and TGA/DTA analysis completed the characterization of the synthesized derivatives.

3.2.1. Synthesis and characterization of the derivative 1



Scheme 3. Synthesis of the derivative **1**.

The ^1H NMR spectrum of the derivative **1** is shown in **Figure 17**. The characteristic signals that confirmed the formation of the desired product are the triplets at 3.06 and 4.65 ppm, attributable to the macrocycle- $\text{CH}_2\text{CH}_2\text{SO}_3^-$ groups on the bridges.

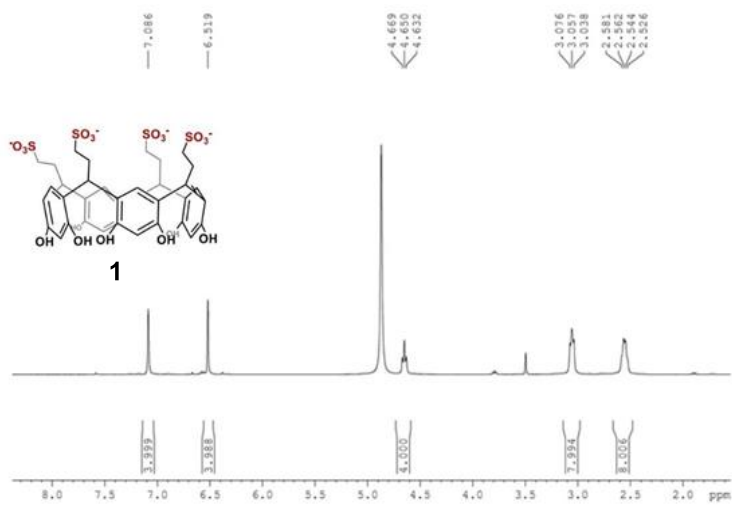


Figure 17. ^1H NMR (600 MHz, D_2O , 298 K) of the derivative **1**.

^{13}C NMR spectrum (**Figure 18**) confirmed the structure of **1** thanks to the presence of a signal at 29.65 ppm attributable to the methyne bridge and at 50.03 ppm attributable to the CH_2SO_3^- group.

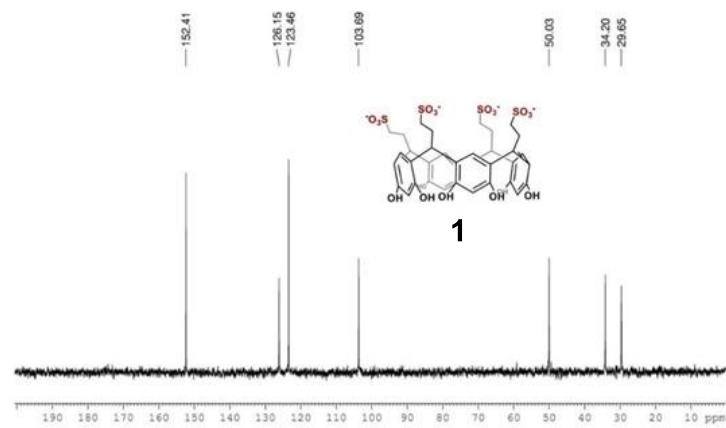


Figure 18. ^{13}C NMR (150 MHz, D_2O , 298 K) of the derivative **1**.

FT ICR HR MS in negative ion mode was reported in **Figure 19** and was in accord with the molecular mass of **1**, in fact the mass spectrum showed the presence of two ion peaks at m/z 229.0177 and 481.0255 attributable at $[\text{M}-4\text{H}]^4$ and $[\text{M}-2\text{H}+2\text{Na}]^2$ respectively.

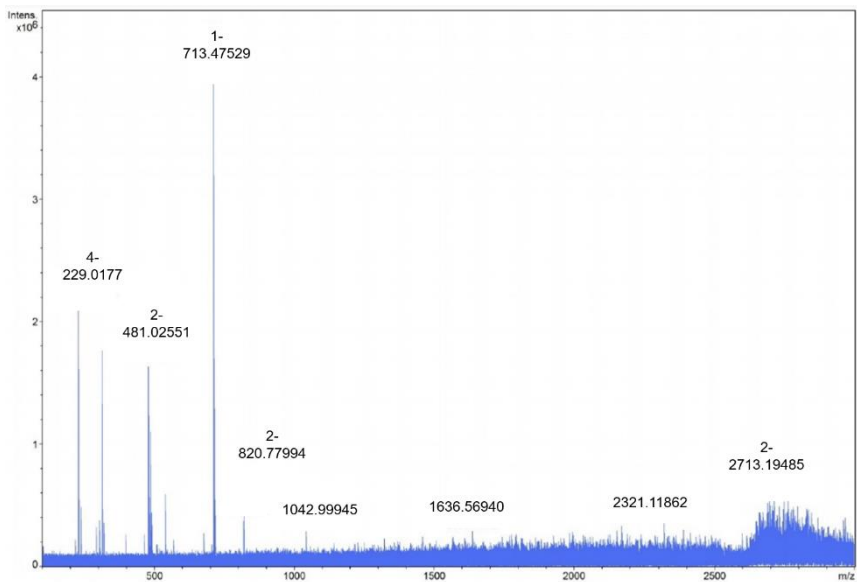


Figure 19. Negative-ion mode mass spectrum of the derivative **1**.

Close inspection of the FT-IR spectrum shown in **Figure 20** shows an intense band at 3425 cm^{-1} corresponding to the $-\text{OH}$ stretching groups, while at 1350 cm^{-1} cs. are present the bands attributable to the stretching of the $-\text{S}=\text{O}$ group.

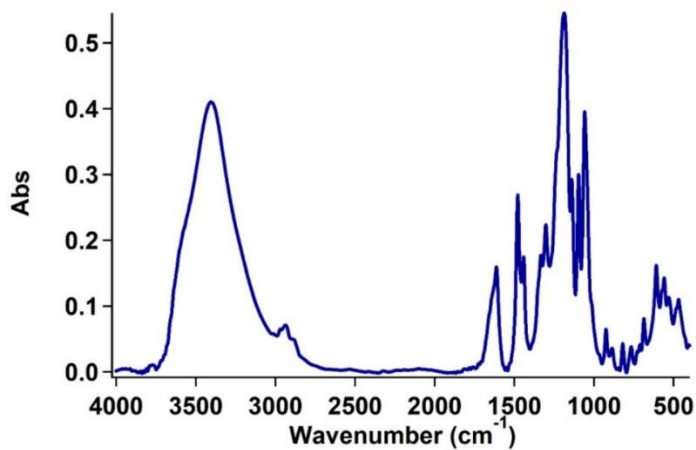


Figure 20. FT IR spectrum of derivative **1**.

In **Figure 21** it is shown the thermogravimetric analysis (TGA) of derivative **1**. The measurement was carried out in the temperature range 25 - 900 °C in the reactive atmosphere. The TGA analysis shows the presence of four degradation events. The first event, at 25-100 °C is attributable to the loss of water and solvent residues. The second event occurs at 225 °C, whereas the third degradation event starts at a temperature of about 330 °C and also extends over a hundred degrees. The last event, that theoretically is due to the degradation of the macrocycle, is centered at about 730 °C and extends from 450 °C to about 880 °C.

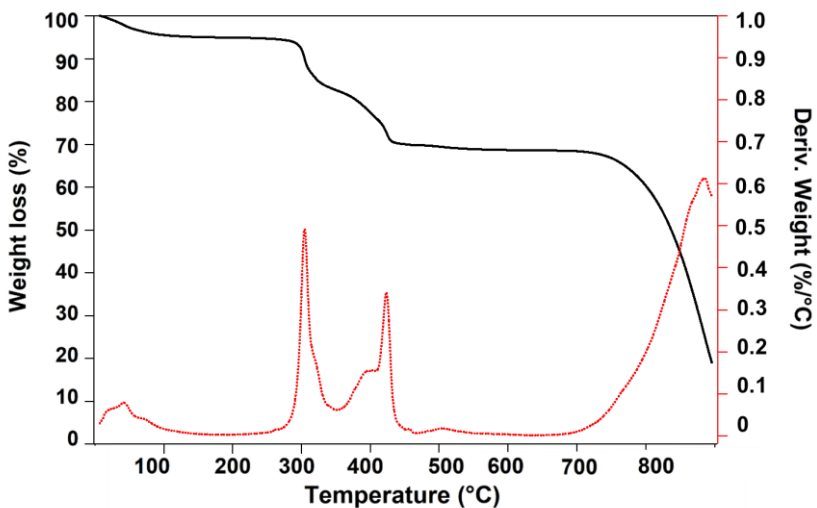


Figure 21. TGA / DTG of derivative **1**.

3.2.2 Synthesis and characterization of the derivatives **2** and **3**

Analogously to **1**, the structures of derivatives **2** and **3** were confirmed by ^1H and ^{13}C NMR spectra and the data obtained were in accord with those reported in literature.⁵⁴ The thermogravimetric profiles of **2** and **3** are reported into the experimental section.

3.3 Products testing of dispersing and retarding properties of derivatives

The dispersing and retarding abilities of the water-soluble macrocycles **1**, **2** and **3** were investigated by performing workability tests at the R&D laboratory of the BI-QEM S.P.A in Buccino (SA).

The dispersing performances of the tetrasulfonate macrocycles **1**, **2** and **3** were measured in cement mortars by *slump tests* (see section **1.5.1**).^{1,2} As reported in **Figure 22**, different dosages of macrocycles (i.e. 0.2-0.8% by weight of cement, bwoc) were tested, and their ability as flowable agents for mortar systems was ascertained at *water/cement* (w/c) ratio of 0.50. Our goal was to gain useful data regarding the relationship between the structure of macrocycles **1**, **2** and **3** (i.e. number of hydrophilic OH groups) and their dispersing performance. We start our investigation with the resorcin[4]arene **1** bearing 8 OH groups at the upper rim, and as reported in **Figure 22**, the dispersing ability of this derivative was rather limited. In fact, low spread values of 180-200 mm were measured in the range 0.2-0.8 % by weight of cement (bwoc), these values were significantly lower than those obtained with commercial plasticizers, such as Disperbeton 45 (a sulfonate naphthalene-formaldehyde plasticizer manufactured and distributed by BI-QEM SPECIALTIES S.p.A). Differently, the pyrogallol[4]arene macrocycle **2** (**Figure 22**), bearing 12 polar OH functions at the upper rim, showed a superior dispersing capability. In fact, a dosage of 0.50 % of **2** was sufficient to reach a spread value of 270 mm ca (**Figure 22**), instead derivative **1** didn't provide any dispersing properties even at high dosages (a similar behavior was displayed by **3**, that was not reported in **Figure 22**). Pyrogallol[4]arene **2** showed higher performances in terms of dispersibility in comparison with the ones observed with the

resorcin[4]arenes **1**. This phenomenon has been related to the more hydrophilic nature of **2**, due to the presence of 12 OH groups at its upper rim, that are responsible of the greater chelating effect toward the Ca^{++} ions. Therefore, the adsorption of **2** on the cement particle surfaces and the following formation of $\text{Ca}^{++}@2$ chelates lead to the creation of a thick layer all around the grain. This effect is combined to the electrostatic repulsion between the cement particles to determine the flocculation process.^{22,23,22}

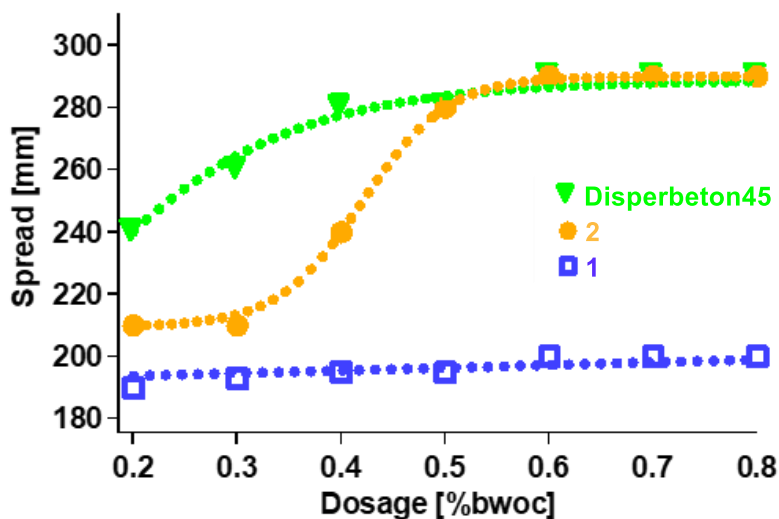


Figure 22. Slump test for the studies of the dosage-dependent effect of the synthesized macrocycles **1** and **2** on mortar spread value (bottom) and

comparison with Disperbeton 45 (commercial by BI-QEM SPECIALTIES S.p.A). The dosage-dependent effect of the derivative **3** is not reported because of its limited dispersion capability.

Once obtained these results, derivatives **1**, **2** and **3** were used for investigations on their spread retention ability on mortar (**Figure 23**). In detail, slump tests were performed over time. SPs additives can confer retention of fluidity over time to the fresh cement mortars in which they are added: consequently, a measurement of this properties allows to understand if the tested additives could be defined as a workability retainer and/or a water reducer. Thus, the spread of cement mortars (**Figure 23**) was studied with dosing the 0.5 % bwoc of macrocycle and by setting the water/cement ratio at 0.5; finally, the evolution of mortar fluidity (by slump test) was measured over time (up to 120 min).

The results reported in **Figure 23** display that the derivative **3** does not show any fluidizing property. In accordance with the data reported previously in **Figure 23**, the derivative **1** shows a very low initial spread diameter that means a poor fluidizing capability. Instead, pyrogallol[4]arene **2** shows a high initial spread value comparable to commercial plasticizers, such as Disperbeton 45 (a sulfonate naphthalene-formaldehyde plasticizer manufactured and distributed by BI-QEM SPECIALTIES SpA). Finally, in the mortar doped with the derivative **2**, the fluidity retention of the paste reduced slower than with the one doped with the commercial plasticizers.

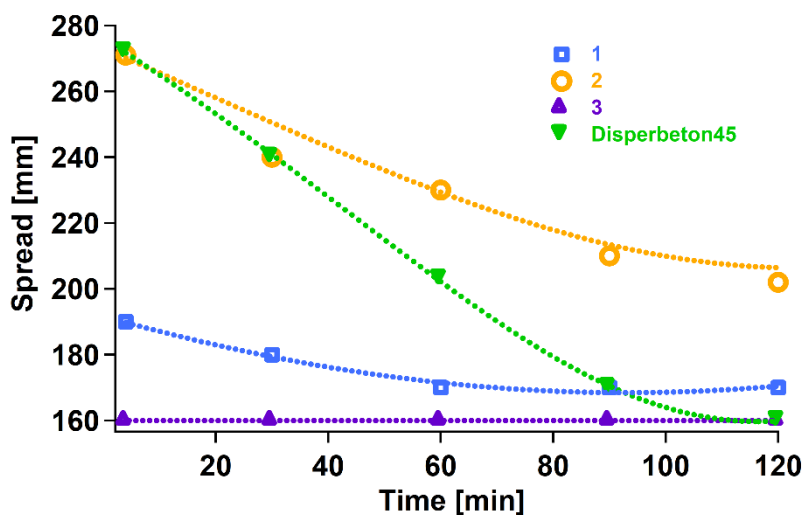


Figure 23. Monitoring of the spread value of fresh cement mortars mixed with the synthesized sulfonated macrocycles (0.5% bwoc) ($w/c = 0.5$) during time.

Data previously reported in literature⁵⁵ show that soluble sulfate salts can depress the dispersing abilities of anionic SPs such as PCEs.⁵⁵ Specifically, both sulfate anions and the anionic groups of SPs can compete for the adsorption on the cementitious surface. Even more efforts have been focused on the design of novel superplasticizers insensible to the presence of sulfate anions in recent years. Then, the sulfate anion tolerance of pyrogallol[4]arene **2** macrocycle was investigated by

⁵⁵ Ilg, M.; Plank, J. Synthesis and Properties of a Polycarboxylate Superplasticizer with a Jellyfish-Like Structure Comprising Hyperbranched Polyglycerols. *Ind. Eng. Chem. Res.* **2019**, *58*, 12913–12926.

dissolving different amounts of sodium sulfate (0.2–0.8 % bwoc) in the mortar mixture doped with **2** (0.2 %) and performing slump tests ($w/c = 0.50$). As reported in **Figure 24**, the sulfate ions slightly affect the dispersing performances of **2** because it was observed only a slight increase of the spread values after the addition of Na_2SO_4 from 0 to 0.5 % bwoc.

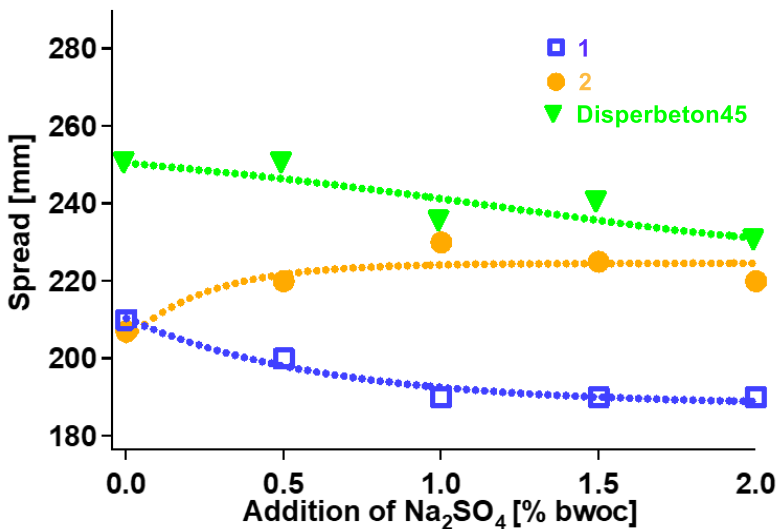


Figure 24. Investigation of the sodium sulfate effect on the dispersing performance of **2** and **1** dosed at 0.2% bwoc, in comparison to a commercial naphthalene-based plasticizer branded Disperbeton 45 at w/c of 0.5.

We envisioned that this result is due to the anionic recognition abilities of **2** which could establish H-bonding interactions with the SO_4^{2-} anions in

solutions and so by blocking with this mechanism their access to the grains surface, as represented in **Figure 25**. As highlighted in the model reported in **Figure 25 c**, the derivative **2** is adsorbed on the cement particle surface by electrostatic interactions between the anionic functions of **2** and the cations of the cementitious particles surface (**Figure 25 c**). In this way, the pyrogallolarene skeleton stretches out into the water solution and under these conditions, the upper rim of pyrogallolarene **2** can let the -OH groups to establish H-bonding interactions with sulfate anions (**Figure 25 a**).⁵⁶

The model shown in **Figure 25** was corroborated by a ¹H NMR titration experiment in which the concentration of **2** was kept constant, varying the sulfate anion concentration (**Figure 25 d**), in accord with a standard protocol described in literature.⁵⁶ The aromatic signal of **2** was strongly affected by the addition of sulfate anion (in the form of sodium salt, from 0 to 40 mM in D₂O solution) to the 0.001 M solution of **2** in D₂O, indeed it has undergone a significant downfield shift.

In compliance with literature⁵⁶ this phenomenon indicated that the hydroxy groups interact with a fast complexation equilibrium with the anionic guest through H-bonding interactions.⁵⁶ According with the **Figure 25 b**, the pyrogallolarene molecules can limit the access of the sulfate anion to the cementitious surface because they can create such a wall between them. It is also probable that the presence of the adsorbed supramolecular complex $\text{SO}_4^{2-}@\mathbf{2}$ can increase the electrostatic repulsion ($\text{SO}_4^{2-} \cdots \text{SO}_4^{2-}$) among the grains, this effect can explain the slight increase of the spread observed in **Figure 25**. DFT-calculations were

employed to investigate the structure proposed for the H-bonding complex $\text{SO}_4^{2-}@\mathbf{2}$.

The first step involved the obtaining of the lowest energy-structure of the supramolecular complex $\text{SO}_4^{2-}@\mathbf{2}$ through Monte Carlo conformational search (Amber force field, H_2O as solvent) that was successively optimized by DFT calculations at the B3LYP/6-31G(d,p) level of theory (**Figure 25**). From a close inspection of the DFT-optimized structure of $\text{SO}_4^{2-}@\mathbf{2}$ (**Figure 25 b**) complex it was observed the presence of two H-bonding interactions involving the vicinal OH groups with H-bond donating free valence (**Figure 25 a**) and two oxygen atoms of the sulfate anion. More detailly, the two H-bonds show a $\text{O}-\text{H}\cdots\text{O}=\text{S}$ mean distance of 2.53 Å and an $\text{O}-\text{H}\cdots\text{O}=\text{S}$ angle of 172.1°; they can be classified as strong H-bonds because these distances meet the required parameters.^{56c}

-
- ⁵⁶ (a) Casnati, A.; Sansone, F.; Ungaro, R. *In Advances in Supramolecular Chemistry*; Gokel, G. W., Ed.; Cerberus Press Inc.: South Miami, 2004; Vol. 9, 165-218.
(b) Hirose, K. *In Analytical Methods in Supramolecular Chemistry*; Schalley, C. A., Ed.; Wiley-VCH: Weinheim, 2007.
(c) Steiner, T. The Hydrogen Bond in the Solid State. *Angew. Chem.* **2002**, 41, 48–76.
(d) Connors, K. A. *Binding Constants*; John Wiley & Sons: Chichester, 1987.
(e) Fielding, L. Determination of Association Constants (K_a) from Solution NMR Data *Tetrahedron* **2000**, 56, 6151–6170;
(f) Hirose, K. J. Spectrofluorometric Study of the Inclusion Complexation of Fluorescent Whitening Agents and β -Cyclodextrins *Inclusion Phenom. Macrocyclic Chem.* **2001**, 39, 193–209.

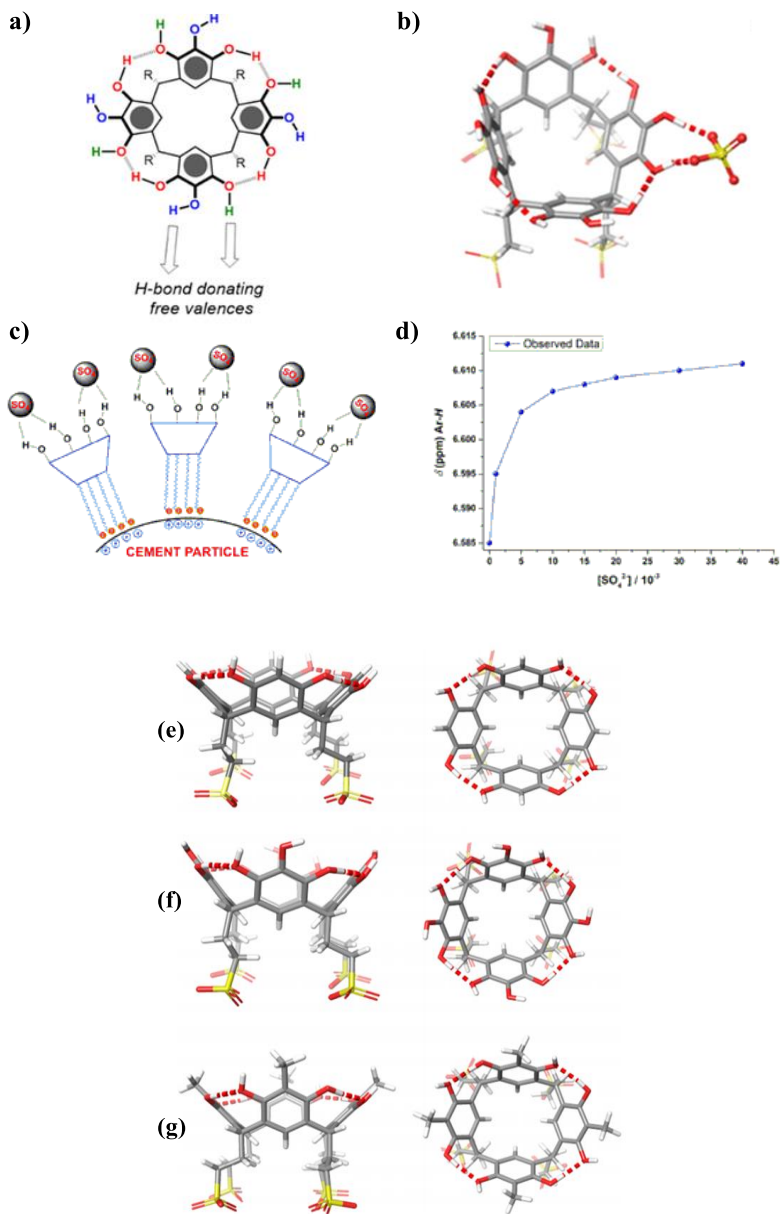


Figure 25. (a) Intramolecular hydrogen bonds donating free valences in macrocycle **2**. b) DFT-optimized structure of the compound where the

red dashed lines represent intramolecular and intermolecular H-bonding interactions. (c) Sketch of the H-bonding interactions between the synthesized macrocycles SPs and sulfate anions. (d) Complexation induced shift of the ^1H NMR signals of the aromatic signals of the derivative **2** (0.001 M), upon addition of the sulfate anions in D_2O . (DFT)-optimized structures of derivatives: (e) Tetrasulfonate Resorcin[4]arene **1**, (f) Pyrogallol[4]arene **2** and (g) Tetrasulfonate Methylresorcin[4]arene **3** at the B3LYP/6-31G(d,p).

The water-reduction abilities of SPs additives are a useful parameter in order to define their efficiency. In accord with these considerations, the macrocycles **1-3** were also tested for their ability to reduce the water required to prepare the cement mix, without affecting the workability to produce high-strength concrete. Water reduction capability was tested preparing a calibration curve with cement slurries at different water/cement ratios. Then, samples of grout were doped with the desired specimens and their spread diameter were measured changing the % of active at a settled w/c of reference. From the comparison of the water quantity contained into the samples and the blank, it is possible to extrapolate the power of reduction.

As it is possible to observe from the results in **Figure 26**, the samples **1** and **3** are not definable as water reducer superplasticizers. Instead, interesting results were obtained with the derivative **2** which shows the 23.6 % of water reduction capability. This additive can be classified for

this reason between the second-generation SPs because it can be comparable to the SMF and SNF used as reference.^{1,2}

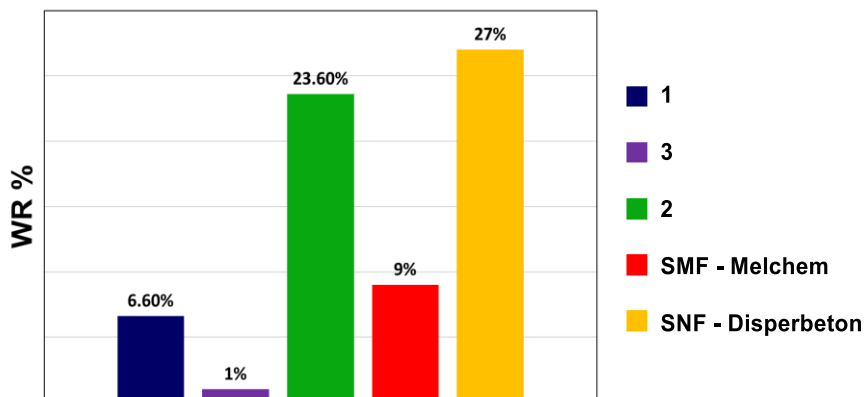


Figure 26. Water reduction test of mortar matrix doped with experimental compounds compared with commercial references

Finally, we studied the influence on the setting time of the water-soluble macrocycles **1** and **2** at a dosage of 0.5 wt % and a w/c of 0.5 on mortar. Resorcinarene sulfonate **1** and pyrogallolarene **2** behave as setting retarders because they generate a delay of the dormant period responsible

for an initial setting time of 8 h. These results are aligned with the ones already reported into literature for β -CD^{57,58}.

It could be hypothesized, that the macrocyclic delays the quiescent phase hydration of the cement, for a dual reason: a) the macrocyclic backbone generates the steric hindrance between cement grains; b) the formation of chelates between the OH groups on the macrocycle and Ca^{2+} . These mechanisms determine the formation of a thick adsorption layer constituted by macrocyclic- Ca^{2+} chelates and a water film of solvation that prevents the nucleation and solid phase growth of the hydration products and thus delay the hydration of the cement (**Figure 27**).^{59,60}

⁵⁷ Lv, S.H.; Gao, R.; Cao, Q.; Li, D.; Duan, J. Preparation and characterization of polycarboxymethyl- β -cyclodextrin superplasticizer. *Cem. Concr. Res.* **2012**, *42*, 1356–1361.

⁵⁸ Lv, S.-H.; Gao, R.-J.; Duan, J.-P.; Li, D.; Cao, Q. Effects of β -Cyclodextrin Side Chains on the Dispersing and Retarding Properties of Polycarboxylate Superplasticizers. *J. App. Polym. Sci.* **2012**, *125*, 396–404.

⁵⁹ Li, Y.; Zheng, J.; Guo, H.; Lu, M. Preparation and Application of New Polycarboxylate Superplasticizers with Mild Retarding Performance Based on Monovinyl β -Cyclodextrin Monomer. *J. Disper. Sci. Technol.* **2015**, *36*, 369–379.

⁶⁰ Li, Y.; Guo, H.; Zhang, Y.; Zheng, J.; Li, Z.; Yang, C.; Lu, M. Synthesis of Copolymers with Cyclodextrin as Pendants and its End Group Effect as Superplasticizer. *Carbohydr. Polym.* **2014**, *102*, 278–287.

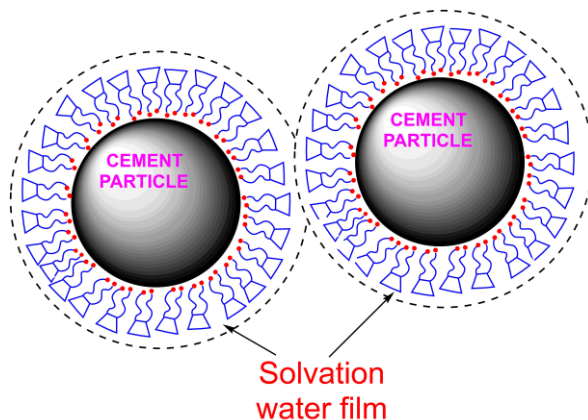


Figure 27. Schematic representation of the formation of water and SPs shell on cement grains.

Due to its retarding properties, the pyrogallol[4]arene **2** can be used as a retarding additive for cementitious systems. Adding retarding admixtures can be a successful strategy to ensure the workability of cement in hot climate sites or in the presence of a high Ca^{2+} concentration. Moreover, retarding admixtures are also employed to amplify the window of workability of gypsum slurries with their strong retarding effect. Indeed, gypsum slurries with a very low moisture content, generally have a fast setting time (less than 15 min), so it is often necessary to use additives in combination with retarders to guarantee their workability for longer times.

3.4 Conclusions

From the analysis of the results, it was shown that the fluidizing properties of these macrocycles are highly dependent by the number of OH groups on the upper rim.

In fact, derivative **3**, which has a methyl group on position 2 of the aromatic rings, shows no dispersant properties at all. These properties are slightly greater with resorcinol-based derivative **1** but still not comparable with the superior properties displayed by tetrasulfonated pyrogallol[4]arene **2**. The dispersing ability of derivative **2** is also not affected by the presence of sulphate anions in the cement matrix. This effect is due to the anion recognition capabilities of this macrocycle, which is able to complex the sulphate anion via H-bonding interactions, as it has been demonstrated through NMR titrations and computational calculations using DFT.

Thus, given the current interest in the synthesis of new dispersant molecules, our studies can be considered as interesting investigation for the future design of SPs based on macrocycles with improved fluidization capabilities and setting time performance.

3.5 Experimental section with details for the synthesis of derivatives 1, 2 and 3.

High resolution mass spectra were acquired on a Bruker Solarix FT-ICR mass spectrometer equipped with a 7T magnet. The mass spectra were calibrated externally, and a linear calibration was applied. All reaction solvents were dried by activated 3 Å molecular sieves. All chemicals reagents grade were used without further purification and were used as purchased. Reaction temperatures were measured externally. Reactions were monitored by TLC silica gel plates (0.25 mm) and visualized by UV light 254 nm, or by spraying with H₂SO₄-Ce(SO₄)₂. NMR spectra were recorded on a Bruker Avance-600 [600 (¹H) and 150 MHz (¹³C)], Avance-400 [400 (¹H) and 100 MHz (¹³C)] or Avance-300 MHz [300 (¹H) and 75 MHz (¹³C)] spectrometers. Chemical shifts are reported relative to the residual solvent peak. IR Spectroscopy analysis and Thermal analysis were recorded at the Research & Development Laboratory of BI-QEM SPECIALTIES S.P.A. respectively with FT-IR 4100 Type A (JASCO EUROPE) and with TGA Q500 (TA Instruments), in air atmosphere up to 900 °C with a heating rate of 10 °C/min.

Compounds **1**, **2** and **3** were obtained following a slightly modified procedure than that reported previously in literature.⁵⁴ A two-phase mixture of 2-(2-bromoethyl)-1,3-dioxane (0.250 mol) and an aqueous solution of Na₂SO₃ (0.500 mol in 250 mL) was stirred for 48 h under reflux and nitrogen atmosphere. The reaction mixture was allowed to cool to room temperature, and 250 mL of water were added. Then it was washed twice with 450 mL of ethyl ether in order to remove the unreacted

starting material. To the aqueous phase was successively added ethanol (500 mL), the appropriate aromatic monomer (1,2,3-trihydroxybenzene, 1,3-dihydroxybenzene, 1,3-dihydroxy-2-methylbenzene: 0.403 mol), and 75 mL of a solution 37 % of HCl. The reaction mixture was refluxed under nitrogen atmosphere for 48 hours. Then the solvent was removed under vacuum and cold methanol was added. The obtained precipitate was filtered and washed with cold methanol to give: **1** in 90 % of yield as a yellow solid; **2** in 92 % of yield as a yellow solid; **3** in 80 % of yield as a white solid. Derivative **1**. ^1H NMR (400 MHz, D_2O , 298 K): δ 7.08 (s, 4H, ArH), 6.52 (s, 4H, ArH), 4.65 (t, $J = 7.9$ Hz, 4H, $-\text{CHCH}_2$), 3.05 (t, $J = 7.4$ Hz, 8H, $-\text{CH}_2\text{SO}_3\text{Na}$), 2.55 (m, 8H, $-\text{CHCH}_2$). ^{13}C NMR (150 MHz, D_2O , 298 K) δ 152.4, 126.1, 123.5, 103.70, 50.0, 34.2, 29.6. FT-ICR HR ESI MS (negative ion mode), m/z calcd for $\text{C}_{36}\text{H}_{36}\text{O}_{20}\text{S}_4^{4-}$: 229.0176, found: 229.0177; m/z calcd for $\text{C}_{36}\text{H}_{36}\text{O}_{20}\text{S}_4 \text{Na}_2^{2-}$: 481.0245, found: 481.0255. Derivative **2**. ^1H NMR (600 MHz, D_2O , 298 K): δ 6.61 (s, 4H, ArH), 4.59 (t, $J = 7.8$ Hz, 4H, $-\text{CHCH}_2$), 2.88 (t, $J = 7.8$, 8H, $-\text{CH}_2\text{SO}_3\text{Na}$), 2.46 (m, 8H, $-\text{CHCH}_2$). ^{13}C NMR (150 MHz, D_2O , 298 K) δ 141.3, 133.9, 125.1, 115.9, 50.0, 34.5, 29.1. Derivative **3**. ^1H NMR (600 MHz, D_2O , 298 K): δ 7.02 (s, 4H, ArH), 4.61 (t, $J = 7.98$ Hz, 4H, $-\text{CHCH}_2$), 2.86 (t, $J = 7.3$ Hz, 8H, $-\text{CH}_2\text{SO}_3\text{Na}$), 2.55 (m, 8H, $-\text{CHCH}_2$), 1.82 (s, 12 H, $-\text{CH}_3$). ^{13}C NMR (150 MHz, D_2O , 298 K) δ 149.4, 125.4, 121.2, 114.9, 49.8, 49.3, 34.2, 29.0, 8.8. FT-ICR HR ESI MS (negative ion mode), m/z calcd for $\text{C}_{40}\text{H}_{44}\text{O}_{20}\text{S}_4^{4-}$: 243.0333, found: 243.0334; calcd for $\text{C}_{40}\text{H}_{44}\text{O}_{20}\text{S}_4\text{Na}^{3-}$: 331.7074, found: 331.7076; calcd for $\text{C}_{40}\text{H}_{44}\text{O}_{20}\text{S}_4 \text{Na}_2^{2-}$: 509.0558, found 509.0560.

3.5.1 FT-IR Analysis of Derivatives 1, 2 and 3. FT-IR Analyses were carried out on a Jasco V-630 Spectrophotometer in KBr dispersion. $\nu_{(\text{OH})}$ stretching vibration at 3425 cm^{-1} ; $\nu_{(\text{S}=\text{O})}$ stretching vibration at 1180 cm^{-1} and 1050 cm^{-1} .

3.5.2. TGA / DTG Analysis of Derivatives 1, 2 and 3. Thermogravimetric Analyses were acquired on a TA Instrument Q500 thermogravimetric analyzer up to 900°C , $10^\circ\text{C}/\text{min}$ ramp in air atmosphere. Decomposition profile plots are shown into supporting information.

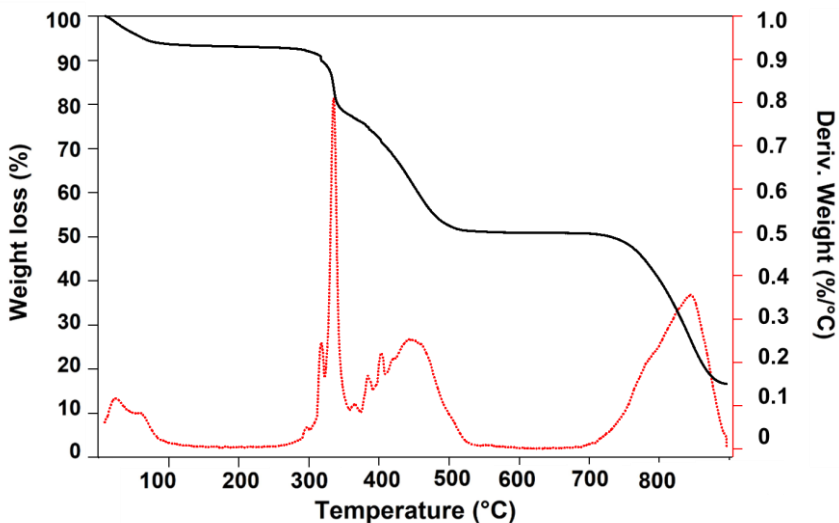


Figure 28. TGA / DTG of derivative 2.

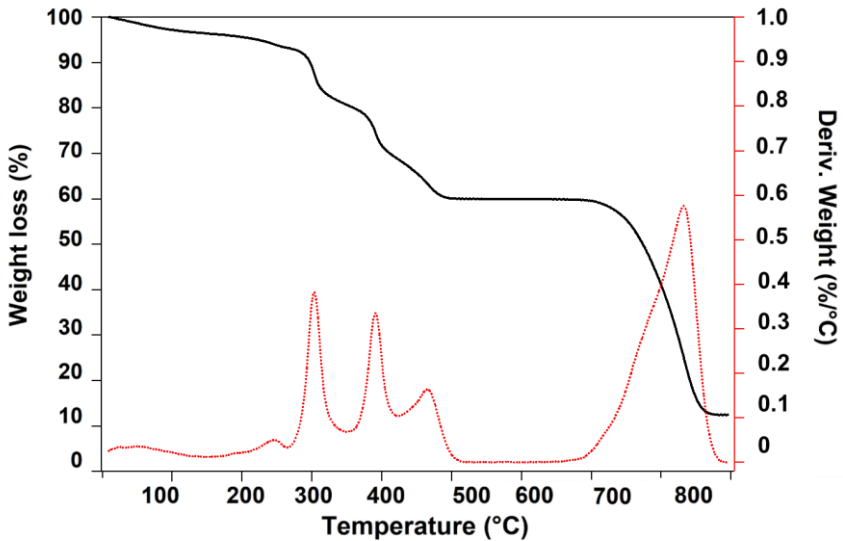


Figure 29. TGA / DTG of derivative 3.

3.6 Applicative workability tests of derivative 1,2 and 3 on fresh mortar

3.6.1 Mortar test materials and lab equipment. Mortar test materials and lab equipment. An Ordinary Portland Cement CEM IIA 42.5 RLL (Italcementi) in compliance with UNI EN 197-1 and a sand CEN Standard Sand compliant to DIN EN 196-1 (Normensand) were used in this study. Mortar performance was tested according to the current standard norms.

Spread tests performed were compliant to ASTM C143 (“Standard Test method for slump hydraulic-cement concrete”). The equipment used were an automatic mortar mixer model E093 (Matest S.p.A.) in

compliance with ASTM C305M specifications (“Mechanical mixing of hydraulic cement pastes and mortars of plastic consistency”) and an automatic flow table model M092 (LBG srl) in compliance with ASTM C230M specifications (“Standard Specification for Flow Table for Use in Tests of Hydraulic Cement”). All spread tests were carried out at $w/c = 0.5$, according with requirements of EN196-1:2016 (Methods of testing cement, Part 1 - Cap. 6: Preparation of mortar) / EN 480-1:2011 (Admixture for concrete, mortar and grout - Test methods part 1: Preparation of control mortar).

Setting time determination was performed with Vicat apparatus in compliance with ASTM C191 specifications (“Standard test method for time of setting of hydraulic cement by Vicat needle”). All setting time tests were performed at $w/c = 0.5$, according with EN196-1:2016 / EN 480-2:2011 (Admixture for concrete, mortar and grout - Test methods part 2: Determination of setting time).

The solid content of all the derivatives was estimated at 105 °C for 30 minutes with moisture analyzer model name Crystaltherm (Gibertini) to calculate the specific dosage of additives.

3.6.2. Study of the dosage-dependent effect, slump tests and setting time evaluation of new performing additives 1, 2 and 3 in comparison with commercial plasticizers.

The fluidificant effects of synthesized admixtures were assessed by means of a spread test on mortar and compared with the dispersing performance of commercial admixtures.

All the cement mortars were prepared with the following amounts of materials/ conditions: 450 g of Cement; 225 g of water ($w/c = 0.5$); 1350 g of CEN standard sand; 0.5 % (bwoc) of the additive (100 % active); 4 minutes mixing program (compliant to ASTM C305: 30s low mixing rate, 30s high mixing rate, 2 minutes rest period, 1 minute high mixing rate); the temperature of the test room, the equipment and the materials (plaster, water) was set at 20.0 ± 2.0 °C. After the mix, spread tests were performed by automatic flow-table (15 blows): measurements were performed after 4', 30', 60', 90 and 120', in order to evaluate the spread diameter time dependence of mortar doped with the additive.

Meanwhile the setting time was carried out using the Vicat apparatus in defined time lapse to study the trend of the SPs. The initial setting time occurred in compliance with ASTM C191 specifications, when the penetration of the Vicat probe in the fresh mortar was 4 ± 1 mm.

3.6.3. Investigation of dispersing performance of 1,2 and 3 in the presence of sulfates. The influence of sulfate ions on the new unconventional superplasticizers was determined following the method previously described by Plank and co-workers²⁵ and the results were compared with the effect on commercially available reference additives. The experimental conditions for preparation of the mortar, the determination of the %TS and the requirements for the equipment were the same of the previous experiments. For the following experiments, the investigation was carried out employing low additives dosage (0.2% bwoc) to highlight the effect of the additive on the spread diameter values. The cementitious mortar was doped with different dosages of Na_2SO_4 (i.e., 0.2–2% bwoc) that was added in the cement powder. The test result

was obtained measuring the first slump flow of the cementitious only after 4 minutes.

3.6.4. ^1H NMR Titration of derivative 2 with Na_2SO_4 . A solution of derivative 2 (5 mL, solution A) 0.001 M in D_2O was prepared. In 0.5 mL of this solution, Na_2SO_4 was dissolved in 0.05 M concentration (solution B). 0.5 mL of solution of derivative 2 (solution A), in a NMR tube, was titrated with the Na_2SO_4 solution B in the concentration range: from 0 to 40 mM.

Chapter 4: Poly(EthyleneGlycol)/ β -Cyclodextrin Pseudorotaxanes as Sustainable Dispersing and Retarding Materials in Cement-Based Mortar

4.1 General overview

Cyclodextrins (CDs) (**Figure 30**) are a class of polyhydroxylated macrocycles that are obtained through the enzymatic degradation of starch.^{61,62} Consequently, the cyclodextrins are obtained from renewable resources, and are practically non-toxic. CDs are constituted by D-(+)-glucose units joined together by α -1,4-glycosidic bonds to form macrocyclic compounds that play a pivotal role as hosts in supramolecular chemistry.^{63,64}

⁶¹ Chen, G.; Jiang, M. Cyclodextrin-based inclusion complexation bridging supramolecular chemistry and macromolecular self-assembly. *Chem. Soc. Rev.* **2011**, *40*, 2254–2266.

⁶² Miyauchi, M.; Harada, A. Construction of supramolecular polymers with alternating α -, β -cyclodextrin units using conformational change induced by competitive guests. *J. Am. Chem. Soc.* **2004**, *126*, 11418–11419.

⁶³ Schneider, H.-J.; Hacket, F.; Rüdiger, V.; Ikeda, H. NMR Studies of Cyclodextrins and Cyclodextrin Complexes. *Chem. Rev.* **1998**, *98*, 1755–1786.

⁶⁴ Rekharsky, M. V.; Inoue, Y. Complexation thermodynamics of cyclodextrins. *Chem. Rev.* **1998**, *98*, 1875–1918.

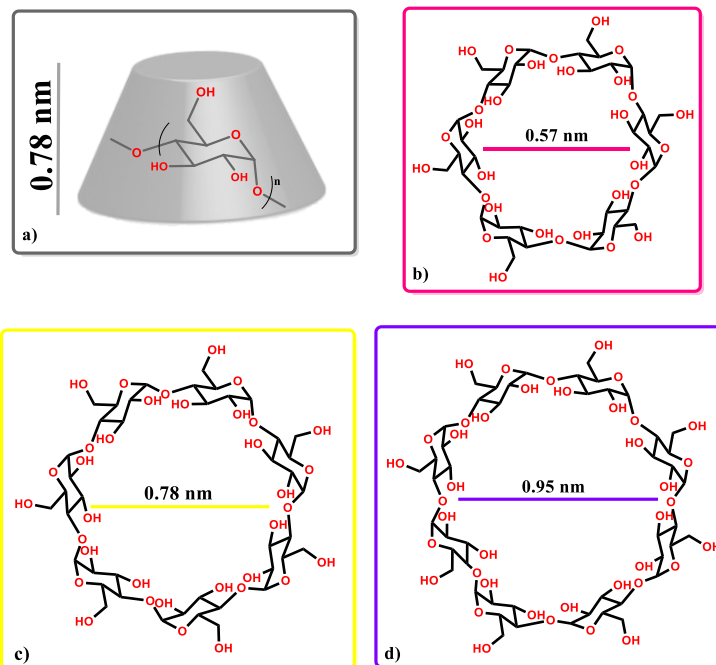


Figure 30. Structure of cyclodextrins: a) toroidal structure; b) α -cyclodextrin; c) β -cyclodextrin; d) γ -cyclodextrin.

The most common members of this family of macrocycles are α -, β - and γ -cyclodextrins (**Figure 30 b , c and d**), which are constituted of six, seven and eight D-glucose units, respectively. Cyclodextrins show a 3D toroidal shape with a hydrophobic cavity and hydrophilic rims (**Figure 30 a**).

Cyclodextrins (CDs) show the primary hydroxyl groups (-CH₂OH) on the smaller rim meanwhile the larger rim is constituted by secondary hydroxyl groups.⁶⁵

The cyclodextrins are useful host in supramolecular chemistry,^{66,67} and are able to form inclusion complexes. The formation of inclusion complexes between the cyclodextrin and hydrophobic guests occurs by inclusion of the guest inside the hydrophobic cavity of the cyclodextrin.⁶⁸ · ⁶⁹ The thermodynamic driving forces of this supramolecular process is the “hydrophobic effect”, that drives the aggregation of nonpolar molecules in an aqueous solution.^{61,62,65}

Due to their versatile nature, CDs have found many applications in different industrial sectors, such as food,⁷⁰ pharmaceutical,⁷¹

⁶⁵ Dodziuk, E. Cyclodextrins and their Complexes: Chemistry, Analytical Methods, Applications. Wiley-VCH; 2006.

⁶⁶ Del Valle, E. M. M. Cyclodextrins and Their Uses: A Review. *Process Biochem.* **2004**, *39*, 1033–1046.

⁶⁷ Chen, G.; Jiang, M. Cyclodextrin-Based Inclusion Complexation Bridging Supramolecular Chemistry and Macromolecular Self-Assembly. *Chem. Soc. Rev.* **2011**, *40*, 2254–2266.

⁶⁸ Mura, P. Analytical Techniques for Characterization of Cyclodextrin Complexes in Aqueous Solution: A Review. *J. Pharm. Biomed. Anal.* **2014**, *101*, 238–250.

⁶⁹ Maazaoui, R.; and Abderrahim, R. Applications of cyclodextrins: formation of inclusion complexes and their characterization. *IJAR* **2015**, *3*, 1030–1030.

⁷⁰ Fenyvesi, É.; Vikmon, M.; Szente, L. Cyclodextrins in food technology and human nutrition: benefits and limitations. *Crit. Rev. Food Sci. Nutr.* **2016**, *56*, 1981–2004.

⁷¹ Jansook, P.; Ogawa, N.; Loftsson, T. Cyclodextrins: structure, physicochemical properties and pharmaceutical applications. *Int. J. Pharm.* **2018**, *535*, 272–284.

chemistry,^{72,73} , medicine,⁷⁴ and environment⁷⁵. Their success is due to their low-cost production, so compatible for the industrial scale.

In the food industry, the CDs can improve the antioxidants and antibacterial properties of additives upon their inclusion inside the cavity. CDs can also mask the bad taste of specific substances or can be also applied in food packing.^{76,77} As specific example, the odour freshener Febreze (Proctor and Gamble) contains cyclodextrins, which are claimed to entrap odour-producing lipophilic molecules.^{76,77}

In the pharmaceutical field the solubility of these biocompatible materials is really appealing to enhance the drugs therapeutic efficacy. For these reasons, the inclusion compounds based on CD are widely used for facilitating the parenteral administration of drugs as reported several times in the literature.⁷⁸ Very recently, Miranda et al.⁷⁹ carried out a

⁷² He, Y.; Hou, X.; Liu, Y.; Feng, N. Recent progress in the synthesis, structural diversity and emerging applications of cyclodextrin-based metal–organic frameworks. *J. Mater. Chem. B* **2019**, *7*, 5602–5619.

⁷³ Ogoshi, T. & Harada, A. Chemical sensors based on cyclodextrin derivatives. *Sensors* **2008**, *8*, 4961–4982.

⁷⁴ Lenik, J. Cyclodextrins based electrochemical sensors for biomedical and pharmaceutical analysis. *Curr. Med. Chem.* **2017**, *24*, 2359–2391.

⁷⁵ Cova, T. F. G. G.; Murtinho, D.; Pais, A. A. C. C.; Valente, A. J. M. Cyclodextrin-based materials for removing micropollutants from wastewater. *Curr. Org. Chem.* **2018**, *22*, 2150–2181.

⁷⁶ Tian, B.; Xiao, D.; Hei, T.; Ping, R.; Hua, S.; Liu, J. The Application and Prospects of Cyclodextrin Inclusion Complexes and Polymers in the Food Industry: A Review. *Polym. Int.* **2020**, *69*, 597–603.

⁷⁷ Stick, R. V.; Williams, S. J. Disaccharides, Oligosaccharides and Polysaccharides. In *Carbohydrates: The Essential Molecules of Life*. Elsevier; 2009, 321–341.

⁷⁸ Jansook, P.; Ogawa, N.; Loftsson, T. Cyclodextrins: structure, physicochemical properties and pharmaceutical applications. *Int. J. Pharm.* **2018**, *535*, 272–284.

⁷⁹ Miranda, M., G.; Santos, V. O. R. E.; Bessa, J. R.; Teles, Y. C. F.; Yahouedehou, S. C. M. A.; Goncalves, M. S.; Ribeiro-Filho, J. Inclusion complexes of non-steroidal anti-

study to investigate the role of CDs as a carrier for active pharmaceutical ingredient (API) capable of improving the pharmacological and biopharmaceutical properties of non-steroidal anti-inflammatory drugs and to reduce the side effects associated with their use.

CD-based inclusion compounds also have applications in the environmental field.⁸⁰ Duan's group has reported the ability of the β -CD to complex pollutants of different nature as a useful system to purify aqueous samples.^{81,82}

SPs currently on the market such as SNF and SMF^{16,16} are obtained from non-renewable sources. In addition, severe pollution problems are related to use and fate of Poly- β -Naphthalene Sulfonate (SNF) and PolyMelamine Sulfonate (SMF) that are widely used in the civil engineering field. In 2002, Ruckstuhl's group demonstrated how the quality of underground water is more and more under pressure for the persistence of SPs and particularly of sulfonated naphthalene SPs and their formaldehyde condensates.⁸³

inflammatory drugs with cyclodextrins: a systematic review. *Biomolecules* **2021**, *11*, 361-383.

⁸⁰ Baudin, C.; Pean, C.; Perly, B.; Gosselin, P. Inclusion of Organic Pollutants in Cyclodextrins and Derivatives. *Int. J. Environ. Anal. Chem.* **2000**, *77*, 233–242.

⁸¹ Duan, Z.; Li, Y.; Zhang, M.; Bian, H.; Wang, Y.; Zhu, L.; Xia, D. Towards Cleaner Wastewater Treatment for Special Removal of Cationic Organic Dye Pollutants: A Case Study on Application of Supramolecular Inclusion Technology with β -Cyclodextrin Derivatives. *J. Clean. Prod.* **2020**, *256*, 120308.

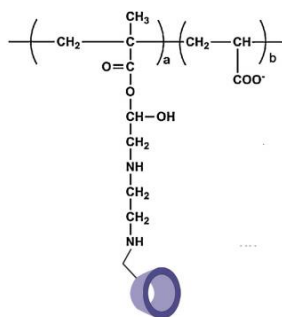
⁸² Duan, Z.; Wei, S.; Bian, H.; Guan, C.; Zhu, L.; Xia, D. Inclusion as an Efficient Purification Method for Specific Removal of Tricyclic Organic Sulfur/Nitrogen Pollutants in Fuel and Effluent with Cyclodextrin Polymers. *Sep. Purif. Technol.* **2021**, *254*, 117643.

⁸³ Ruckstuhl, S.; Suter, M. J.-F.; Kohler H.-P. E.; Giger, W. Leaching and primary biodegradation of sulfonated naphthalenes and their formaldehyde condensates from

Therefore, due to the need for more environmentally friendly additives to provide alternatives to these problems, increasing attention has been focused on the development of biodegradable SPs from renewable sources, and among these, β -CD-based dispersants have proven to meet this demand.

Until now, CD-based SPs have been obtained starting from the modification of polymers with CD-based derivatives or by polymerization of CD-based monomers. In all cases described so far in literature, the cyclodextrin units were covalently grafted on the polymeric backbone.^{57,58}

One example is represented in **Figure 31**, in which the superplasticizer described by Li Y. and collaborators,^{59,60} is a β -CD-based polymer obtained by a radical polymerization^{59,60} starting with a monovinyl β -CD monomer. The material showed excellent superplasticizer properties combined with a strong retarding effect.



concrete superplasticizers in groundwater affected by tunnel construction. *Environ. Sci. Technol.* **2002**, *36*, 3284–3289.

Figure 31. A polymeric material bearing CD used as superplasticizers.⁵⁹
60

Another interesting example of CD-based SPs was discussed by Lv S.H. et al.^{57,58} The poly-carboxymethyl- β -cyclodextrin, PCM- β -CD in **Figure 32**, is covalently functionalized with β -cyclodextrin, and bears PEG-chains. The PCM- β -CD showed an excellent fluidity retention during time and a strong retarding effect.^{57,58}

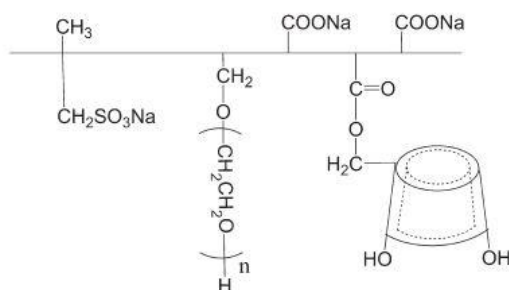


Figure 32. Poly-CarboxyMethyl- β -CycloDextrin PCM- β -CD superplasticizer.^{57,58}

In particular, it was demonstrated that the properties of the β -CD-based PCs in **Figure 33** is due to both the footprint effect between the macrocycles/PEG and the electrostatic effect caused by the anionic groups of the polymer bounded on the surface of cement grains (**Figure 33**).⁵⁷⁻⁶⁰ In PCM-based SPs in **Figure 33**, the carboxylic groups act as anchors to adsorb on the surfaces of cement particles. The poly(ethylene glycol) side chains play a crucial role for the dispersing abilities of this

material, in fact the PEG chains protrude from the cement surface into the pore solution to produce steric hindrance (**Figure 33**).

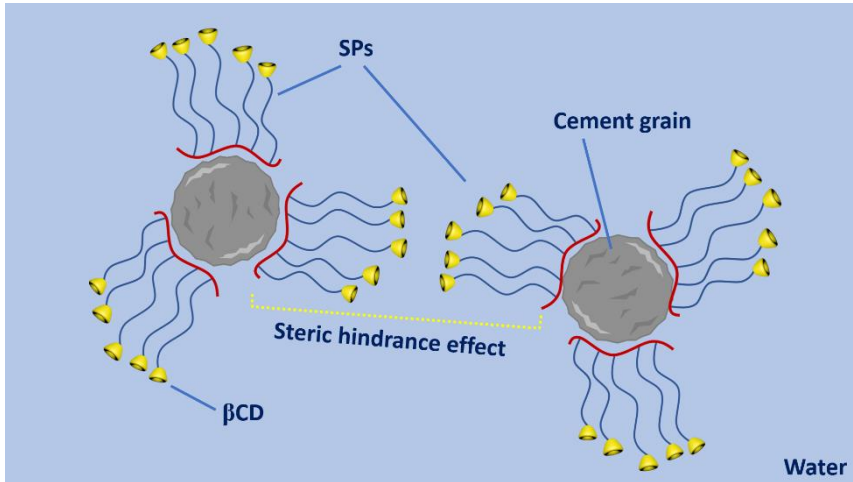


Figure 33. Representation of the working mechanisms of SPs constituted by PEG chains and cyclodextrin units that are covalently grafted on the polymeric backbone.

Even if SP materials constituted by cyclodextrins covalently grafted with PEG chains (in **Figure 31** and **Figure 32**) have found applications as SPs⁵⁷⁻⁶⁰ no information has been reported in literature about the dispersion and retarding effects of PEG@CD-based supramolecular inclusion complexes (see **Figure 34**) in which the PEG chain is included (threaded: PEG@CD) inside the cavity of the β -CD, by secondary interactions, to form pseudorotaxane architectures (**Figure 34**).

Harada introduced the synthesis of a lot of examples of PEG@CD pseudorotaxanes obtained in sustainable conditions.^{84, 85, 86, 87, 88} The formation of pseudorotaxane architectures occur by a self-assembly equilibrium in which a linear molecule, such as PEG derivative (**Figure 34**, axle) is threaded through a macrocycle (**Figure 34**, wheel) such as the cyclodextrins.⁸⁹ The pseudorotaxane architectures are stabilized by intermolecular secondary interactions such as H-bond, electrostatic and van der Waals forces (**Figure 34**) or hydrophobic effect in CD-based pseudorotaxanes.

⁸⁴ Harada, A.; Kamachi, M. Complex formation between poly(ethylene glycol) and α -cyclodextrin. *Macromolecules* **1990**, *23*, 2821–2823.

⁸⁵ Harada, A.; Li, J.; Kamachi, M. The molecular necklace: a rotaxane containing many threaded α -cyclodextrins. *Nature* **1992**, *356*, 325–327.

⁸⁶ Harada, A.; Li, J.; Kamachi, M. Complex Formation between Polyisobutylene and Cyclodextrins: Inversion of Chain-Length Selectivity between β -Cyclodextrin and γ -Cyclodextrin. *Macromolecules* **1993**, *26*, 5267–5268.

⁸⁷ Harada, A.; Li, J.; Kamachi, M. Preparation and properties of inclusion complexes of polyethylene glycol with β -cyclodextrin. *Macromolecules* **1993**, *26*, 5698–5703.

⁸⁸ Harada, A.; Li, J.; Okada, M.; Kamachi, M. Preparation and Characterization of Inclusion Complexes of Poly(propylene glycol) with Cyclodextrins. *Macromolecules* **1995**, *28*, 8406–8411.

⁸⁹ Udachin, K. A.; Wilson L.D.; Ripmeester J.A. Solid Polyrotaxanes of Polyethylene Glycol and Cyclodextrins: The Single Crystal X-ray Structure of PEG- α -cyclodextrin. *J. Am. Chem. Soc.* **2000**, *122*, 12375–12376.

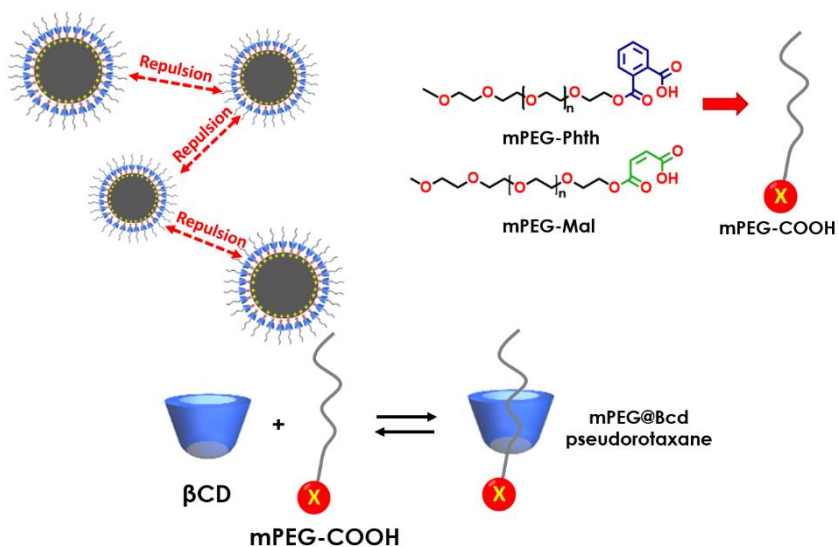


Figure 34. Cartoon representation of pseudorotaxane and its axle and wheel components. The dispersing mechanism envisioned for mPEG-COOH@ β -CD pseudorotaxanes studied in this work.

A CD-based polyrotaxanes was reported by Harada and coworkers.⁸⁵⁻⁸⁸ The supramolecular architectures described in **Figure 35** was constituted by cyclodextrin rings threaded through a PEG chain, as shown by X-ray analysis in which hydrogen bonding interactions between cyclodextrin rings were detected.

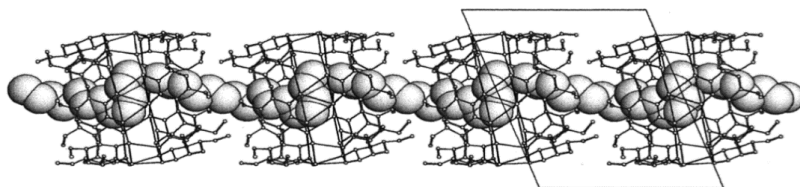


Figure 35. X-ray structure of PEG- β -cyclodextrin.⁸⁹

The synthesis of a pseudorotaxane is obtained by simple mixing of both the components in appropriate solvent without the need of any work-up procedure. Usually, PEG and CDs are both water-soluble and for these reasons, the experimental conditions for the synthesis of β -CD/PEG-based can be considered as sustainable and suitable for applications in industries. Prompted by these considerations we have investigated the SPs properties of pseudorotaxanes formed by threading of linear mPEG-COOH derivatives bearing carboxylic functions (**Figure 36** up), as axle and β -CD as host (**Figure 36** down). In detail, we envisioned that the carboxylic functions (maleic and phthalic functions) could act as anchors on the cement surface through coordination with metal centers (**Figure 34**), while the pseudorotaxane architecture constituted by β -CD wheel threaded along the PEG axle would protrude from the cement surface to generate steric hindrance (**Figure 34**).

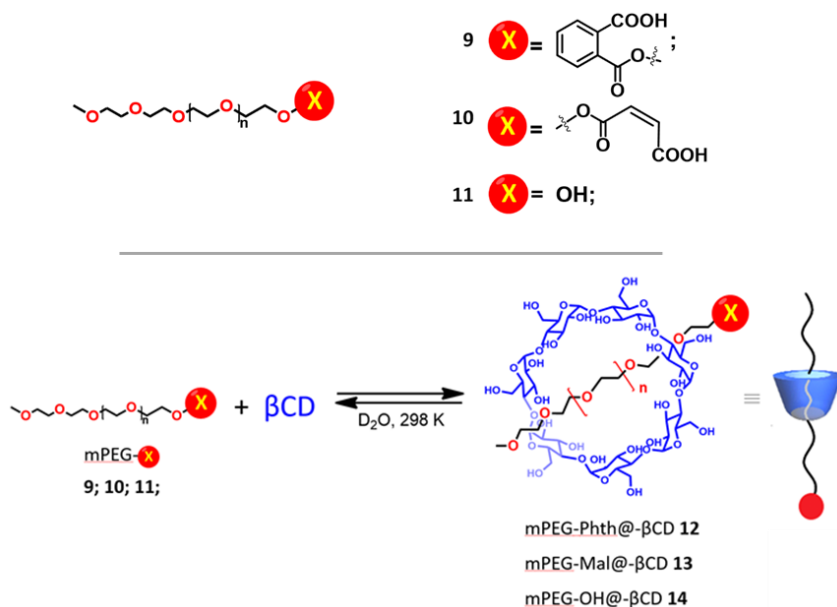
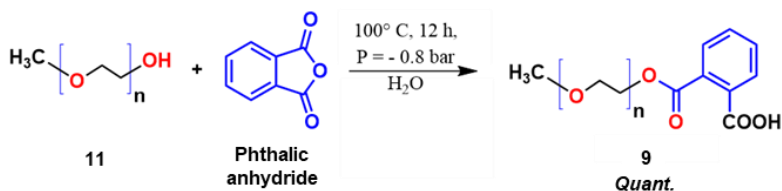


Figure 36. mPEG-COOH derivatives synthesized in this work (top): mPEG-Phth **9**, mPEG-Mal **10**, mPEG-OH **11**. β -CD-based pseudorotaxanes (bottom): mPEG-Phth@- β -CD **12**, mPEG-Mal@- β -CD **13** and mPEG-OH@- β -CD **14**.

In this study,³ we have synthesized the mPEG derivatives **9** and **10** in **Figure 36** (top), by reaction between mPEG₁₀₀₀-OH **11** with phthalic and maleic anhydride, and successively we have obtained the β -CD-based pseudorotaxanes (**Figure 36** bottom) by mixing of components (**9**, **10** or **11** and β -CD) in aqueous solution. For the first time the abilities of these β -CD-based pseudorotaxanes as SPs in cement-based mortar have been studied.

4.2 Synthesis and characterization of the polymeric axis mPEG-Phth **9** and mPEG-Mal **10**

4.2.1 Synthesis and characterization of derivative mPEG-Phth **9**



Scheme 4. Synthesis of derivative mPEG-Phth **9**.

The synthesis of compound **9** (mPEG-Phth) is reported in the **Scheme 4**. The starting mPEG-1000-OH **11** was melted at 60 °C and then 1 equivalent of phthalic anhydride was crushed into a fine powder and mixed into the reaction mixture at 60 °C. The reaction mixture was stirred at 60 °C for 30 minutes until complete solubilization of the phthalic anhydride.

Successively the reaction was heated at 100 °C and under vacuum of -0.8 bar for 12 h, when all the water was completely distilled out. Finally, the colourless waxy product **9** was cooled and stored at room temperature.

The evolution of the reaction was monitored by GPC analysis (**Figure 37**) of samples periodically removed from the reaction mixture. The GPC profile showed how the elution profile of the starting material was gradually shifted at lower retention time, which indicated that the reaction was complete after 12 h.

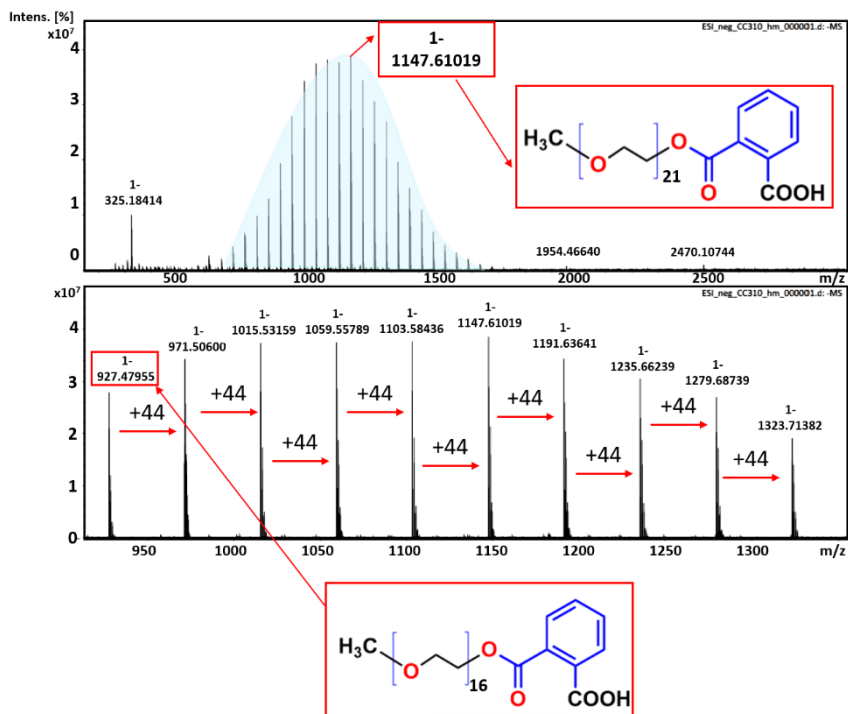
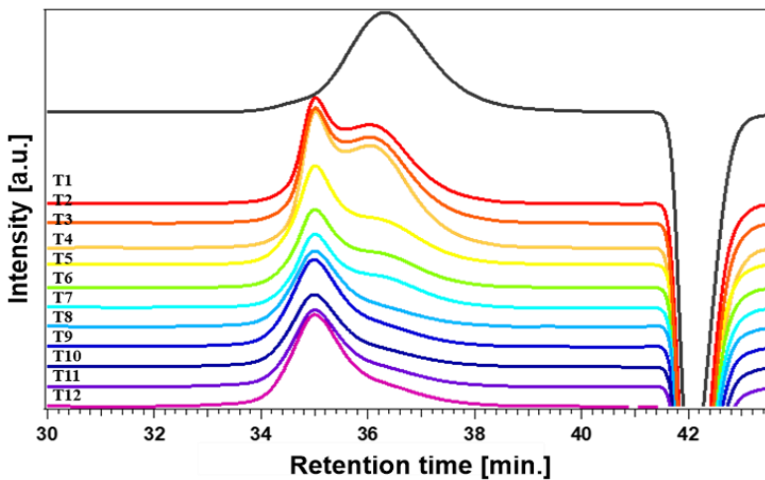


Figure 37. *Top:* Gel permeation chromatograms for the reaction between mPEG-OH **11** in black and phthalic anhydride to obtain the derivative **9**; *Bottom:* positive ESI ion mode FT-ICR HR MS of mPEG-Phth **9**.

Useful information regarding the progress of the esterification of mPEG **11** to mPEG-Phth **9** were obtained by FT-IR spectra (**Figure 38**).

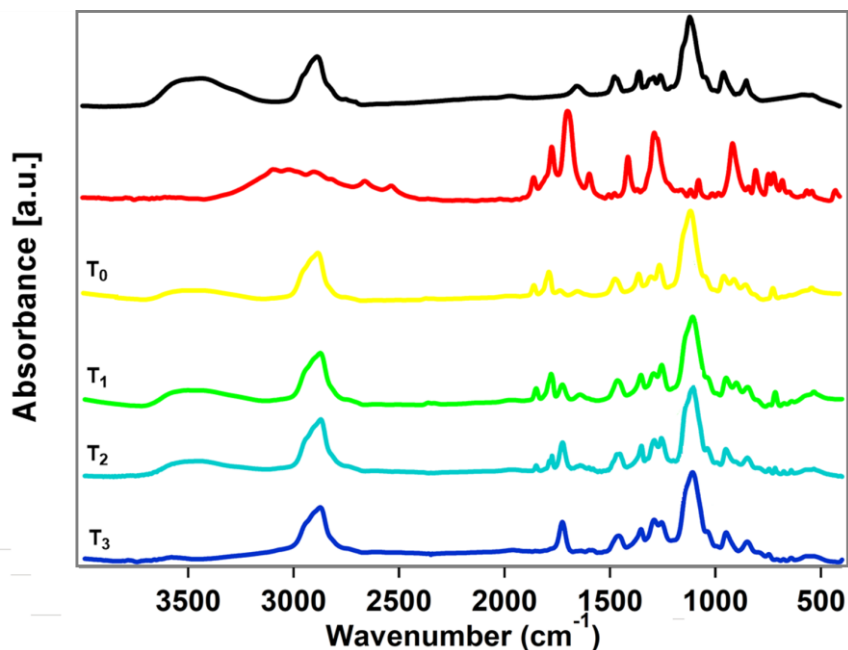


Figure 38. FT-IR spectra of the reaction mixture in **Scheme 4** over time (T₁ = 1 h; T₂ = 3 h; T₂ = 9 h; T₃ = 12 h). In black and red the FT IR spectra of the starting material **11** and mPEG-Phth **9**, respectively.

Detailed analysis of the FT-IR spectra of the reaction mixture in **Figure 38** revealed the disappearance of the band at 3400 cm^{-1} attributable to OH stretching of the starting material mPEG-OH **11**, while a new diagnostic band appeared at 1731 cm^{-1} , that was attributable to the C=O stretching of the new ester bond.

^1H and ^{13}C NMR spectra confirmed the formation of the mPEG-Phth **9** product. In detail, in the ^1H NMR spectrum in **Figure 39**, the $-\text{CH}_2\text{OH}$ signal of the starting mPEG-OH **11** showed a downfield shift of 0.56 ppm after the formation of the new ester bond.

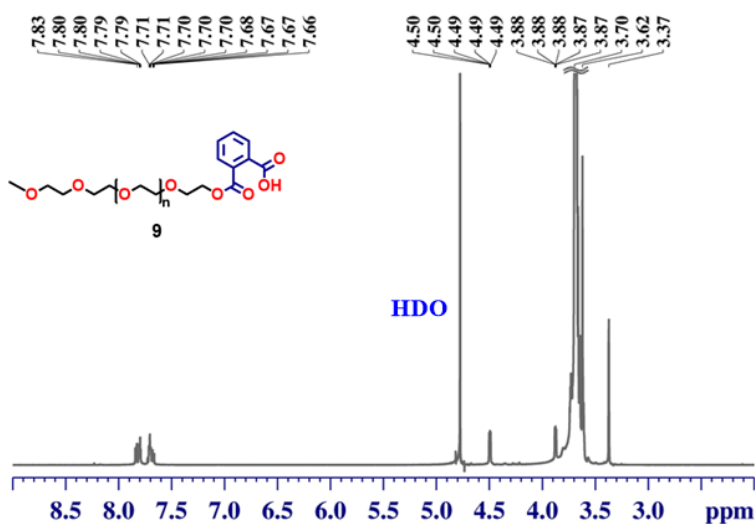


Figure 39. ^1H NMR spectrum (150 MHz, D_2O , 298 K) of derivative mPEG-Phth **9**.

The ^{13}C NMR spectrum in **Figure 40** of derivative mPEG-Phth **9** evidenced two signals at 171.9 ppm and 169.8 ppm attributable to its carbonyl functions.

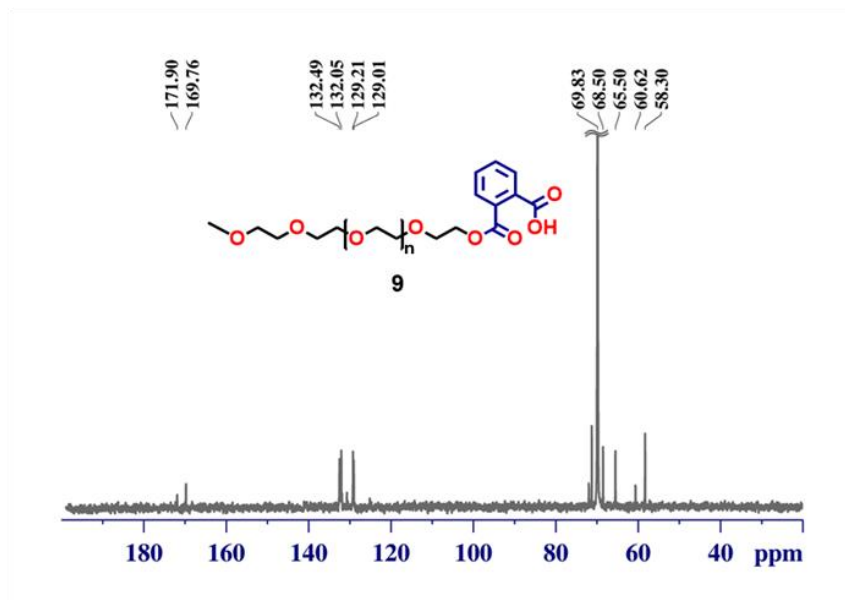


Figure 40. ^{13}C NMR spectrum (150 MHz, D_2O , 298 K) of derivative mPEG-Phth **9**.

DSC investigation of the derivative mPEG-Phth **9** in **Figure 41** highlighted that the synthesized compound **9** presents different behaviour in comparison of the raw material. Indeed, during the heating ramp, the product showed a phase transition at the T_m of 30.7 °C with an enthalpy of 115.1 J/g, while higher values of melting temperature and enthalpy were observed for the starting mPEG-OH **11** (**Figure 41**, left in red).

During the cooling process, a crystallization temperature of 16.8 °C was observed for the product **9**, with $\Delta H = 90.8$ J/g, which is lower than the corresponding value measured for mPEG-OH **11** (**Figure 41**, right in blue).

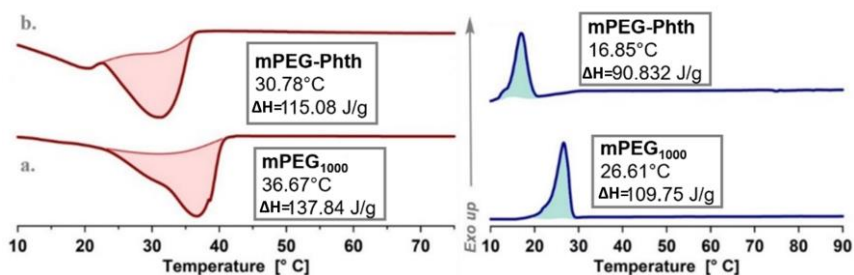


Figure 41. DSC heating (left, in red) and cooling (right, in blue) curves of a) mPEG₁₀₀₀ **11** and b) derivative mPEG-Phth **9**.

The thermal stability (TGA) analysis of the product mPEG-Phth **9** is reported in **Figure 42**, comparing its thermogram to that of the starting materials ones.

The mPEG₁₀₀₀ **11**, (**Figure 42**, black line), starts to lose weight at 191.8 °C while the maximum degradation rate is reached at 217 °C. In comparison, the product mPEG-Phth **9** showed higher thermal stability, as indicated by TGA experiments in **Figure 42**. The TGA analysis of mPEG-Phth **9** shows two steps of degradation: the first step is due to the phthalate group and occurs at 176.4 °C while the second decomposition

step at 299.7 °C was attributable to the polymeric chain (**Figure 42**, light green curve).

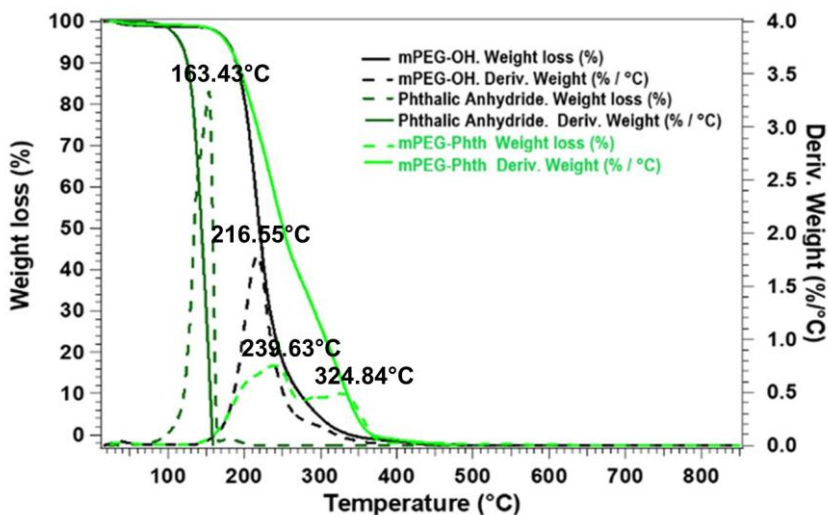
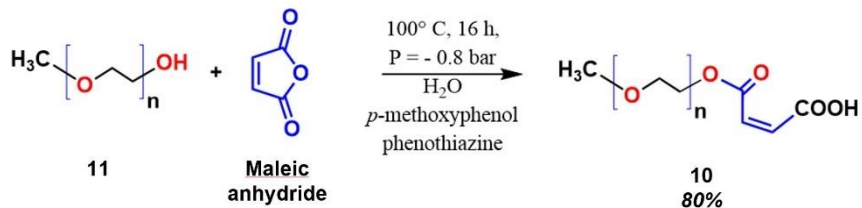


Figure 42. Thermogravimetric analysis of derivatives mPEG-Phth **9**, mPEG-OH **11**, and phthalic anhydride.

4.2.2 Synthesis and characterization of derivative mPEG-Mal **10**



Scheme 5. Synthesis of the derivative mPEG-Mal **10**.

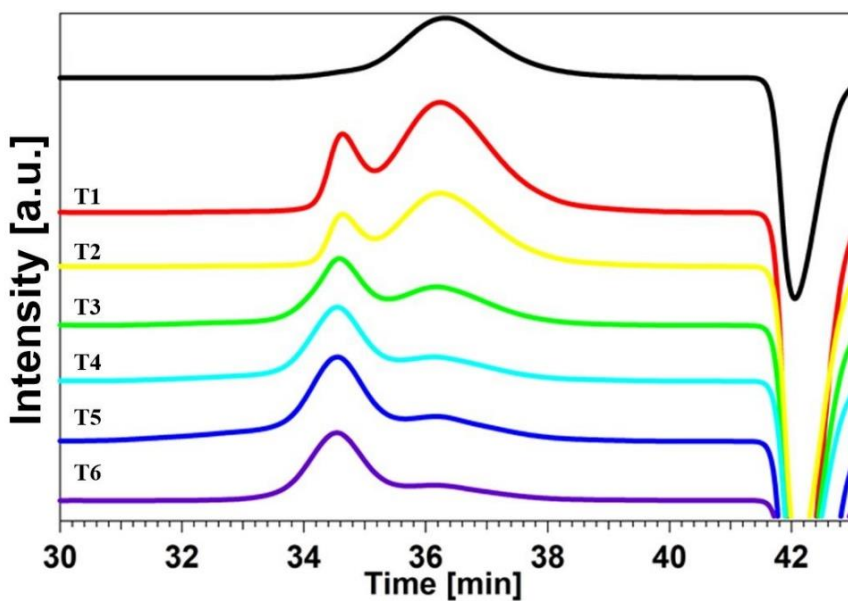
The derivative mPEG-Mal **10** was obtained under different conditions than those reported for the derivative mPEG-Mal **10**.³ Indeed, it was observed that when the functionalization of the mPEG-OH **11** with the maleic anhydride (1.0 equiv) was performed under the conditions already optimized for the phthalic anhydride, the esterification of the starting mPEG-OH **11** was not complete after 12 h. It was assumed that in the presence of oxygen a thermally initiated concurrent homopolymerization of maleic anhydride occurs,⁹⁰ so in order to avoid this undesirable effect, the reaction was repeated in presence of phenothiazine and p-methoxyphenol, which are able to inhibit the radical polymerization of acrylate compounds.

The mPEG-Mal compound **10** was obtained as shown in **Scheme 5**. The starting material mPEG₁₀₀₀-OH **11** was melted at 60 °C and dissolved in water. Then, 1 equivalent of maleic anhydride was crushed into a fine powder and stirred into the reaction mixture at 60 °C. Therefore, to inhibit the radical homopolymerization, we performed the reaction in the presence of phenothiazine (0.05 %, w/w) and p-methoxyphenol (0.1 %, w/w).⁹⁰ The reaction was vigorously mixed at 60 °C for 30 minutes, then a vacuum of -0.8 bar was applied, and the reaction mixture was stirred at 100 °C for 16 h until the complete remotion of water by distillation. Finally, the waxy red product **10** was cooled and stored at room temperature. Under these conditions the 80 % of conversion of

⁹⁰ Levy, L. B. Inhibition of Acrylic Acid Polymerization by Phenothiazine and p-Methoxyphenol. II. Catalytic Inhibition by Phenothiazine. *J Polym Sci A Polym Chem* **1992**, *30*, 569–576.

mPEG1000 to mPEG-Mal **10** was obtained after 16 h, as confirmed by GPC experiments (**Figure 43**).

The reaction progresses were monitored by GPC analysis. As it is possible to observe in **Figure 43** the final product **10** (violet line) shows a shorter retention time than the starting material **11** (black line), that means a new compound with wider M_w has been obtained.



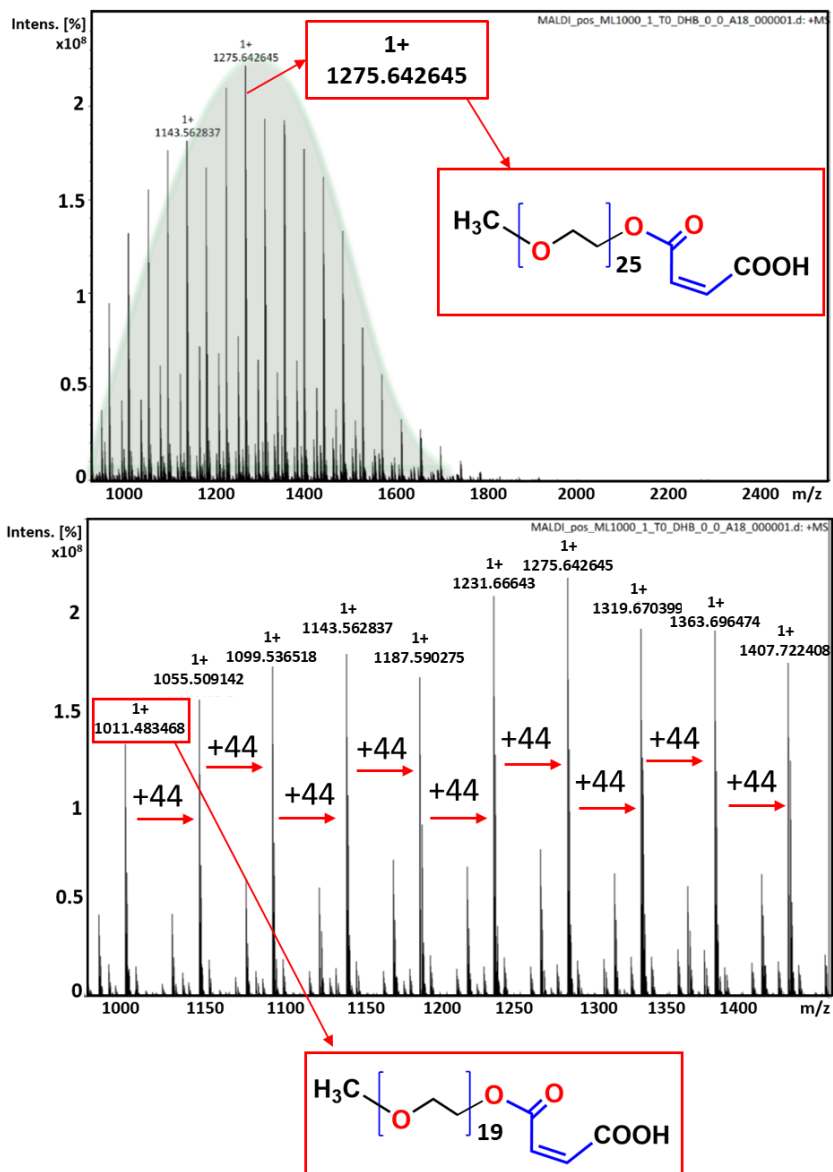


Figure 43. *Top:* Gel permeation chromatograms for the monitoring of the reaction of esterification between mPEG-OH **11** (black) and maleic

anhydride to obtain the derivative mPEG-Mal **10** (violet). *Bottom:* positive MALDI ion mode FT-ICR HR MS of mPEG-Phth **10**.

From the analysis of the FT-IR spectra (**Figure 44**) it was possible to observe the gradual disappearance of the characteristic OH-stretching band at 3400 cm^{-1} of the starting mPEG-OH **11** and the appearance of a new stretching band at 1731 cm^{-1} attributable to the C=O.

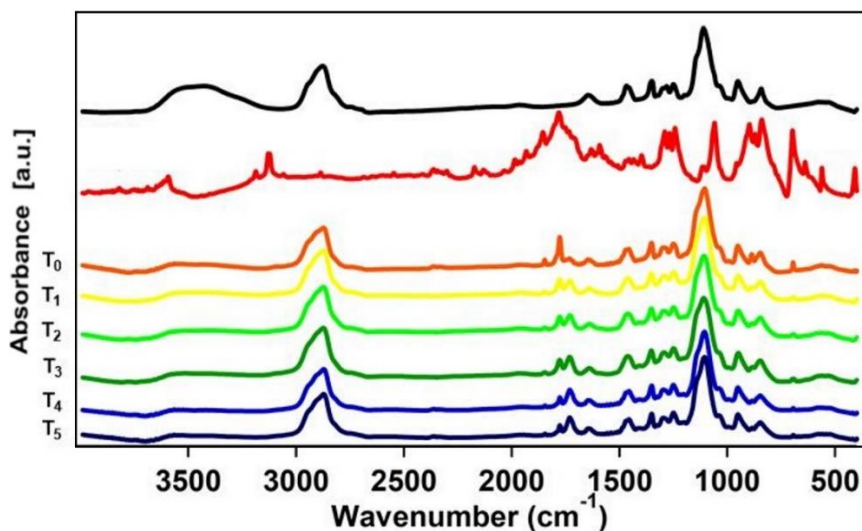


Figure 44. FT-IR spectra of the synthetic process at different stages of the esterification reaction (T_0 = starting time; T_1 = 1 h; T_2 = 3 h; T_3 = 9 h; T_4 = 12 h; T_5 = 16 h). of the compound **10** in comparison with the starting materials, **11** in black and the maleic anhydride in red, respectively.

1D NMR experiments confirmed the functionalization of the mPEG-OH **9** with the maleic anhydride to give the derivative mPEG-Mal **10**. In fact, the ^1H NMR spectrum of the product in **Figure 45** shows the presence of CH=CH signals at 6.36 and 6.53 ppm, while its ^{13}C NMR spectrum in **Figure 46** shows the presence of two resonances at 170.0 ppm and 167.1 ppm attributable to the carbonyl groups.

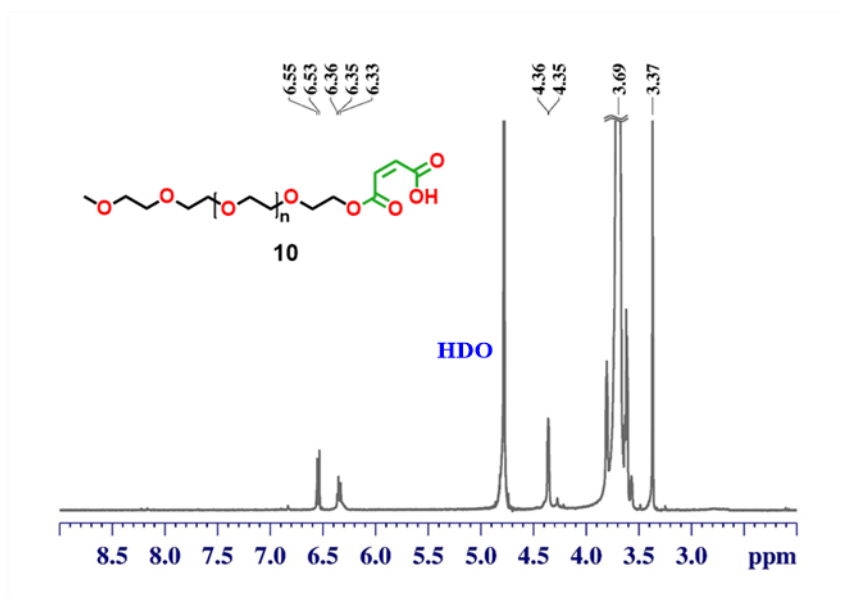


Figure 45. ^1H NMR spectrum (600 MHz, D_2O , 298 K) of derivative mPEG-Mal **10**.

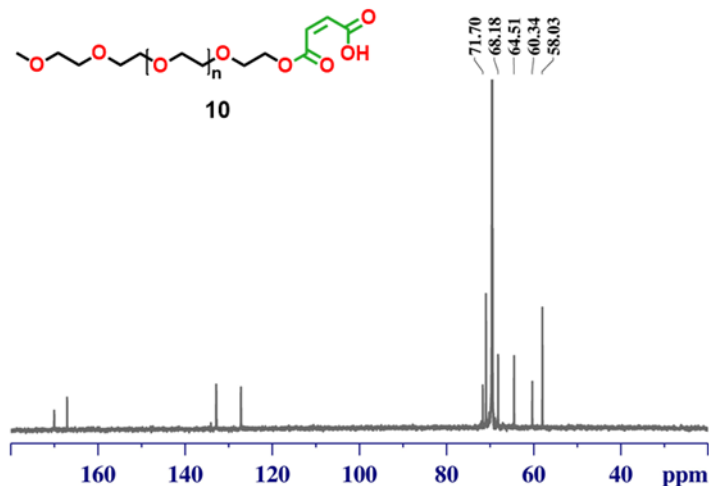


Figure 46. ^{13}C NMR spectrum (150 MHz, D_2O , 298 K) of derivative mPEG-Mal **10**.

The presence of the maleate at the end of PEG chain influences the chemical-physical properties of the PEG blocks as highlighted by DSC investigation. The enthalpy curve of derivative mPEG-Mal **10** also displayed in both the curves of heating and cooling, lower values of T_m and ΔH values, than the starting material: during the heating ramp the T_m was observed at 32.5 °C with a ΔH of 122.8 J/g (**Figure 47**, left in red), instead in the cooling ramp the phase transition occurred at 23.0 °C with a ΔH value of 109.7 J/g (**Figure 47**, right in blue).

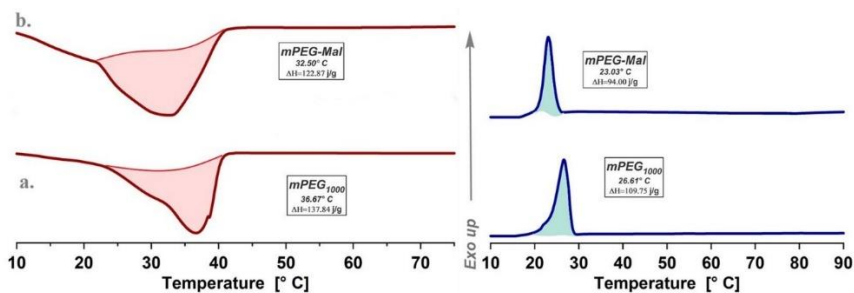


Figure 47. DSC heating (left, in red) and cooling (right, in blue) curves of a) mPEG-OH **11** and b) derivative mPEG-Mal **10**.

The TGA profile of mPEG-Mal **10**, was reported with the dark blue line in **Figure 48** was shifted to a higher temperature compared with the black line of mPEG-OH **11** and the light blue curve of maleic anhydride (**Figure 48**), indicating an increased thermal stability of mPEG-Mal **10** in comparison with the starting raw materials. Also, in the thermogram of mPEG-Mal **10** two steps were detected. The first degradation step was related to the maleate group and it was observed at 152.3 °C, instead the second one at 285.7 °C is caused by the degradation of the polymeric PEG-chain (**Figure 48**).

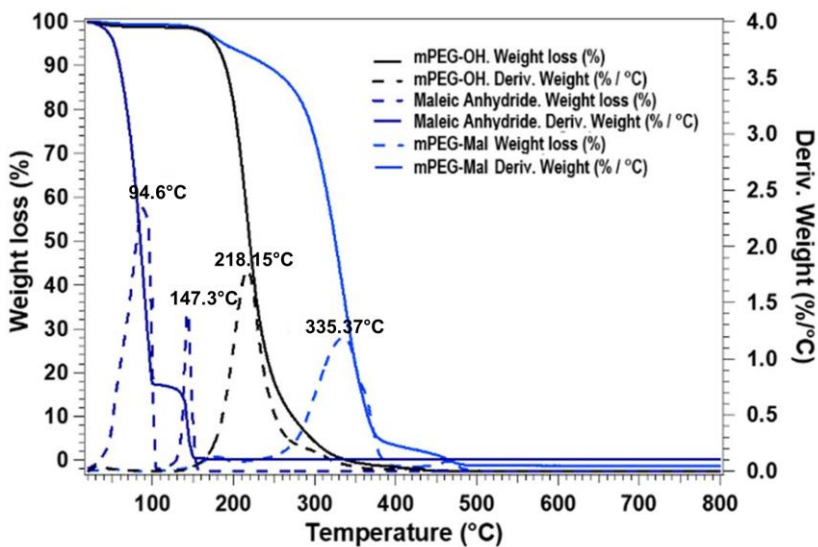


Figure 48. Thermogravimetric analysis of derivatives mPEG-Mal **10**, mPEG-OH **11**, and maleic anhydride.

4.3 Formation and characterization of pseudorotaxanes mPEG-Phth@- β CD 12, mPEG-OH@- β CD 13 and mPEG-OH@- β CD 14

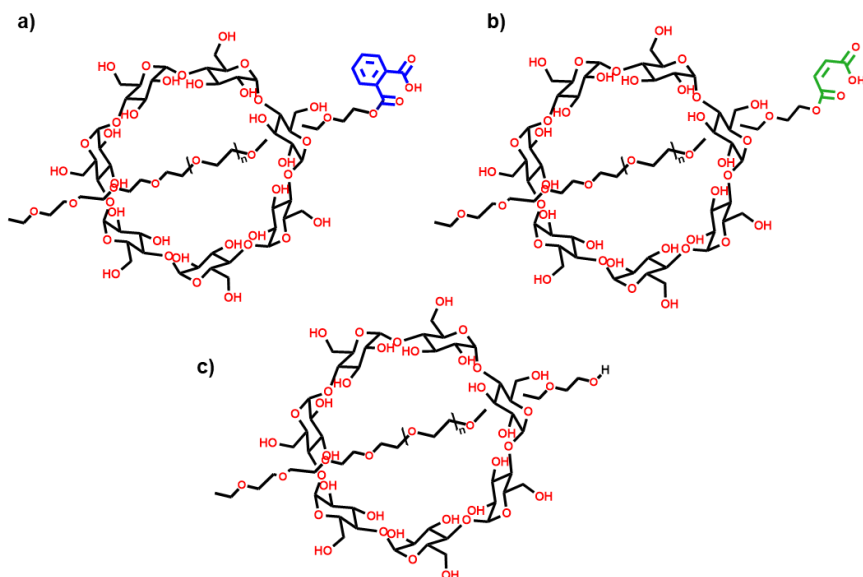
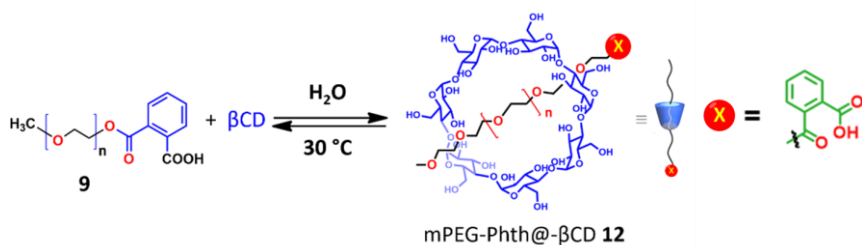


Figure 49. β -CD based pseudorotaxanes: a) mPEG-Phthal@- β CD 12, b) mPEG-Mal@- β CD 13 and c) mPEG-OH@- β CD 14.

The supramolecular systems studied in this thesis (**Figure 49**) were analyzed by ^1H NMR spectroscopy and thermogravimetric analysis and the results were corroborated by molecular dynamics (MD) simulations.

4.3.1 Formation and characterization of pseudorotaxane mPEG-Phth@- β CD 12



Scheme 6. Formation of the β -CD based pseudorotaxanes mPEG-Phth@- β CD **12**.

It was already reported in literature^{89,89} that it is possible to obtain β -CD inclusion complexes, by simple mixing of an appropriate guest in a β -CD-aqueous solution. For this reason, mPEG-Phth **9** and β -CD in D_2O was stirred in equimolar ratio at room temperature for 30 min and the resulting solution was analysed by 1H NMR (400 MHz, 298 K) (**Figure 50**). The formation of pseudorotaxane mPEG-Phth@- β CD **12** (**Scheme 6**) was confirmed by a complexation induced shift (C.I.S.) of the 1H NMR signals of the host and guest molecules.

In **Figure 50**, it is compared the ^1H NMR spectra of free mPEG-Phth **9** and β -CD **10** with the ^1H NMR spectrum of their 1:1 mixture. The formation of mPEG-Phth@- β CD complex **12** is strongly evidenced by the complexation induced shift (C.I.S.) of the anomeric signal of the β -CD **10** (**Figure 50**, in red) that upon complexation with **9**, experiences a $\Delta\delta = \delta_{\text{complex}} - \delta_{\text{free}}$ shift of -0.2 ppm. Readably, the $\text{OCH}_2\text{C}(\text{O})\text{O}$ -Phth protons of the PEG chain of **9** experienced a CIS of -0.2 ppm (**Figure 50**, in blue). Finally, the aromatic signals of the mPEG-Phth **9** experienced a marked downfield shift upon formation of pseudorotaxane (**Figure 50**).

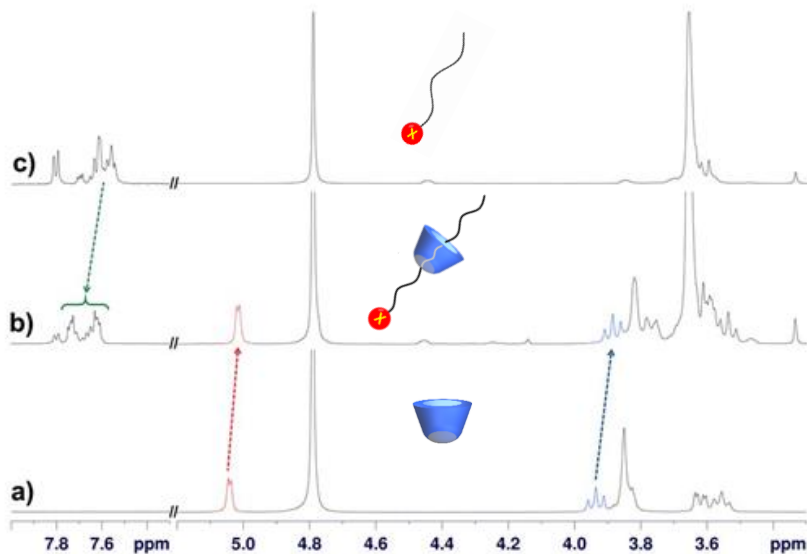


Figure 50. ^1H NMR spectra (600 MHz, D_2O , 298 K) of: (a) β CD; (b) an equimolar mixture ($1 \times 10^{-3}\text{M}$) of β CD and mPEG-Phth **9**; (c) mPEG-Phth **12**.

The structure of the pseudorotaxane **12** was analysed by MD simulation, carried by using YASARA software (version 20.8.23) and AMBER-14 force field.^{91,92} It was built a simulated system that consists of the mPEG-Phth@- β CD complex **12** and 8700 H₂O molecules in a periodic cubic box of size 6.5 nm/side. MD was simulated for 30 ns and snapshots were captured every 10 ps (**Figure 51 a**). We started with initial coordinates of β -CD that were taken by the Cambridge Crystallographic Data Centre (CCDC), while the starting structure of mPEG-Phth **9** in a full-extended conformation was obtained by MD calculations. The minimum-energy structures of mPEG-Phth@- β CD **12** defined by MD (**Figure 51, b-d**) displayed how the phthalate group and a portion of the PEG-axle **9** are inside the inner core of the host to give the final pseudorotaxane mPEG-Phth@- β CD **12**.

⁹¹ Krieger, E.; Vriend, G. YASARA View—Molecular graphics for all devices—From smartphones to workstations. *Bioinformatics* **2014**, *30*, 2981–2982.

⁹² Wang, J.; Wolf, R.M.; Caldwell, J.W.; Koilman, P.A.; Case, D.A. Development and testing of a general amber force field. *J. Comp. Chem.* **2004**, *25*, 1157–1174.

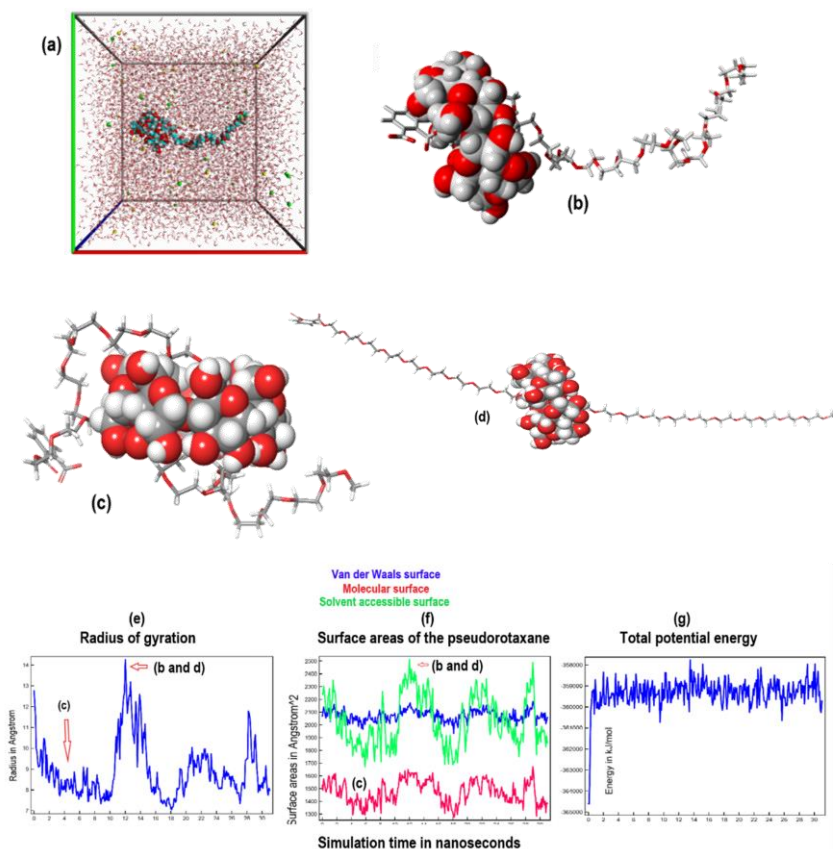


Figure 51. (a) The ray-traced illustration of the simulated complex. The simulation cell boundary is set to periodic. Atoms that stick out of the simulation cell will be wrapped to the opposite side of the cell during the simulation. (b and d) Minimum energy structures of pseudorotaxane mPEG-Phth@-βCD **12** calculated by MD simulation. (c) Instance of a structure of mPEG-Phth@-βCD complex **12** in which the mPEG-Phth chain **9** is all around the βCD macrocycle (closed conformation). (e)

Radius of gyration of the solute as a function of simulation time. (f) Van der Waals (blu), molecular (red), and solvent accessible area (A^2) (green) of pseudorotaxane mPEG-Phth@- β CD **12**.

The trajectory analysis (**Figure 51 e**) highlights that in a period of 10 to 16 ns the radius of gyration of the complex presents the maximum value that results into the pseudorotaxane structures in **Figure 51 b** and **d**. For this reason, in the minimum energy structures of mPEG-Phth@- β CD pseudorotaxane **12**, the polymeric chain adopts a fully extended conformation that has a high solvent accessible surface (**Figure 51 b** and **d**). Thus, in the fully extended conformation mPEG-Phth@- β CD pseudorotaxane **12** can establish H-bonding interactions with water molecules favouring the formation of the solvation water film that plays a crucial role for the dispersing abilities of SPs additives. (see illustration in **Figure 51**).

From the FT IR spectroscopy, it is possible to observe in **Figure 52** that the spectrum of compound **12** (dark green) is the combination of the characteristic functional groups of the starting materials, such as the presence of -OH stretching vibrations in the spectral region around 3600-3000 cm^{-1} due to the β -CD (**Figure 52**, red line), and the presence of the C=O stretching band of the ester group at 1735 cm^{-1} attributable to the polymeric axis **9** (**Figure 52**, light green line) of the mPEG-Phth@ β -CD **12** (**Figure 52**, dark green line).

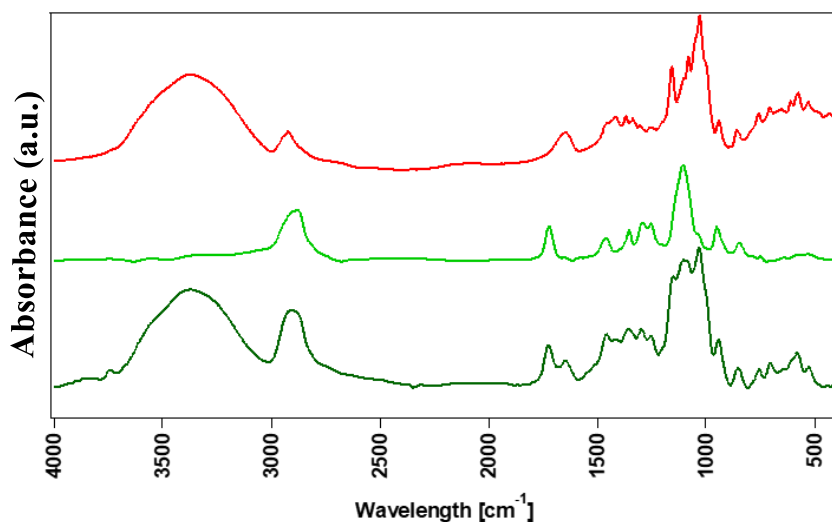


Figure 52. FTIR spectrum of mPEG-Phth@ β -CD **12** (dark green) in comparison with β -CD (red) and mPEG-Phth **9** (light green).

The **Figure 53** shows the TGA-DTA curves of the starting β -CD that presents three events of weight loss: the first step extended until 110 °C and showed the 10-15 % of mass loss due to the evaporation of superficial moisture of the compound. This step is followed by a weight loss of 10 % associated to the removal of moisture in the inner core of the macrocycle that occurs around 110 °C; the third step is observed around 307 °C that is attributed to the degradation phenomenon of β -CD.

The thermogravimetric analysis of the pseudorotaxanes displays a different profile in comparison with the curves of the free components mPEG-Phth **9** and β CD (**Figure 53**).

The initial stage of degradation (onset temperature) of the mPEG-Phth@ β -CD **12** starts at 182.2 °C and this value is very similar to the value of the only free guest mPEG-Phth **12**.

The thermogram of mPEG-Phth@- β CD pseudorotaxane **12** shows three slopes due to three events of degradation at $T_d = 182.2$ °C, $T_d = 298.0$ °C, and $T_d = 478.2$ °C. The values of temperature related to the maximum degradation rate are observed with the DTG curve: 199.5 °C, 318.4 °C and 496.1 °C, instead the free mPEG-Phth **9** shows the maximum degradation rate at 239.5 °C, 324.8 °C.

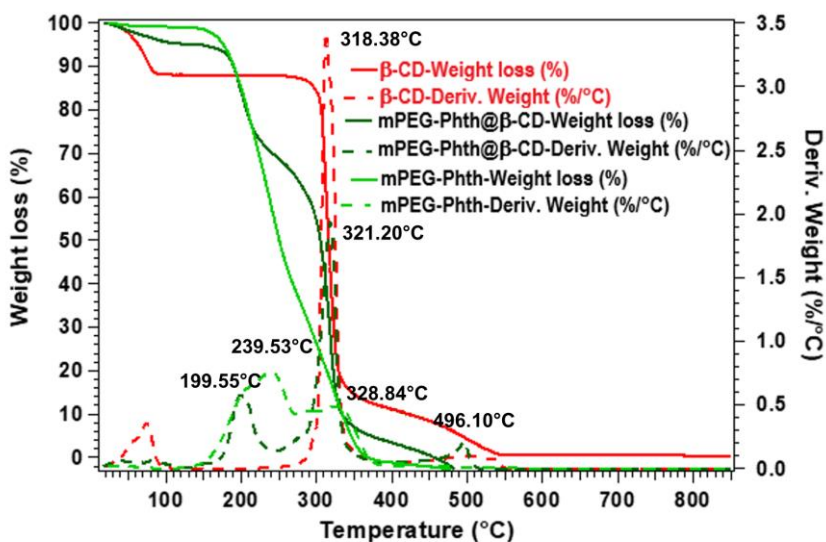


Figure 53. Thermogram of mPEG-Pthal@ β CD **12** (dark green line) in comparison with thermal profile of β -CD (red) and mPEG-Phth **9** (light green).

4.3.2 Formation and characterization of the pseudorotaxane mPEG-Mal@ β -CD **13** and mPEG-OH@ β -CD **14**

The pseudorotaxanes mPEG-Mal@ β -CD **13** and mPEG-OH@ β -CD **14** were obtained following the same procedure as for the first pseudorotaxane **12**. The threading of the polymeric chain into the cyclodextrin cavity was ascertained by a shift of the host and guest signals in the ^1H NMR spectrum due to the complexation equilibrium. In **Figure 54** it is shown the comparison between the proton spectra of free mPEG-Mal **10** and β -CD with the ^1H NMR spectrum of their 1:1 mixture. The formation of the mPEG-Mal@ β -CD complex **13** is highlighted by the shift of the anomeric signal of β -CD that shows a $\Delta\delta = \delta_{\text{complex}} - \delta_{\text{free}} = -0.2$ ppm. It was interesting to observe that the $-\text{CH}_2\text{C}(\text{O})\text{O}-$ protons of the mPEG-Mal polymeric chain **10** were up-field shifted. An interesting shift was also observed for the vinylic signals of the mPEG-Mal **10** guest that upon formation of the pseudorotaxane experienced a shift of 0.15 ppm.

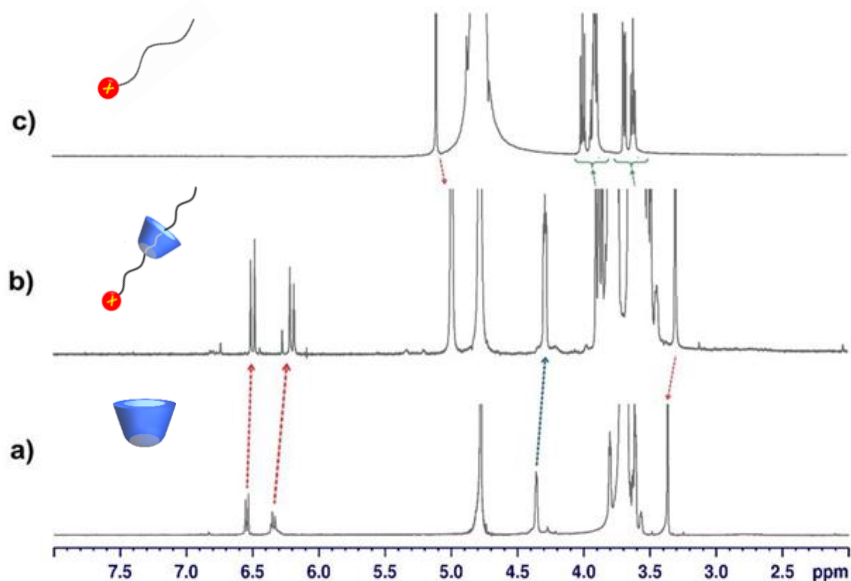


Figure 54. ^1H NMR spectra (600 MHz, D_2O , 298 K) of: (a) $\beta\text{-CD}$; (b) equimolar mixture of mPEG-Mal **10** and $\beta\text{-CD}$; (c) mPEG-Mal **10**. Marked the ^1H NMR signals that suffer a significant complexation induced shift upon formation of the pseudorotaxane.

The comparison of the infrared spectra of the starting materials and the final compound mPEG-Mal@ $\beta\text{-CD}$ **13** was reported in **Figure 55**.

The FT-IR spectrum of the mPEG-Mal@ $\beta\text{-CD}$ pseudorotaxane **13** shows a band at 3500 cm^{-1} due to the OH groups of the $\beta\text{-CD}$ (**Figure 55**, red line), at 1735 cm^{-1} is present the C=O stretching band of the ester group of mPEG-Mal **10** (**Figure 55**, light blue line) and of its C=C stretching at

1631 cm^{-1} in the curve of the pseudorotaxane mPEG-Mal@ β -CD **13** (Figure 55, dark blue line).

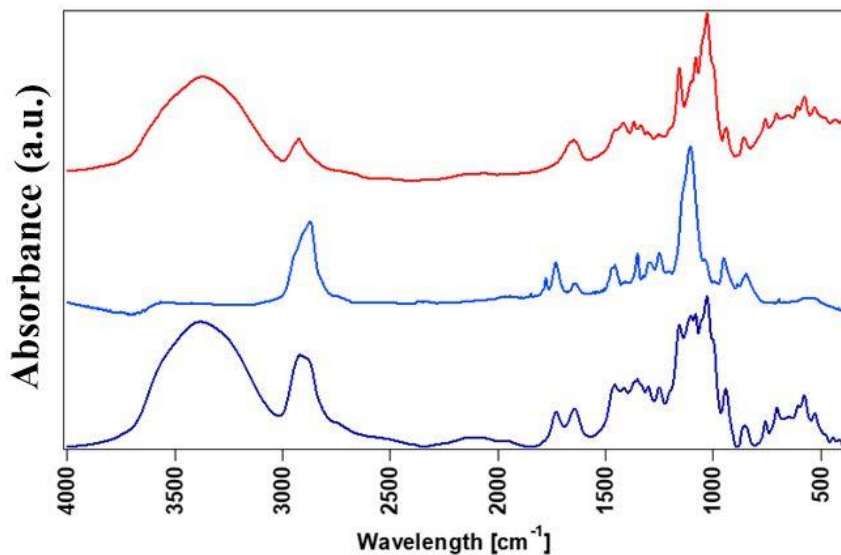


Figure 55. FTIR spectrum of mPEG-Mal@ β -CD **13** (dark blue) in comparison with mPEG-Mal **10** (light blue) and β -CD (red).

The thermal curve of the complex mPEG-Mal@ β -CD **13** is quite different from those of the free host and guest **10** (Figure 56). Around the solvent evaporation temperature of 100 $^{\circ}\text{C}$, the loss of surface and intrinsic macrocycle water is observed for complex **13**. After this step, the temperature of the onset of degradation can be defined, which occurs at

153.2 °C, which is very close to that observed for the free mPEG-Mal **10** alone.

From the thermogram analysis of the mPEG-Mal@- β CD pseudotaxane **13**, it is possible to distinguish three weight losses at: $T_d = 178.46$ °C, $T_d = 298.0$ °C, and $T_d = 478.2$ °C. The corresponding temperature values for the maximum degradation rate are calculated through the derivative of the weight loss and correspond to the temperatures of 233.73 °C, 320.49 °C and 494.5 °C.

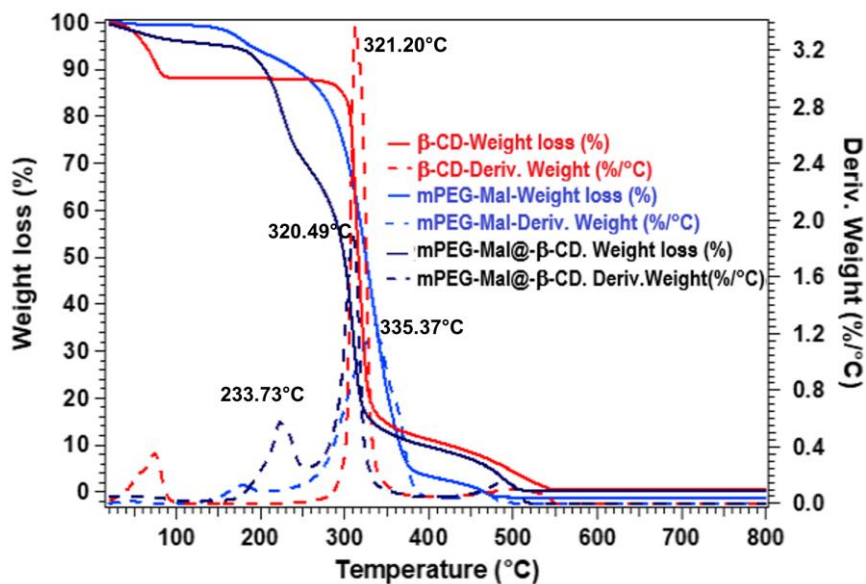


Figure 56. Thermogram of mPEG-Mal@ β CD **13** (dark blue line) in comparison with thermal profile of β -CD (red) and mPEG-Mal **10** (light blue).

4.3.3 Formation and characterization of pseudorotaxane **14**

In analogous way, the formation of the inclusion complex mPEG-OH@- β CD **14** was ascertained by ^1H NMR experiments (600 MHz, D_2O , 298 K.) (Figure 57), which evidenced a shift of the signal of OMe group upon addition of β CD (1 equiv), with a $\Delta\delta = (\delta_{\text{complex}} - \delta_{\text{free}}) = 0.03$ ppm.

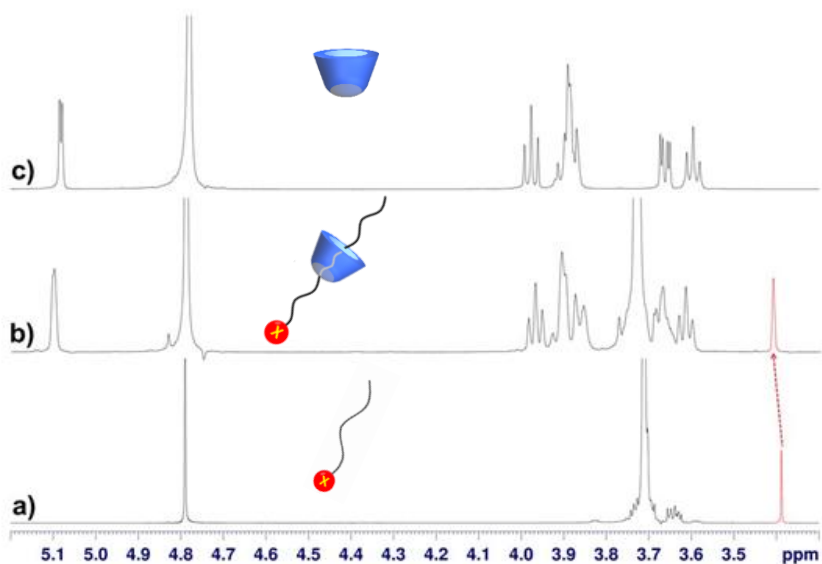


Figure 57. ^1H NMR spectra (600 MHz, D_2O , 298 K) of: (a) mPEG-OH **11**; (b) an equimolar mixture ($1 \times 10^{-3}\text{M}$) of β CD and mPEG-OH **11**; (c) β CD.

The comparison of the infrared profiles of the starting materials and the final compound **14** is reported into **Figure 58**. For the compound **14** (**Figure 58**, grey curve), it is possible to observe the bands attributable to the stretching of OH groups at 3500 cm^{-1} of both the β -CD and the mPEG-OH **11** (**Figure 58**, red and black line respectively) meanwhile the C-O and C-O-C stretching of the β -CD are observed in the spectral region of $1085\text{-}1050\text{ cm}^{-1}$ and $1150\text{-}1085\text{ cm}^{-1}$ (**Figure 58**, grey line).

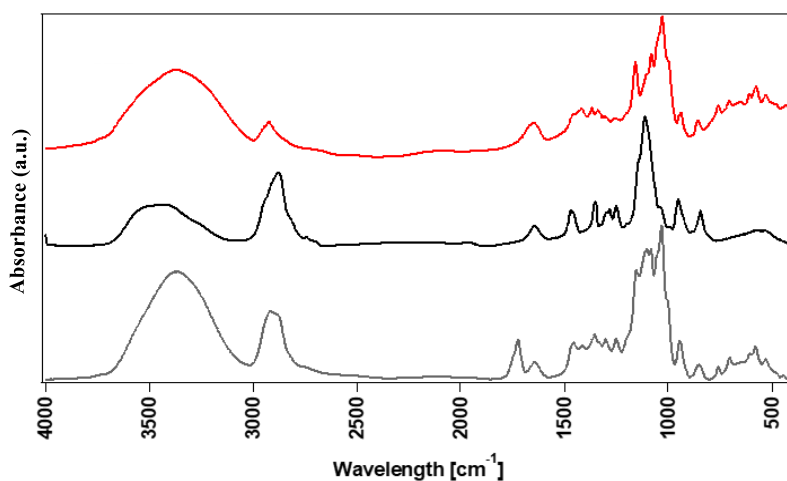


Figure 58. FTIR spectrum of mPEG@ β -CD **14** (grey) in comparison with mPEG₁₀₀₀ **11** (black) and β -CD (red).

To complete the characterization, the thermogram of the mPEG@ β -CD **14** was reported in the **Figure 59**. The thermic profile of the compound shows mainly two important degradation steps: the first is very close to the one observed with the mPEG₁₀₀₀ **11** and occurs at $176.08\text{ }^{\circ}\text{C}$

meanwhile the second one starts at 305.48 °C and involves the degradation of the β -CD that correspond to a T_{\max} of 182.11 °C and 318.96 °C respectively.

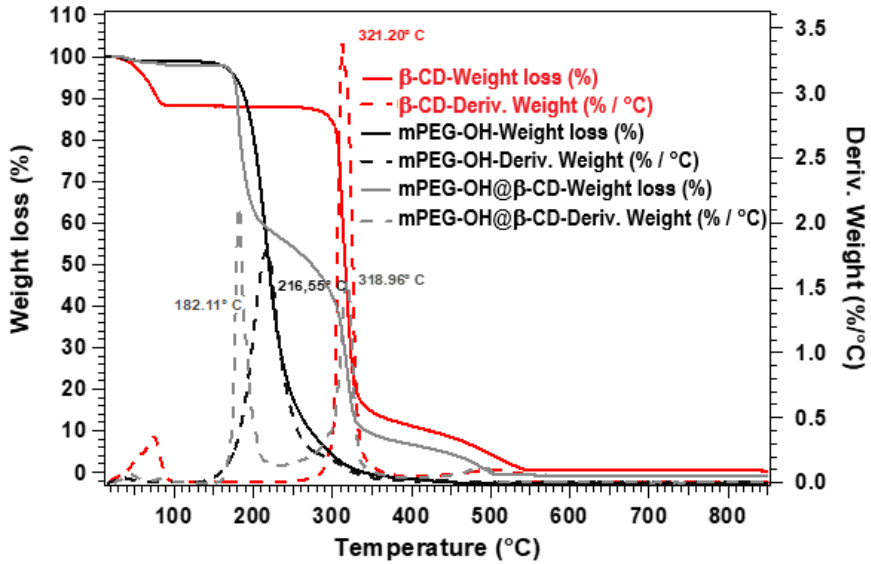


Figure 59. Thermogram of mPEG@ β CD **14** (dark green line) in comparison with thermal profile of β -CD (red) and mPEG₁₀₀₀ **11** (black).

4.4 Products testing of dispersing and retarding properties of derivatives

Therefore, with the aim to investigate the effects of the dosage of PEG@- β CD pseudorotaxanes on the fluidity of the cement mortar by slump tests

that were performed at different dosages of pseudorotaxane (i.e. 0.2-0.8 wt. % cement, bwoc), and with different mPEG-COOH/ β CD molar ratios (**Figure 60**) with the industrial test described in the section **1.5.1**.

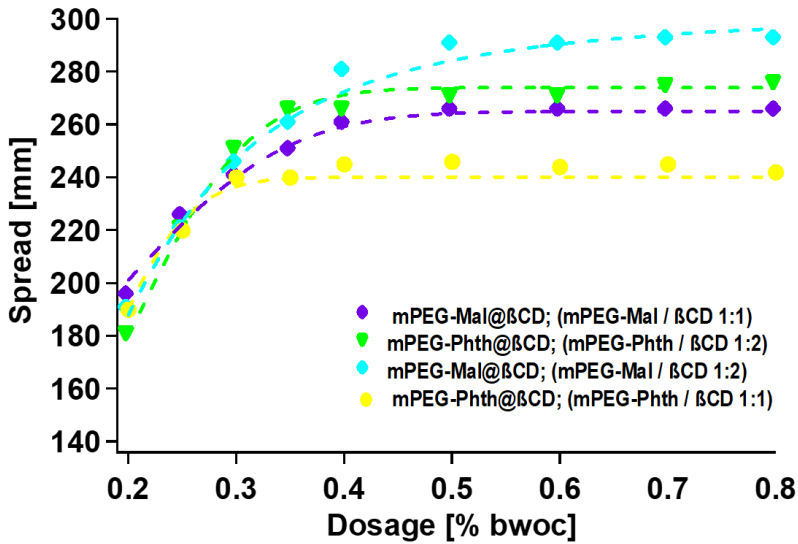


Figure 60. Slump tests measured at different dosage of mPEG-COOH@ β -CD pseudorotaxane at different mPEG-COOH/ β -CD molar ratio.

The aim of this study was to find the best mPEG-COOH/ β CD molar ratio in terms of performance. As observed in **Figure 60**, the fluidizing activity of the 1:1 mixture of mPEG-COOH and β CD was modest, whereas

superior fluidizing abilities were observed with the 1:2 mPEG-COOH/ β CD mixtures.

For example, at the dosage of 0.5 % for the 1:2 mPEG-Mal **10**/ β CD mixture, a spread value of approximately 290 mm could be obtained, which was much larger compared to 260 mm obtained with the 1:1 mPEG-Mal **10**/ β -CD ratio (**Figure 61**).

The higher flocculation efficiency of mixtures with an excess of β CD can probably be related to the formation of β CD-Ca⁺⁺ chelates.⁹³ Once the complex is adsorbed on the surface of the cement particles leading to the formation of Ca⁺⁺ chelates, the formation of a thick layer occurs, which together with the phenomenon of electrostatic repulsion between the cement particles, determines the dispersion process.

We also investigated the influence of the mPEG-COOH/ β CD mixtures in cement mortar by means of slump tests over time (**Figure 61**) to verify the efficiency of the pseudorotaxanes. The values of the spread diameters of cementitious pastes were measured over time (**Figure 61**) and were compared with those of the free host and guest components (β CD and mPEG-COOH derivatives) (**Figure 61**).

The trend of the spread over time (**Figure 61**) is named fluidification and is a typical property of SPs that guarantees the workability over time of the fresh cementitious mortars: therefore, estimating the fluidifying ability

⁹³ Liu, Y.; Zou, C.; Li, C.; Lin, L.; Chen, W. Evaluation of β -Cyclodextrin–Polyethylene Glycol as Green Scale Inhibitors for Produced-Water in Shale Gas Well. *Desalination* **2016**, *377*, 28–33.

of an additive means understanding how to classify it, if as a workability retainer and/or a water reducer.

For this reason, we evaluated the spread of cement mortars using a dosage of 0.5% bwoc (**Figure 61**) of the pseudorotaxanes and using a water/cement ratio of 0.5. Once the slurries were prepared, the evolution of the fluidity of the mortar was monitored over time up to 120 minutes by measuring the spread values of the cement paste diameters. As observed in the reported graph in **Figure 61**, the dispersion capacity of the individual components mPEG-Phth **12**, mPEG-Mal **10**, mPEG-OH **11** and β -CD is very low. From these results it was assumed that β -CD and the free derivatives of mPEG **9**, **10** and **11** individually cannot be used as fluidifying admixtures for concrete.

The situation changes for the equimolar mixture obtained between mPEG-Phth **9** and β -CD. It was measured an initial diffusion value of approximately 265 mm (**Figure 61**), that was much higher than that observed for the free components mPEG-Phth **9** (170 mm) and β -CD (240 mm). As the ratio of β -CD/mPEG-Phth **9** increased from 1:1 to 2:1, both a significant increase in the diffusion values at 280 mm and the fluidity retention of the mortar decreased more slowly than in the presence of β -CD alone. Similarly, studies were carried out for the pseudorotaxane mPEG-Mal@- β CD **13**, obtained by mixing mPEG-Mal **10** and β -CD in a ratio of 1:2, which showed excellent fluidity retention and high initial diffusion of about 290 mm. Thus, the mPEG-Phth@- β CD inclusion complex **12** provides excellent slump retention, in the first 60 min, the size

of the paste diameter slightly decreased from 280 to 270 mm and then reached after two hours the value of 240 mm.

Interestingly, mPEG-Mal@- β CD **13** shows better performance than mPEG-Phth@- β CD complex **12**: in fact, derivative mPEG-Mal@- β CD **13** shows better slump retention as the diameter of its mortar was reduced from 290 to 260 mm. Therefore, the loss of fluidity of the mPEG-Phth@- β CD **12** and mPEG-Mal@- β CD **13** pseudorotaxanes was 14.2% and 10.3% within 2 hours of the test. With the mPEG-OH@- β CD **14** inclusion complex produced by mixing mPEG-OH **9** and β -CD in both 1:1 and 1:2 ratios, initial spread values of 240 mm were observed, i.e. behaviour very similar to that of free β CD. This result led us to deduce that non-functionalized mPEG-OH **11** fails to improve the fluidizing properties of cementitious systems.

Finally, it can also be concluded that the carboxyl functionalization on the PEG chain may play a very important role in improving the adsorption capacity of pseudorotaxanes on cement granules.

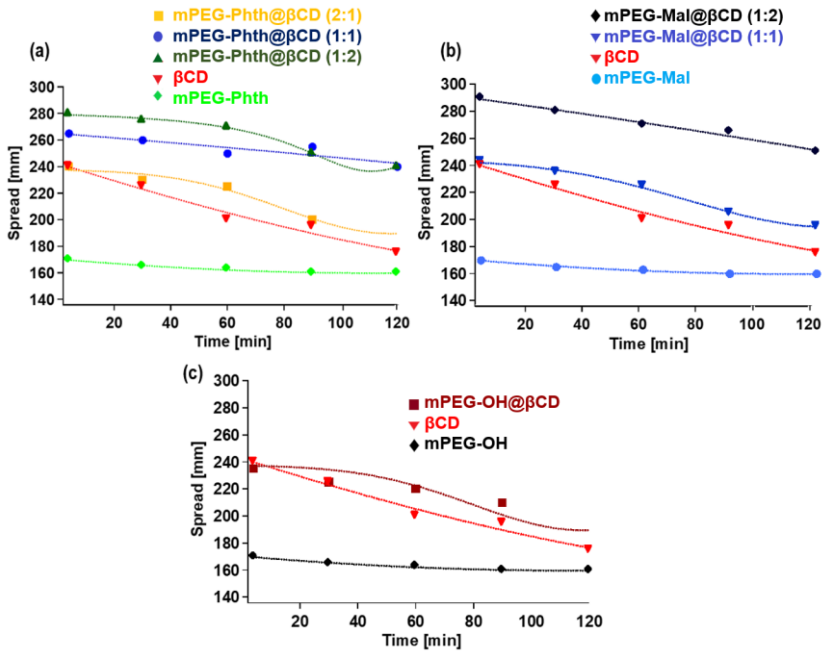


Figure 61. Spread test results of fresh cement mortars admixed with the pseudorotaxanes and their free constituents β -CD and mPEG-X with different molar ratios reported into the graphs: (a) mPEG-Phth@ β -CD **12**, mPEG-Phth **9**, and β -CD; (b) mPEG-Mal@ β -CD **13**, mPEG-Mal **10**, and β -CD; (c) mPEG-OH@ β -CD **14**; mPEG-OH **11**, and β -CD. (0.5 % bwoc) (w/c = 0.5).

A further investigation involved the study of the setting time of mPEG@- β -CD pseudorotaxanes. It is widely known in the literature⁹⁴ that sugar-

⁹⁴ Thomas, N. L.; Birchall, J. D. The Retarding Action of Sugars on Cement Hydration. *Cem. Conc. Res.* **1983**, *13*, 830–842.

based derivatives such as cyclodextrins show a retarding effect that slows down the concrete curing phase.

We have observed that the mPEG-Phth@- β CD **12** and mPEG-Mal@- β CD **13** pseudorotaxanes generate a retarding effect with an initial setting time of 8 hours.

The retarding effect was also observed in other CDs-based SPs, and is attributable to the steric hindrance⁵⁷⁻⁶⁰ of the macrocyclic skeleton. In addition, the ability of the CD to chelate Ca^{2+} prevents both the nucleation phase and solid-phase growth of the hydration products that produces a delay of the hydration of the cement (**Figure 62**).^{57-60,95}

Indeed, it is well known that the formation of a thick layer of long adsorption additives consisting of chelated Ca^{2+} macrocycles and a film of water of solvation (**Figure 62**) leads to a slowing down of the growth of hydration products.

⁹⁵ Meng, Y.; Liao, B.; Pang, H.; Zhang, J.; Song, L. Cyclodextrin-modified polycarboxylate superplasticizers as dispersant agents for multiwalled carbon nanotubes *J. Appl. Polym. Sci.* **2019**, *136*, 47311-47317.

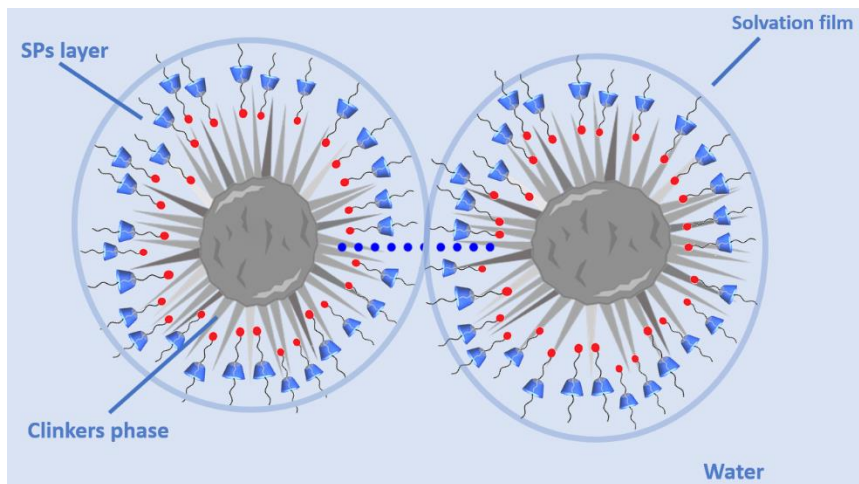


Figure 62. Sketch of the proposed dispersing mechanism with the pseudorotaxanes mPEG-COOH@ β -CD.

4.5 Conclusions

In conclusion in this chapter, an example of sustainable additives based on pseudorotaxanes for applications in the field of cement-based building materials is reported. Initially, the polymer chain end of Methoxy-PEG-OH was functionalized with phthalate and maleate groups using a sustainable one-pot, solvent-free synthetic approach.

The formation of pseudorotaxanes between mPEG-COOH and β CD was studied in solution both by ^1H NMR titration experiments and thermogravimetric studies. The fluidization capabilities of mPEG-COOH/ β CD mixtures were investigated by assessing the effect of dosage

and by monitoring the fluidization activity over time of fresh cementitious mortars.

The free components were analysed separately and do not show dispersant properties. On the other hand, 2:1 mixtures of mPEG-COOH/ β CD really show excellent dispersing properties as the initial spread values are very large, e.g. 280-290 mm. It was also pointed out that at the same time mPEG-COOH/ β CD mixtures also show a severe retarding effect with an initial setting time of 8 h.

However, due to the current interest focused on the synthesis of new sustainable dispersant and retardant additives, the information reported here plausibly represents preliminary studies that will be useful for the design of new supramolecular-based SPs with improved fluidization capabilities and setting time performance.

4.6 Experimental section with details for the synthesis of derivatives 9, 10, 11, 12, 13 and 14

All chemicals reagents grade were used without further purification and were used as purchased. Reaction temperatures were measured externally. NMR spectra were recorded on a Bruker Avance-600 [600 (^1H) and 150 MHz (^{13}C)], Avance-400 [400 (^1H) and 100 MHz (^{13}C)] or Avance-300 MHz [300 (^1H) and 75 MHz (^{13}C)] spectrometers. Chemical shifts are referenced to the residual non deuterated solvent peak (H_2O : ^1H NMR $\delta =$

4.78). IR, GPC and thermal analysis were recorded respectively with FT-IR 4100 Type A (JASCO Europe), with TGA Q500 (TA Instruments) and GPC Waters Alliance at the Research & Development Laboratory of BI-QEM SPECIALTIES S.P.A. DSC TA DSC25P instrument (Trios) was used for the calorimetric measurements. Each experiment consisted of a heating ramp from 5 °C to 150 °C at a rate of 10 °C/ min in the air atmosphere and at P = 1 atm.

Gel permeation chromatography (GPC) measurements were obtained with GPC Waters Alliance e2695 instrument equipped with a refractive-index RI 2414 detector and Waters Ultrahydrogel 120, 250, 500 in series columns. H₂O/NaNO₃/NaOH (0.1 M) was used as an eluent at a flow rate of 0.7 mL/min at 40 °C. Data processing was performed with Empower 3 software. The molecular weight of the polymers was calculated on the basis of PEG calibration curve (SI). KBr tablets were used to analyze samples for the FT-IR measurements.

4.6.1 Synthesis of derivative mPEG-Phth 9

mPEG-OH was melted at 60 °C and the powdered phthalic anhydride (38.1 g, 0.25 mol) was crushed into a fine powder and added into the reaction flask containing the liquid polymer (250 g, 0.250 mol). The entire reaction was mixed at 80 °C for 12 h at P = 1 atm to obtain the white waxy derivative mPEG-Phth **9**. ¹H NMR (600 MHz, D₂O, 298 K): δ 7.79-7.83 (overlapped, 2H, ArH), 7.66-7.71 (overlapped, ArH, 2H), 4.49 (m, -

OCH₂CH₂OCOPh), 3.88 (m, -OCH₂CH₂OR) 3.62-3.70 (PEG *backbone*), 3.37 (s, 3H, O-CH₃). ¹³C NMR (100 MHz, D₂O, 298 K): δ 171.9, 169.7, 132.5, 132.0, 129.2, 129.0, 69.8, 68.5, 65.5, 60.6, 58.3.

4.6.2 Synthesis of derivative mPEG-Mal 10

mPEG-OH was melted at 60 °C and the maleic acid (19.6 g, 0.21 mol) was crushed, added to the stirred polymer (200 g, 0.21 mol). After the complete solubilization of the raw materials, phenothiazine (0.05 %, w/w) and p-methoxyphenol (0.1 %, w/w) were placed into the reaction mixture. The stirred reaction was carried on at 100 °C for 12 h at P = - 0.8 bar, finally a red waxy product was collected. ¹H NMR (600 MHz, D₂O, 298 K): δ 6.54 (d, *J* = 12.2 Hz, 1H, RCO₂-CH=CH-R), 6.35 (d, *J* = 12.2 Hz, 1H, RCO₂-CH=CH-R), 4.35 (m, -OCH₂CH₂OCOR), 3.59-3.69 (PEG backbone), δ 3.37 (s, 3H, O-CH₃). ¹³C NMR (100 MHz, D₂O, 298 K): δ 170.0, 167.1, 132.9, 128.8, 71.7, 68.2, 64.5, 60.3, 58.0.

4.6.3 Formation of pseudorotaxane 12, 13 and 14

The synthesis of β-CD@mPEG-COOH pseudorotaxanes was performed under atmospheric pressure in a flask starting with the solubilization of β-CD (10 g, TS = 93 % wt, 8.8×10⁻³ mol) in 250 mL of deionized water.

After this step, the waxy axis (1/0.5; 1/1; 1:2 β -CD/mPEG-COOH molar ratio) was melted at 60 °C and then added to the mixing mixture of β -CD in water, and the resulting solution was stirred at 25 °C for 30 minutes. At the end, the water was evaporated to dryness under vacuum and the β -CD@mPEG-COOH pseudorotaxanes were then dried and stored at RT.

4.6.4 Differential scanning calorimetry (DSC)

DSC analysis was conducted using a DSC TA DSC25P instrument. Each measurement consisted first of a heating ramp from 5 °C to 150 °C at a rate of 10 °C / min in the oxidative atmosphere and at P = 1 atm that is followed by an equilibration state. At the end, a cooling step of 5 °C / min was applied to the samples until reaching 5° C.

4.6.5 FT-IR characterizations

FT-IR spectra of the axis **9**, **10** and **11** and of the pseudorotaxanes **12**, **13** and **14** were recorded on a Jasco V-630 Spectrophotometer preparing KBr pellets. mPEG-Phth **9** $\nu_{(C=O)} = 1731.76 \text{ cm}^{-1}$; mPEG-Mal **10** $\nu_{(C=O)} = 1728.87 \text{ cm}^{-1}$.

4.6.6 TGA / DTG Analysis of Derivatives the axis 9, 10 and 11 and of the pseudorotaxanes 12, 13 and 14

Thermogravimetric investigations were performed on a TA Instrument Q500 thermogravimetric analyser up to 900°C, 10°C/min ramp in air atmosphere.

4.6.7 Molecular Dynamics Simulation

Yasara Structure software (version 20.8.23) was used for the Molecular dynamics and AMBER 14 as force field.

A cubing box (6.5 nm) containing pre-equilibrated water molecules ($d = 0.997$ g/mL) at pH = 12 and 298 K was used as unit cell and MD were simulated for 10 ns and a snapshot was taken each 10 ps. The starting coordinates of β -CD were taken by The Cambridge Crystallographic Data Centre (CCDC), while the coordinates of the pseudorotaxane mPEG-Phth@ β -CD **12** were obtained by molecular mechanics calculation using a mPEG chain with a lower number of (-CH₂CH₂O-) units.

The minimized structures of the mPEG@ β -CD pseudorotaxane showed that the polymer chains interact through multiple H-bonds with water molecules.

In detail, it was observed that the pseudorotaxane complex is stabilized through a variable number 2-10 of hydrogen interactions between the PEG

axis and the host macrocycle, and the rest of the PEG axis is solvated by water.

From 4 ns to 7.5 ns, the simulation shows that the PEG chain is folded around the CD and because of this, an increase in the number of hydrogen bonds is observed.

Consistently, the number of solute-solvent interactions decreases and the radius of the complex is reduced to 0.7 nm.

The minimized energy structure of the mPEG-Phth@CD pseudorotaxane **9** shows the protrusion of the carboxyl function from the CD cavity, which through H-bonds interacts with the hydroxyl groups of the macrocycle partially covered by a section of the PEG chain (**Figure 63**).

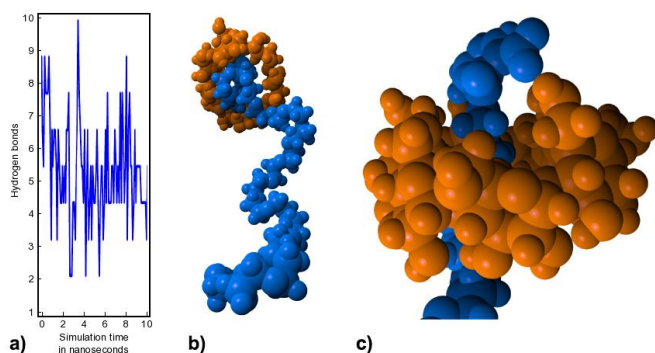


Figure 63. mPEG-Phth@-βCD **12** (a) Number of H-bonds as function of the simulation time. (b and c) Enlargements of the minimized pseudorotaxane system obtained during the MD simulation.

Moreover, the mPEG-Mal@- β CD pseudorotaxane **13** behaves in the same way as the derivative mPEG-Phth@CD **12**. The minimized structure of the mPEG-Mal@- β CD pseudorotaxane **13** displays even for this system that the polar group represented by the carboxylic function of the axle, can go through the macrocycle to forms H-bond interactions with the OH function of the β CD (**Figure 64**).

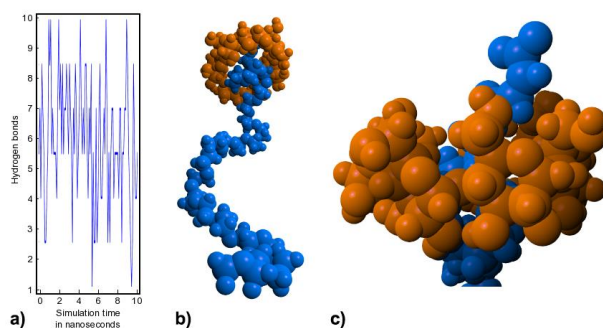


Figure 64. mPEG-Mal@- β CD **13**. (a) Number of H-bond interactions depending on the simulation time. (b and c) magnification of the minimized pseudorotaxane structure obtained during the MD simulation.

4.7 Applicative workability tests of derivative **12**, **13** and **14** on fresh mortar

4.7.1 Mortar test materials and lab-based equipment

The cement used into this work was an Ordinary Portland Cement, CEM IIA 42.5 RLL (Italcementi) in compliance with UNI EN 197-1, instead

the sand (Normensand) used was the CEN Standard Sand to follow the DIN EN 196-1 for the slump and Vicat tests. The performance of the cementitious system was ascertained through tests, according to the current laws. The water content of all the specimens was defined at 105 °C for 30 minutes to calculate the dosage of additives (moisture analyzer model name Crystaltherm Gibertini).

The measurement of the spread diameters was determined with the Slump test setting the w/c at 0.5, in accordance with ASTM C143 ("Standard Test method for slump hydraulic-cement concrete") and EN196-1:2016 (Methods of testing cement, Part 1 - Cap. 6: Preparation of mortar) / EN 480-1:2011 (Admixture for concrete, mortar and grout - Test methods part 1: Preparation of control mortar). The lab accessories used were an automatic mortar mixer model E093 (Matest S.p.A.) conforming to ASTM C305M specifications ("Mechanical mixing of hydraulic cement pastes and mortars of plastic consistency") and an automatic flow table model M092 (LBG srl) conforming to ASTM C230M specifications ("Standard Specification for Flow Table for Use in Tests of Hydraulic Cement").

The Vicat apparatus was used to define the setting time for all the mortar doped with the 0.5% bwoc of samples (100% active), setting the w/c at 0.5 to follow the standards ASTM C191 ("Standard test method for time of setting of hydraulic cement by Vicat needle") and EN196-1:2016 / EN 480-2:2011 (Admixture for concrete, mortar and grout - Test methods part 2: Determination of setting time).

4.7.2 Mortar tests

Cementitious pastes were realized following these conditions: 450 g of CEM II 42.5 R; 225 g tap water ($w/c = 0.5$); 1350 g CEN standard sand; 0.5 % (bwoc) of the additive (100 % active). The standard mixing program requires a 4-minute mixing schedule (according to ASTM C305: 30s low mixing, 30s high mixing, 2 minutes rest, 1 minute at high mixing). All the lab equipment, the room and the materials used should have the temperature set at 20.0 ± 2.0 °C. Mortar was assested with 15 strokes of the automatic flow table. After mixing, spread diameters were recorded three times to report the average values. The measurement of the spread values was performed at specific time lapse: after 4', 30', 60', 90 and 120'. To evaluate the dosage-dependent effect, pastes were doped with a range of percentage of active to measure the initial spread diameters.

The Vicat apparatus was employed to define the setting time over a defined time window to analyse SPs trends. The initial setting time was defined at the point where the penetration of the Vicat needle into the fresh mortar was 4 ± 1 mm, in accordance with ASTM C191 specifications.

Chapter 5: Modified carboxymethylcellulose-based scaffolds as new potential ecofriendly superplasticizers with a retardant effect for mortar: from the synthesis to the application

These studies were the object of the abroad research that was carried out during the research activities at the Bauhaus Universität of Weimar. The investigations were based on modified complex carbohydrates and on their use as new potential sustainable SPs for cement-based materials. All the investigations were done under the *Prof. Andrea Osburg's* supervision, *Deputy Head of the F. A. Finger Institute for Building Materials Engineering at the Chair of Construction Chemistry and Polymeric Materials ChemPoWer of the Bauhaus-Universität in Weimar, Germany.*

5.1 General overview

Carboxymethylcellulose (CMC) is an ecofriendly compound that is obtained from the modification of cellulose as a by-product of industrial processes in sugar companies (**Figure 65**).⁹⁶ This interesting material is a complex carbohydrates⁹⁷ that consists of modified glucopyranose units in

⁹⁶ Alizadeh, A.S.; Mousavi, M.; Labbafi, M. Synthesis and Characterization of Carboxymethyl Cellulose from Sugarcane Bagasse. *J. Food Process. Technol.* **2017**, *8*, 1-6.

⁹⁷ Nevell, T. P.; Zeronian, S. H.; Cellulose Chemistry and Its Applications; Eds.; Ellis Horwood series in chemical science; E. Horwood; Halsted Press: Chichester, West Sussex, England, New York, 1985.

which some hydrogen atoms of the hydroxyl groups are substituted by carboxymethyl moieties with a different degree of substitution (**Figure 65**). The glucopyranose monomers are joined together through β -glycosidic bonds into the final sugar-based polymer. Cellulose⁹⁸ is one of the most abundant complex carbohydrate on earth and for its availability different cellulose derivatives are used in several commercial sectors.

The use of cellulose-based derivatives is very wide and the applications range extends from the food sector to the pharmaceutical, cosmetical, electronic and engineering sectors.⁹⁹ The role of nanocellulose as an additive in food has been highlighted but only with the development of low-cost production processes its application in food companies has been possible. After exploring its used such as emulsifier or functional food ingredient¹⁰⁰, it was highlighted its role in material sciences as functional recyclable packaging.¹⁰¹

Recently, cellulose has found applications also into the civil engineering field as shown by Wicklein et al. that in 2015¹⁰² studied to enhance the

⁹⁸ Aspinall, G. O. *The Polysaccharides*. 2: Ed.; Molecular biology; Acad. Press: New York, 1983.

⁹⁹ De Amorim, J.D.P., De Souza, K.C., Duarte, C.R. Plant and bacterial nanocellulose: production, properties and applications in medicine, food, cosmetics, electronics and engineering. A review. *Environ Chem Lett* **2020**, *18*, 851–869.

¹⁰⁰ Gómez, H.C.; Serpa, A.; Velásquez-Cock, J.; Gañán, P.; Castro, C. Vegetable nanocellulose in food science: a review. *Food Hydrocoll* **2016**, *57*, 178–186.

¹⁰¹ Gómez H., C.; Serpa, A.; Velásquez-Cock, J.; Gañán, P.; Castro, C.; Vélez, L.; Zuluaga, R. Vegetable Nanocellulose in Food Science: A Review. *Food Hydrocolloids* **2016**, *57*, 178–186.

¹⁰² Wicklein, B.; Kocjan, A.; Salazar-Alvarez, G.; Carosio, G.; Camino, G.; Antonietti, M.; Bergstrom, L. Thermally insulating and fire-retardant lightweight anisotropic foams based on nanocellulose and graphene oxide. *Nat. Nanotechnol.* 2015, *10*, 277–283.

energetical properties of buildings using materials made from renewable resources. It was highlighted that suspensions based on cellulose can show better insulating properties than traditional polymer-based insulating materials in the building materials.¹⁰²

Moreover, Hisseine et al. in the 2019¹⁰³ discussed another application of cellulose derivative into concrete: it was analysed the effect of the replacement of structural materials with cellulose filaments instead of the conventional synthetic fibres employed nowadays.¹⁰³ Analysis of the results showed that properties such as compressive strength, elasticity and toughness of the cementitious systems were very promising. In detail, it was observed that the cellulose filaments enhanced the mechanical performances of cement-based matrices at the nano/micro-level that were investigated after their introduction. These nanofibers materials increase the hydration grade of silicate clinker phase, improving the final mechanical properties.

CMC is very versatile and for this reason is one of the most intriguing and widely used backbones among all the derivatives commonly used.¹⁰⁴

¹⁰³ Hisseine, O.A.; Wilson W.; Sorelli L.; Tolnai, B; Tagnit-Hamou, A. Nanocellulose for improved concrete performance: a macro-to-micro investigation for disclosing the effects of cellulose filaments on strength of cement systems. *Constr. Build. Mater.* **2019**, 206, 84–96.

¹⁰⁴ Qiu, X.; Hu, S. “Smart” Materials Based on Cellulose: A Review of the Preparations, Properties, and Applications. *Materials* **2013**, 6, 738-781.

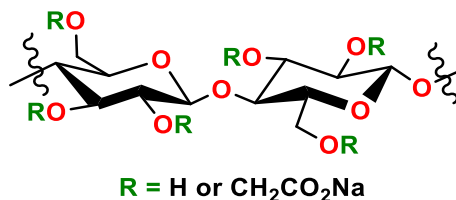


Figure 65. Chemical structure of carboxymethylcellulose.

As introduced in the **Chapter 4**, many studies have been conducted to highlight the polluting effect of the main classes of SPs that are on the market nowadays. After their modification, a cutting-edge application of polysaccharides is to use them as additives in cement-based mortar, called superplasticisers, to provide more sustainable construction materials for the engineering field.

It is already known since 1996 that SNFs can affect the environment differently as discussed by Gälli et. al.¹⁰⁵ For example their synthetic process requires the use of toxic products such as formaldehyde, which is a known carcinogenic agent, furthermore these products affect the quality of wastewater that if mistakenly conveyed in the purification systems damaging the surrounding environment to create a danger for human and environmental health.

The growing concern of the environmental impact of the petrochemical additives currently on the market has led to the aim of obtaining new

¹⁰⁵ Galli, R.; Kiayias, G. Environmental Impact of Superplasticizers. *R.B.M.* **2014**, 2, 427-448.

biodegradable dispersing agents for mortar and concrete mixtures with high performances comparable to the ones of additives such as the PCEs.

The search for new additives with low environmental impact could also reduce the use of non-renewable sources. Using starting materials such as carbohydrates is a promising strategy as already observed from literature studies.¹⁰⁶ Biodegradable admixtures may exhibit different properties on mortar and concrete.

In literature, numerous examples of carbohydrates have been investigated such as anionic cellulose derivatives like hydroxyethyl cellulose, carboxymethyl cellulose, hydroxypropyl cellulose or various starch esters and microbial exopolysaccharides (i.e. pullulan, dextran, curdlan), alginates, marine polysaccharides (such as agar) and plant exudates (locust bean gum) for the development of bio-based additives.^{107,108,109}

One interesting example of the employment of carbohydrate-based SPs was reported by Lasheras-Zubiato et al. in 2012.¹¹⁰ These studies showed the different effect on the properties of fresh concrete that can give the ionic and non-ionic groups of chitosan derivatives, a carbohydrate with

¹⁰⁶ Vieira, M. C.; Klemm, D.; Einfeldt, L.; Albrecht, G. Dispersing Agents for Cement Based on Modified Polysaccharides. *Cem. Concr. Res.* **2005**, *35*, 883–890.

¹⁰⁷ Veen, U.; Lamberti, V.J.M.A.; Bleeker, I.P. Etherified polysaccharide and concrete comprising the same, Wo Pat. Appl. 1999055632 **1999**, 1 – 47.

¹⁰⁸ M. Hibino, Effect of viscosity enhancing agent on self-compactibility of fresh concrete, *Am. Concr. Inst. SP-195* **2000**, 305 – 320.

¹⁰⁹ Glenn, G.M.; Miller, R.M.; Orts, W.J. *Moderate strength lightweight concrete from organic aquagel mixtures* Ind. Crops Prod. **1998**, *8*, 123 – 132.

¹¹⁰ Lasheras-Zubiato, M.; Navarro-Blasco, I.; Fernández J.M.; Álvarez, J.I.; Effect of the addition of chitosan ethers on the fresh state properties of cement mortars. *Cement Concrete Comp.* **2012**, *34*, 964-973.

thickening properties that is second to cellulose for its abundance. It has been observed how chitosan derivatives can modify the working life of mortars and can act as thickening agents, furthermore, being water solubility that is an unavoidable parameter for a superplasticizer, the solubility of such compounds has been improved by introducing polar functional groups.

Another example of sugar-based additives was introduced very recently in the literature through the studies carried on by the Prof. Andrea Osburg's group¹¹¹ where I spent my research period abroad. The performances of starch-based superplasticisers were investigated for their rheological behaviour on mortar and their effect on the clinkers hydration processes.

In their work, it was demonstrated the importance to hydrolyse starch (**Figure 66**) and to implement the anionic charges on it to obtain efficient dispersant SPs for mortar systems. Indeed, the molecular weight and the amount of introduced anionic groups of these biopolymers have been discovered as key parameters for the thickening or fluidifying properties of cementitious matrices to which these additives are added. Furthermore, it was also observed that these additives were also able to bind the first hydration product of the clinkers, affecting the hydration rate of cement that resulted into a retardant effect associated with these compounds.

¹¹¹ Partschefeld, S.; Osburg, A. Synthesis of dispersing agents from starch – Influence on rheological properties and early age hydration of OPC. *Constr. Build. Mater.* **2020**, *240*, 17913.

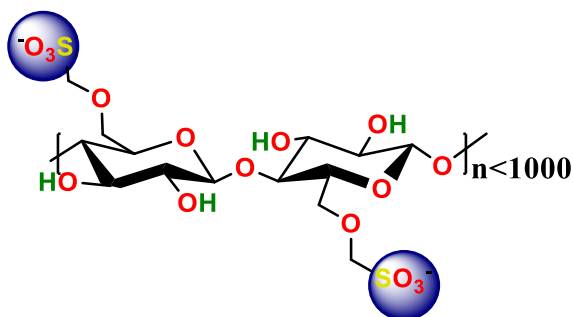


Figure 66. Starch superplasticizers.^{111,113}

In this study,⁴ we have focused our attention on design of a novel cellulose-based SP. Indeed, after developing SPs based on cyclodextrin inclusion complexes (**Chapter 4**), we set ourselves the goal of further expanding the pool of renewable compounds with the CMC to supply the petrochemical ones.

So in this study, we have produced the CMC-based SPs in **Figure 67** slightly modifying the procedure already introduced into literature by Fox et al,¹¹² and Partschefeld and Osburg.^{111,113} The first step was to carry on the hydrolysis reaction of the starting carboxymethylcellulose at different temperatures to obtain several hydrolysed derivatives. Then the synthesized compounds were successively sulfoethylated for different times of reaction to explore the best conditions of reaction to obtain the

¹¹² Fox, J.D.; Robyt, J.F. Modification of starch granules by hydrolysis with hydrochloric acid in various alcohols, and the formation of new kinds of limit dextrans, *Carbohydr. Res.* **1992**, 227, 163–170.

¹¹³ St. Partschefeld, A. Osburg. Bio-Based Superplasticizers for Cement-Based Materials. International Congress on Polymers in Concrete, ICPIC. 2018, 77– 82.

most dispersant compounds in aqueous solution (**Figure 67**). Finally, the materials obtained was investigated by slump tests in order to study their dispersing properties.

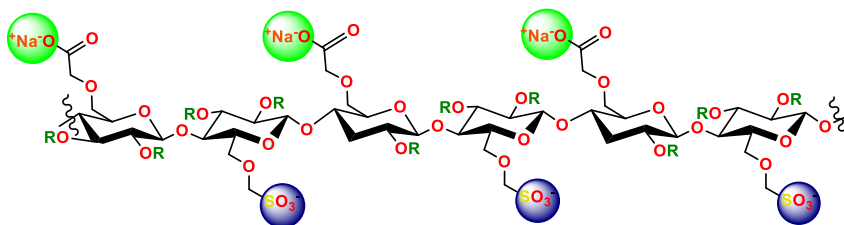
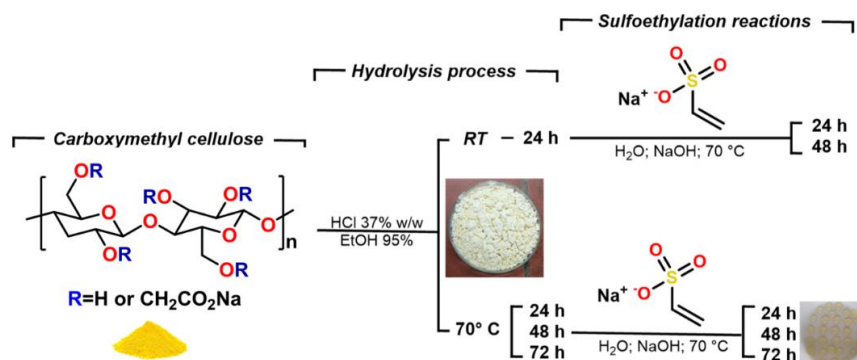


Figure 67. Synthetized CMC SPs.

5.2 Synthesis of new water-soluble carboxymethylcellulose-based SPs



Scheme 7. Overview of the synthesis workflow.

Specimens	Temperature of hydrolysis (°C)	Time of hydrolysis (h)	Time of sulfo-ethylation at 70 °C (h)
15	RT	24	24
16	RT	24	48
17	70 °C	24	24
18	70 °C	48	24
19	70 °C	48	48
20	70 °C	72	72
21	70 °C	72	72

Table 4. Library of synthesized CMC SPs obtained with several temperature and times of hydrolysis and sulfo-ethylation.

The development of these additives in **Scheme 7** was divided into two steps by revisiting the procedure previously reported^{111,113}: the first one was to modify the size of polymer (a) and the second one to functionalize it with sulfonic groups to amplify the interaction with the cement surfaces (b). For the depolymerization step of the CMC, first it was swelled the powder into ethanol solution and successively was performed the acid hydrolysis to obtain a lower value of M_w . In detail, the reactions of hydrolysis were performed first at room temperature, stopping the degradation at defined times (see **Table 4**). In addition, new reaction of hydrolysis was performed at 70 °C (see **Table 4**).

The degraded compounds were solubilized into an aqueous solution of sodium hydroxide and after the addition of sodium vinylsulfonate

(**Scheme 7**), the mixture was stirred for different times at 70 °C (see **Table 4**. Library of synthesized CMC SPs obtained with several temperature and times of hydrolysis and sulfo-ethylation). The goal was to investigate the optimal reaction conditions to increase the water solubility of the material.

Each product in **Table 4** was analyzed with different investigations reported into the experimental section.

5.3 Products testing the dispersing and retarding properties of derivatives

The investigations of the dispersing, retarding and hardening behaviour of hydrolysed and sulfoethylated compounds were investigated by performing applicative tests on mortar at the Laboratory of building chemistry and polymeric materials of the Department of Civil Engineering of the Bauhaus University of Weimar.

The thixotropic properties of the cement slurries doped with the synthesized products were studied through rheological analysis to understand the changes involving the dynamic viscosity and the shear stress of the pastes using rheometer (**Figure 68**). The investigations started with the checking of the rheological features of the blank and of the cement doped with the degraded starting materials (additives **15** and **16**), biodegradable backbones hydrolysed at room temperature and sulpho-ethylated for 24 h and 48 h at 70 °C, respectively. It was observed

that the CEM II 42.5 R doped with the additives **15** and **16** (**Scheme 7**) behave as thickening agents because the grout so obtained showed high values of shear stress and dynamic viscosity, so the measurements were not recorded.^{111,114,115,116}

Better results were obtained arising the temperature of hydrolysis from room temperature to 70 °C (**17**, **18**, **19**, **20**, **21**): for example in **Figure 68** it is possible to observe the rheologic properties of the derivative **20** that shows the ability to gradually reduce both the shear stress (**Figure 68** a. full graph, b. enlargement) and the dynamic viscosity (**Figure 68** c. full graph, d. enlargement) of the CEM II 42.5R cement but its profile is still too close to the blank. It was so empirically confirmed how the rheological parameters are strongly influenced by the molecular weight of the material and the ionic groups anchored on the scaffolds, confirming that these two parameters can strongly influence both shear stress and dynamic viscosity values as reported in literature.¹¹¹

After prolonging the hydrolysis process from 48 to 72 h, these parameters were improved for the sample **21**. In detail, the graph in **Figure 68** displays how the sample **21**, obtained from longer hydrolysis and sulpho-ethylation times (72 h), showed a lower value of shear stress and dynamic viscosity (**Figure 68**).

¹¹⁴ Lachemi, M.; Hossain, K.M.A.; Lambros, V.; Nkinamubanzi, P.C.; Bouzoubaâ, N. Performance of new viscosity modifying admixtures in enhancing the rheological properties of cement paste. *Cem. Concr. Res.* **2004**, *34*, 185-193.

¹¹⁵ Papo, A.; Piani, L. Effect of various superplasticizers on the rheological properties of Portland cement pastes. *Cem. Concr. Res.* **2004**, *34*, 2097-2101.

¹¹⁶ Lapasin, R.; Longo, V.; Rajgelj, S. Thixotropic behaviour of cement pastes. *Cem. Concr. Res.* **1979**, *9*, 309-318.

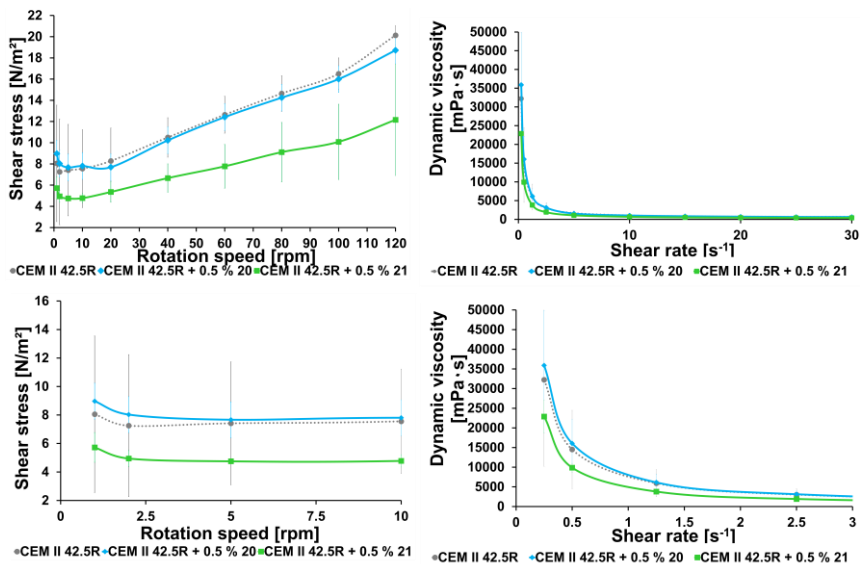


Figure 68. Studies of the shear stress in dependence on rotation speed and of the dynamic viscosity [(a) full graph, (b) enlargement], (c) full graph, (d) enlargement] of the cement CEM II 42.5R at $w/c = 0.5$ with 0.5 % of additives. Test conditions: 0.5 % bwoc of SPs; $w/c = 0.5$; CEMIIA42,5RLL = 30 g (EN197-1); deionized H₂O = 15 g.

Cement particles can adsorb negatively charged superplasticizers because their surface is composed of different mineral phases whose counter-ions can lead to the adsorption of SPs molecules on the cement grains.¹¹⁷ When

¹¹⁷ Zhang, Y.R.; Kong, X..M.; Lu, Z.B.; Lu, Z.C.; Hou, S.S. Effects of the Charge Characteristics of Polycarboxylate Superplasticizers on the Adsorption and the Retardation in Cement Pastes. *Cem. Concr. Res.* **2015**, *67*, 184–196.

the cement comes into contact with water, the surface is heterogeneously charged and clinker phases can bind additives.

We carried on studies of the aqueous phase of the cement by adsorption measurements by the phenol-sulphuric acid method¹¹⁸ and all the synthesised SPs were not detected in the supernatant phase, demonstrating that these additives are able to fully bind mineral surfaces through the electrostatic interaction between the cement surface and the -SO₃ groups.

Adsorption was also facilitated by the structure of the polymer, which with its anionic carboxylate groups can chelate Ca²⁺ on the surface of the cement. This leads to the formation of a layer of SP on the surface that cannot encounter water, slowing down the hydration process and altering the growth and morphology of hydration products.⁹⁴

In **Figure 69** the calorimetric studies were reported and they show the effect of the cellulose-based superplasticizer (w/c ratio 0.5, by addition of 0.5 wt % bwoc of additives) on the kinetics of the hydration of CEM II/A-LL 42.5 R in early stage by isothermal calorimetry.

Additives can sensitively influence the hydration reactions, indeed the only reference presents a dormant period of 2.5 h (**Figure 69**, grey line). The rate of the hydration and the heat release profiles showed a longer

¹¹⁸ Cuesta, G.; Suarez, N.; Bessio, M.I. Quantitative determination of pneumococcal capsular polysaccharide serotype 14 using a modification of phenol-sulfuric acid method. *J. Microbiol. Methods* **2003**, *52*, 69–73.

quiescent period when carbohydrate-based SPs are added to the pastes, as already studied in the literature.

Analysis of the most significant results obtained and reported in **Figure 69** (black line) shows that cellulose extends the dormancy period because it is able to strongly chelate the first mineralogical phase involved, the aluminates.

Calcium sulphate chelates the aluminates by slowing their interaction with water to form ettringite.^{119,120} The additives synthesised (**17-21**) are able to amplify this effect as they further stabilise the ettringite layers, causing a delay in the hydration of the aluminates and consequently lengthening the dormant phase (**Figure 69**).

A strong delaying effect on the dormancy period before C₃S hydration is observed using the following samples: the dormant period is particularly prolonged when using the starting CMC and samples **16** (**Figure 69**, violet line) and **17** (**Figure 69**, blue line) hydrolysed and sulpho-ethylated for 24 h, both of which show a very similar trend (**Figure 69**).

Extending the hydrolysis time to 48 h, with sample **18** (**Figure 69**, red line), a dormant period is observed that is reduced even though it still takes almost 6 h. Only with samples **19** (**Figure 69**, green line), **20** (**Figure 69**, green line) and **21** (**Figure 69**, yellow line) is there a slight delaying effect of almost 4 h on the hydration of the clinkers involved in

¹¹⁹ Zhou, Q.; Glasser, F. P. Kinetics and Mechanism of the Carbonation of Ettringite. *Adv. Cem. Res.* **2000**, *12*, 131–136.

¹²⁰ Brown, P.W.; Bothe, J.V. The Stability of Ettringite. *Advances in Cement Research* **1993**, *5*, 47–63.

this phase. The length of the quiescent period is correlated to the molecular weight of the additives, indeed reducing the M_w of the SPs, the delay is also reduced (**Figure 69**).

The heat release values of the additives are very low in the sample **17** (**Figure 69**, blue line) and with the starting CMC, that explains the strong retardant effect of these compounds.

The samples **18-21** were synthesized increasing the temperature of hydrolysis that means to obtain backbones with a lower M_w . It was very interesting to observe that with the specimens **18-21**, we observe the maximum main heat release value if compared to the reference cement (**Figure 69**). For example, the maximum of thermal energy released with the only cement is 14.5 J/g·h (**Figure 69**, dotted grey line). This value is higher than the one measured for the sample **21** of 4.28 J/g·h (**Figure 69**, dotted yellow line).

After 48 hours, the investigation of the heat release profiles displays that the compounds reach the same heat released values as the black at the same degree of hydration. This result explains that CMC based-SPs influence the hydration reactions only for 48 hours, after this period the specimens reach the same degree of hydration as the reference (**Figure 69**).

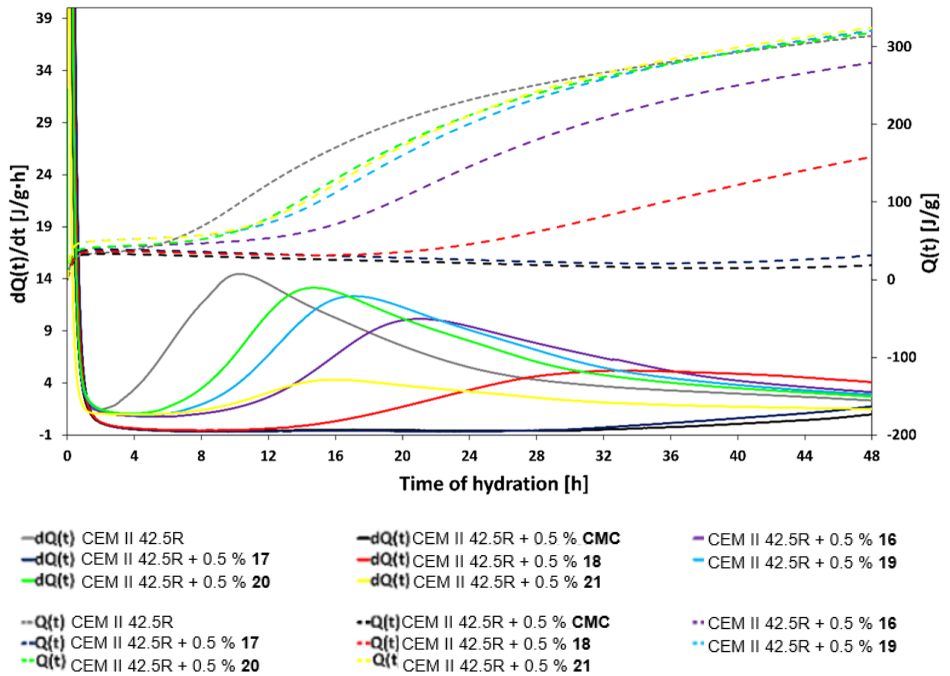


Figure 69. Calorimetry studies of the cellulose-based superplasticizer studied with a w/c ratio = 0.5 on the early hydration of CEM II 42.5 R.

The analysis of the setting times was performed through ultrasounds measurements for the reference CEM II 42.5 R and the CMC-SPs synthesised with the w/c ratio=0.5 and a dosage of 0.5 wt %. Setting point results are shown in **Figure 70**. The initial and final setting time of the blank alone were 326 min and 444 min respectively corresponding to an ultrasonic velocity of 1417.37 m/s and 1794.41 m/s. The starting CMC prevented the cement from curing up to 5 days, while samples **16**, **17** and **18** showed a severe lag effect up to more than 36 hours.

The initial and final setting times were reduced compared to the starting material and the previous modified samples as the M_w was reduced by increasing the hydrolysis temperature, with samples **19** (**Figure 70**, dotted light blue line), **20** (**Figure 70**, dotted grey line), **21** (**Figure 70**, dotted yellow line). However, these products still behave as retarding agents: in fact, the value of the initial and final setting time obtained with sample **19** (**Figure 70**, dotted light blue line) were $T_i=798$ min and $T_f=912$ min, respectively.

A slightly reduced setting point was observed with sample **20** (**Figure 70** dotted grey line), in fact the initial and final hardening values were after 609 min and 729 min, respectively.

Finally, the lag period of sample **21** started after 930 min and ended after 1069 min (**Figure 70**, dotted yellow line).

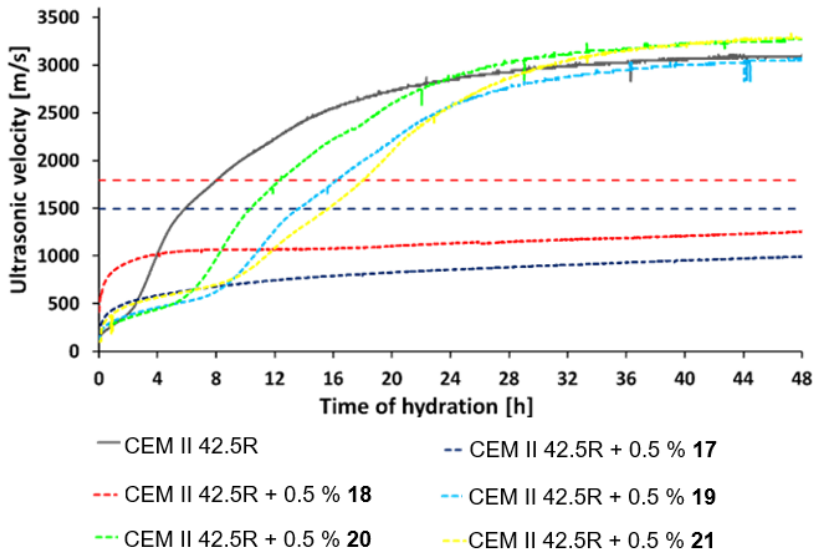


Figure 70. Setting time analysis through Ultrasonic measurements of the CEM II 42.5 R at $w/c = 0.5$ (solid grey line) and with 0.5 % bwoc of additives (derivative **17** dotted blue line; derivative **18** dotted red line; derivative **19** dotted light blue line; derivative **20** dotted grey line; derivative **21** dotted yellow line).

The flowability effect of CMC-based SPs was investigated by slump tests on mortar systems (**Figure 71**). The tests of all the samples were conducted at $w/c=0.5$ and with a percentage of active of 1% bwoc.

The results were compared with the ones obtained without the SPs as a reference. The starting CMC did not display any fluidizing property (data not shown). The derivatives **15**, **16**, **17** (**Figure 71**) on the mortars do not fluidize the mortars and for this reason they are classified as thickening

agents. As observed in **Figure 71** the only reference does not show any fluidizing properties instead the pastes doped with CMC-SPs showed that at 0.5% bwoc it determines good ability of fluidification. Indeed, sample **18**, hydrolyzed at 70 °C for 48 hours, is the first sample to behave as a SP but only with derivatives **19**, **20** and **21** we measured very good spread diameters values (**Figure 71**).

The evolution of the fluidity of the mortars doped with **19** (**Figure 71**, dotted light blue line), **20** (**Figure 71**, dotted grey line) and **21** (**Figure 71**, dotted yellow line) was measured during time and all the derivatives showed an initial spreading diameter of almost 240 mm that remained almost constant for 2 hours (**Figure 71**). This means that the synthesized additives can prolong the workability time within the first 120 minutes when the doped pastes are very flowable (**Figure 71**).

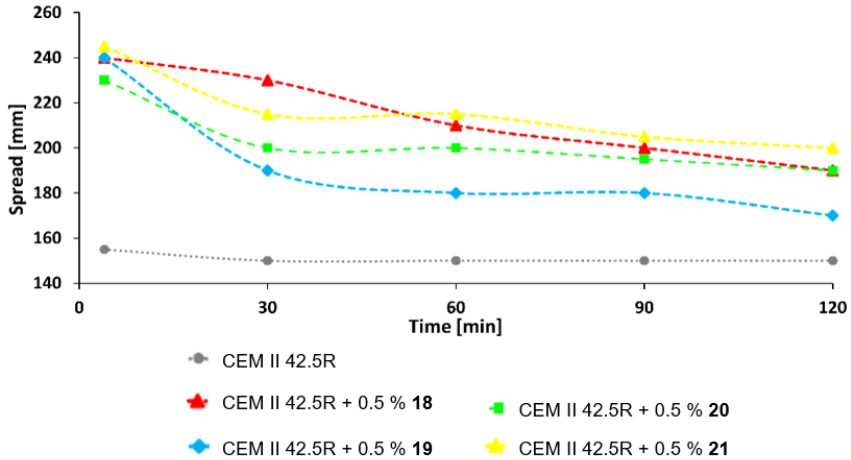


Figure 71. Investigations of the fluidifying properties by slump test of CEM II 42.5R doped with and 1 % bwoc of additives with a w/c=0.5 (UNI EN 197-1): derivative **17** dotted blue line; derivative **18** dotted red line;

derivative **19** dotted light blue line; derivative **20** dotted grey line; derivative **21** dotted yellow line.

Studies on the mechanical behaviour of cement paste doped with the derivatives **19** (**Figure 72**, light blue), **20** (**Figure 72**, green) and **21** (**Figure 72**, yellow) under compressive and flexural stresses after 28 days showed that the increase of the anionic charge state and the reduction of the molecular weight increase the mechanical properties from 78 N/mm³ to 93 N/mm³ regard to the compression parameter of hardened cement mixed with bio-based superplasticizers. Instead, the flexural benchmark still remains a relatively vulnerable aspect as reported into **Figure 72**.

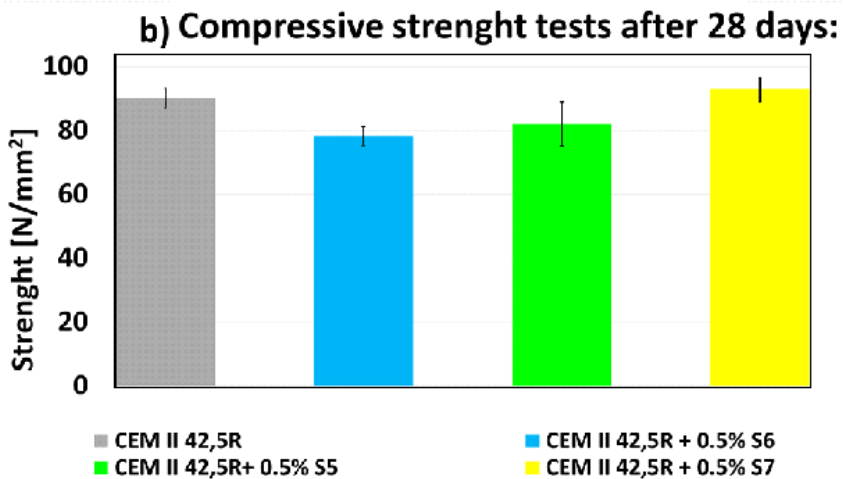
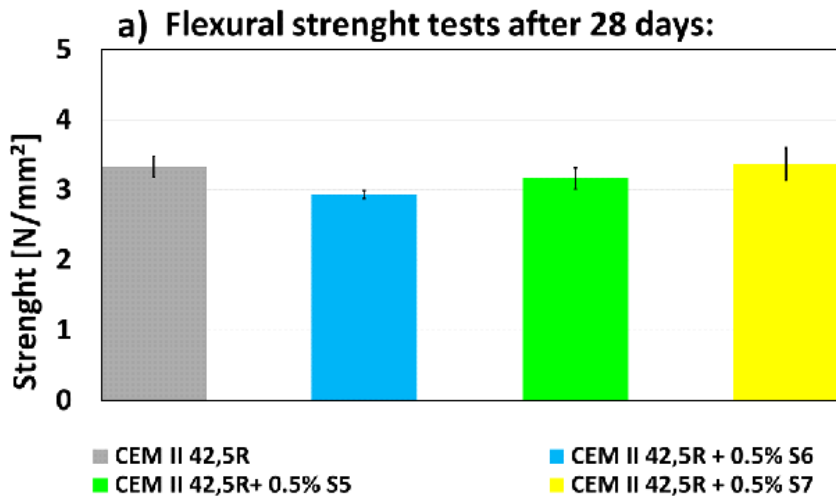


Figure 72. Mechanical properties for (a) bending and (b) compression of mortar CEM II 42.5 R, as the only reference and mortar doped with **19**

(blue), **20** (green) and **21** (yellow) (**Table 4**) and at w/c = 0.35 and 1 % bwoc after 28 days.

CT measurements in **Figure 73** have highlighted the contribution of CMC-SPs on the diameter and size pores of cementitious set matrices. Using the samples **19**, **20** and **21** SPs it is observed the reduction of air bubbles and of the size of the capillary pores. In particular, the main porosity using **19**, **20** or **21** decreases in a range of 40.63 % to 60.94 % in comparison to the reference after 7 days. The Sample **19** shows the highest decrease in porosity after 28 d of 81.8 % (**Table 5**). In addition, the CT images show a significant reduction of air voids (**Figure 73**).

Table 5. X-ray CT to analyze the pore structure of mortar matrixes after 7 and 28 days.

Specimens	% of porosity after 7 days	% of porosity after 28 days
CEM II 42.5 R	64	33
19	25	6
20	38	12
21	28	9

Table 5. X-ray CT to analyze the pore structure of mortar matrixes after 7 and 28 days.

From the analysis of the porosity of the specimens, it was observed that at higher charge contain and lower M_w , the porosity of the final materials improves, which means less exposure to environmental conditions, longer durability of the cement matrix (**Figure 73**).

Using the **19**, **20** and **21** SPs the durability of the hardened cement will not be affected by time and external factors such as environmental pollution (**Figure 73**).

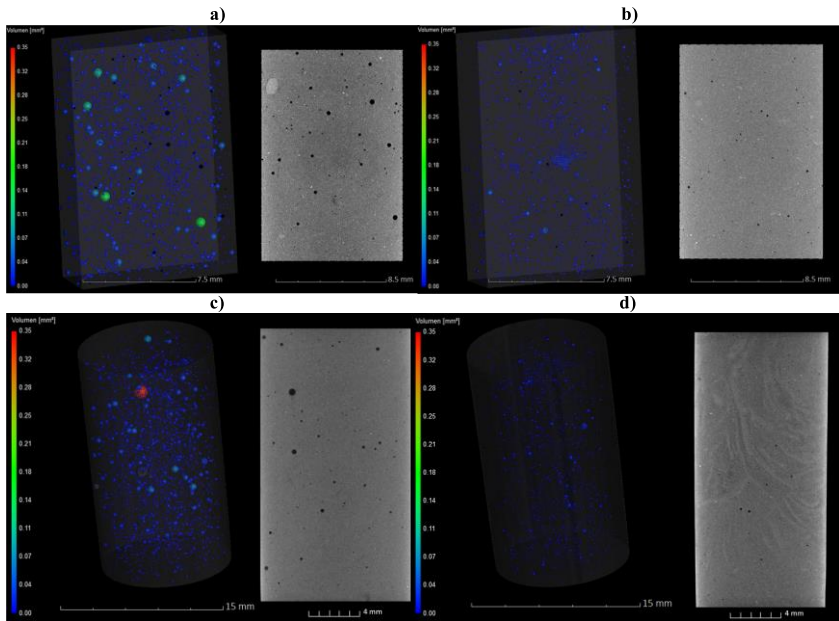


Figure 73. 3D and 2D area void fractions of **21** SP b) after 7 days and d) 28 days compared with the only reference CEM II 42.5 R a) after 7 days and c) after 28 days.

Through ICP measurements of the aqueous solutions contained in the cementitious pores, the retarding effect of CMC-based SPs was confirmed by analysing the most abundant ionic species found in the liquid phase (Ca^{2+} , K^+ , S^{6+} , Na^+ , Si^{4+} , Al^{3+} , followed by small traces of Mg^{2-} and Fe^{3+}).

Each cement sample doped with the synthesized **17-21** SP derivatives showed the same behaviour, for these reasons only the

analysis of sample **19** has been reported, where the abundance of individual ions in a sample obtained with cement alone and with the addition of the SPs was compared as observed in **Figure 74**.

It is very evident that the increase in Ca^{2+} content in the sample doped with additive **19** is shifted to longer timescales. The Al^{3+} concentration reflects the production of the hydrate products obtained from the fast reactions of the aluminate that occur during the initial phase of cement hydration.

The Al^{3+} levels in the first hour of reaction are lower than the corresponding level in the reference, which highlights the retarding effect typical of carbohydrate admixtures. Consistently, the level values of S^{6+} and Si^{4+} also decrease slowly over time. The concentrations of K^+/Na^+ follow the same trend in the sample mixed with **19** and in the blank. After the dormancy period, the second hydration process involving silicates occurs.

This reaction led to the formation of portlandite and $\text{Ca}(\text{OH})_2$ which increases the pH value of the already alkaline environment of the cement which was monitored as shown in **Figure 75**. The pH fluctuates around 12 and after 6 hours, it reaches the maximum value which is shifted to longer times (12 hours after mixing the cement slurry) with sample **19**.

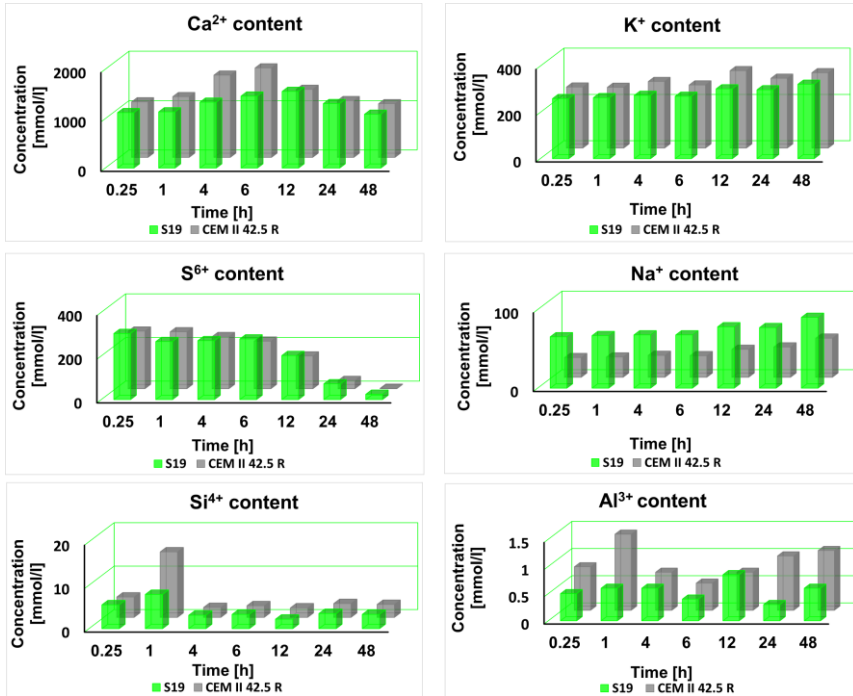


Figure 74. Pore solution chemistry of derivative **19** (green) and the only reference (grey).

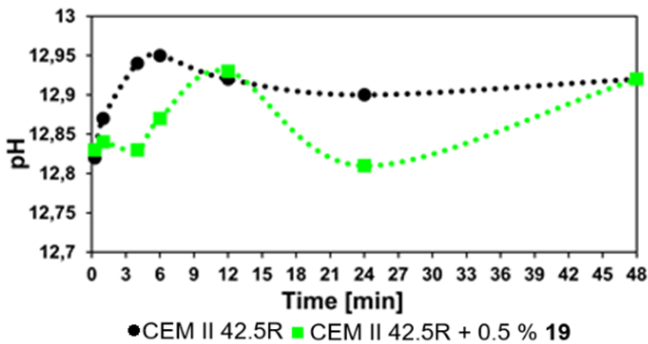


Figure 75. Evolution during time of the pH during the process of hydration of cement powder (grey) and of the cement doped with the additive **19** (green).

5.4 Conclusions

This study was focused on the research and development of new cellulose ethers, so several synthetic strategies were adopted to obtain new compounds for the study of their fluidifying properties as new SPs for mortar systems. These additives are based on carboxymethylcellulose, a water-soluble carbohydrate that has shown an interesting plasticizing effect on mortar.

Carboxymethylcellulose is a "green" complex polymer which is used as a thickening agent. The shear stress and dynamic viscosity values were closely dependent on the M_w weight because only by increasing the hydrolysis temperature from RT to 70 °C was it possible to reduce the size of the starting material. Moreover, only by combining acid hydrolysis and the addition of anionic fillers to the main backbone, was it easy to modify its physicochemical properties. Indeed, by making these modifications to the CMC, potential new superplasticizers were obtained. Through workability tests it was observed that they give fluidity to the mortar and from the overall observation of the data several demonstrations of the strong retarding effect of the synthesized additives were obtained. Indeed, studies of their setting times and calorimetric investigations revealed their retarding function, which was also confirmed by pore solution analysis and absorption experiments of the synthesized additives on the cement.

Our preliminary studies on the final matrices, through mechanical strength tests and CT analysis of the mortar over time, have highlighted the promising properties of these new bio-based additives. Indeed, these

new CMC-SPs broaden the spectrum of possible eco-friendly SPs by proposing an environmentally friendly alternative to the family of petrochemical additives currently on the market to provide innovation in building materials engineering.

5.5 Experimental section for the synthesis of derivatives 15-21

5.5.1 Hydrolysis procedures at variable temperatures and reaction times

25 g of CMC were poured into 200 mL of ethanol (Carl Roth GmbH & Co. KG, Karlsruhe, Germany) and stirred for 5 minutes. Then 10 mL of an aqueous solution of HCl (37 %) (Carl Roth GmbH & Co. KG, Karlsruhe, Germany) was added to the mixture at room temperature, and then the mixture was heated at 70 °C and stirred for a variable time (24h, 48 h and 72h). Then the reaction mixture cooled to room temperature and added 100 mL of an aqueous solution of NaOH (Carl Roth GmbH + Co. KG, Karlsruhe, Germany; purity 98 wt.%, 10 % w/w) under stirring. The solid phase was separated by centrifugation at 2215 G for 5 minutes (Eppendorf® Centrifuge 5804 R) and washed with ethanol (3x100 mL). A pale-yellow solid was obtained that was stored at 30 °C for 72 h.

5.5.2 Sulfo-ethylation of the hydrolysed substrates

The sulfo-ethylation of the hydrolysed products was performed starting from 5 g of the hydrolysed backbone. The hydrolysed products were mixed at 30 °C for 12 h in 200 mL of deionized water. Then, the reaction

temperature was set at 70 °C and added of 1.2 g of NaOH (Carl Roth GmbH + Co. KG, Karlsruhe, Germany; purity 98 wt.%) and stirred for 60 min. Then, 16.2 g of sodium vinyl sulfonate was added dropwise. The reaction mixture was stirred at 70 °C for different times (see **Table 4**. Library of synthesized CMC SPs obtained with several temperature and times of hydrolysis and sulfo-ethylation.), then cooled and stored at room temperature.

5.6 Characterization and testing through applicative tests on mortar

5.6.1 Rheological properties investigations

The thixotropic properties of the cement slurries were so studied preparing grout pastes following these conditions: 30 g cement, 15 g of deionized water at $w/c = 0.5$ with 1 % bwoc percentage of additive. Immediately after the mixing, the specimen was immediately insert into the sample loader with the spindle. The test was performed for each sample three times and a mean value was calculated. The results per each SPs were compared with the reference without additive.

5.6.2 Adsorption studies of CMC SPs on cement grains through UV-Vis-spectroscopy

The investigations were carried out following the phenol method already reported in the literature at a wavelength of 490 nm.¹¹⁸ An aqueous solution of 0.02 M $\text{Ca}(\text{OH})_2$ (Carl Roth GmbH + Co. KG, Karlsruhe,

Germany; purity 96 wt.%) was prepared to mimic the alkaline conditions of the prepared mortar at a w/c ratio of 0.5. Each sample was prepared with a ratio between the water solution and cement of 0.5 and 0.5 % of additive by weight of cement. The suspension was stirred for 2 h at room temperature. After the mixing time, the supernatant was separated from the precipitate by centrifugation at 2215 G for 20 min and the supernatant was filtered (membrane filters with a 0.45 μm pore size) and used for SPs detection. 5 wt% phenol solution and 96 wt% sulphuric acid were added to the supernatant. This exothermic reaction develops a yellow colour solution. The concentration of the blank and the sample containing the additive is measured with a spectral photometer (Schott Instruments, UvLine 9100) at a wavelength of 490 nm. The average of 10 absorbance measurements for each sample is recorded. The concentration of the superplasticizers in the supernatant was determined by using a calibration line with various concentrated glucose solutions and comparing the concentration values obtained with those of the blank without additive.

5.6.3 Isothermal calorimetric studies of early-stage hydration processes

The hydration process was studied through calorimetry at 20 °C. Per each sample, there were followed the same conditions: w/c= 0.5 and 0.5% of active. The 5 g of cement powder were added to the solution of water and SP. After mixing the slurry in the vial, it is then inserted inside the calorimeter. The heat flow was measured for 48 h.

5.6.4 Investigations of the composition of the pore solution analysis

Different stages of the hydration process of the cement were investigated through the analysis of the composition of the liquid phase of the suspension made with lime solution, cement powder and additives. At the ratio between lime and cement of 20 and 0.5% of active, 5 grams of cement were mixed with the 0.02 M Ca(OH)_2 water solution and with 0.5% bwoc of SPs for several defined times: 15', 1h, 4h, 6h, 12h, 24h and 48h. The hydration reaction was stopped mixing the centrifuge tubes at 2215 G at 20 °C, the supernatant was filtered and 1 ml was diluted in 20 ml of HNO_3 to stabilize the pore solution for the ICP-measurements.

5.6.5 Initial and final setting time evaluation

The determination of the point of the beginning and the end of the setting of mortar was defined preparing cementitious paste of the only reference setting the w/c at 0.5 and starting with 450 g of cement powder and 225 g of deionized water. The automatic penetration of the needle was carried with Vicat apparatus in a defined time lapse, after a delay of 2 hours to occur the setting points.

The reference points of the beginning and of the end of the loss of plasticity were defined respectively after 326 minutes and 444 minutes from the mixing of the grout.

For the ultrasonic velocity measurements, the obtaining of the cementitious paste required 300 g of cement, 150 ml of deionized water for the only CEM II 42.5 R. The investigation of the setting times of the samples was performed using the 0.5 % bwoc of each additive. From the only reference, the CEM II 42.5R it was estimated that the ultrasonic velocity was 1417,37 m/s for the initial and 1794.41 m/s for the final

point. By the comparison of the results of the ultrasonic velocity of the samples with the one of the references, the characterization of the values was extrapolated per each sample.

5.6.6 Workability tests

The samples for the workability tests were prepared by mixing cement, deionized water, sand and superplasticizers. Mortar mixer was used for mixing inert materials, cement, deionized water and SPs into a cementitious paste following these conditions: 0.5 % bwoc; w/c=0.5; CEM II 42.5 R = 450 g (EN197-1); H₂O=225 g; Standard sand=1350 g (EN 196). After the mix, to evaluate the trend of the additive on mortar, the spread values were obtained measuring in a specific time lapse the mean values of three measurements of diameters after 4', 30', 60', 90 and 120'. The sand for the Slump tests, setting time estimation and for the mechanical tests is the CEN-standard sand (Normesand) in accordance with the current legislation. The investigations were carried on with the water/cement ratio w/c=0.5, using 0.5% and 1% bwoc of the additives.

5.6.7 Estimation of the mechanical properties of the hardened mortar

For the bending and compressive strength tests, the specimens were prepared following the method DIN EN 197-1 and the specimens were cured until the test age of 7 and 28 days into prism shapes. The prism shaped samples were prepared complying to the legislation in force and three measurements were determined for each specimen. Average values were obtained per each investigation. Bending stress was applied on the long surface of prism specimens using a bend tester (ASTM C 348) even on triplicate samples.

5.6.8 Computed tomography analysis

Grout specimens were prepared in cylindrical vials starting from 5 g of anhydrous cement, deionized water, $w/c=0.5$ for the reference and $w/c=0.4$ and 1% bwoc of active. All the samples were scanned after 7 and 28 days.

6. Summary

6.1 Final conclusions

With this PhD research project, it was set the goal of developing new and performing superplasticizers for the civil engineering field.

In detail, we started broadening the possible applications of well-known supramolecular compounds, the resorcinarenes and pyrogallolarenes. So, water-soluble tetrasulfonate resorcin[4]arene **1** and pyrogallol[4]arene **2** macrocycles were synthesized and investigated for their behaviour as superplasticizers in mortars. Applicative tests clearly shown that these polyhydroxylated compounds are able to work as cement dispersants and it was demonstrated that they can behave as SPs even in presence of sulfate anions because these species don't affect their fluidificant properties.^{1,2}

Moreover, further investigations about their setting time indicated that the compounds **1** and **2** are able to prolong the workability time because they showed retarding effect on cementitious systems.

Successively, due to the growing concerns related to the environmental pollution related to the use of the commercial SPs currently on the market, the research was also focused on the possibility to develop more sustainable additives. We explored the possibility of exploiting supramolecular complexes to mimic commercially available additives, but increasing process and raw material sustainability.

So pseudorotaxane complexes between β -CD and mPEG-derivative bearing carboxylic acid function **9** and **10** were produced and investigated for their dispersing capabilities in cement-based mortars.³ Mortar tests indicate that mPEG-COOH@ β -CD interpenetrated supramolecules show excellent dispersing abilities. Additionally, even the second class of compounds, the supramolecular complexes, show a retarding effect that made these compounds perfect to be employed in warm seasons.

Finally, the studies were focused on the research and development of new cellulose ether derivatives as innovative superplasticizers for cementitious matrixes.⁴ The new water-soluble admixtures were synthesized using a complex carboxymethylcellulose-based backbone that was first hydrolysed and then sulfo-ethylated to change its nature as thickening agent. Through applicative tests on mortar, their effect on cement as fluidificant and retarder was ascertained, widening the pool of compounds that were produced into this PhD project.

Scientific contributions:

- Capacchione, C.; Picariello, D.; Della Sala, P.; Talotta, C.; Neri, P.; Bruno, I.; Pauciulo, A.; Bartiromo, A. R.; Gliubizzi, R.; Gaeta, C. Dispersing and Retarding Properties of Water-Soluble Tetrasulfonate Resorcin[4]arene and Pyrogallol[4]arene Macrocycles in Cement-Based Mortar. *ACS Omega* **2020**, *5*, 18218–18225 [DOI:[10.1021/acsomega.0c01837](https://doi.org/10.1021/acsomega.0c01837)].
- Capacchione, C.; Della Sala, P.; Bruno, I.; Pauciulo, A.; Bartiromo, A. R.; Iannece, P.; Neri, P.; Talotta, C.; Gliubizzi, R.; Gaeta, C. Poly(Ethylene Glycol)/ β -Cyclodextrin Pseudorotaxane Complexes as Sustainable Dispersing and Retarding Materials in a Cement-Based Mortar. *ACS Omega* **2021**, *6*, 12250–12260. [DOI: [10.1021/acsomega.1c01133](https://doi.org/10.1021/acsomega.1c01133)].
- Capacchione, C.; Partschefeld, S.; Gliubizzi, R.; Gaeta, C.; Osburg A. Modified carboxymethylcellulose-based scaffolds as new potential ecofriendly superplasticizers with a retardant effect for mortar: from the synthesis to the application. *MDPI (paper accepted on the 23rd of June 2021)*.
- XXXIX National Conference of the Division of Organic Chemistry - SCI, CDCO, Turin (Italy), 8-11th September, 2019. Poster session.
- 1st School of High-Resolution Mass Spectrometry (1st HR MS School) - Department of Chemistry and Biology of the University of Salerno, Fisciano (Italy), 2nd-3rd December 2019.

- Internal seminary at the F. A. Finger Institute for Building Materials Engineering at the Chair of Construction Chemistry and Polymeric Materials ChemPoWer, Bauhaus-Universität in Weimar, Germany - **February, 17th 2020.**
- Final workshop at the F. A. Finger Institute for Building Materials Engineering at the Chair of Construction Chemistry and Polymeric Materials ChemPoWer, Bauhaus-Universität in Weimar, Germany - **September, 8th 2020.**